PB81-104499

A Study of Visibility in Carbon and Emery Counties, Utah

(U.S.) National Oceanic and Atmospheric Administration, Silver Spring, MD

Prepared for

Bureau of Land Management
Washington, DC

Jul 80

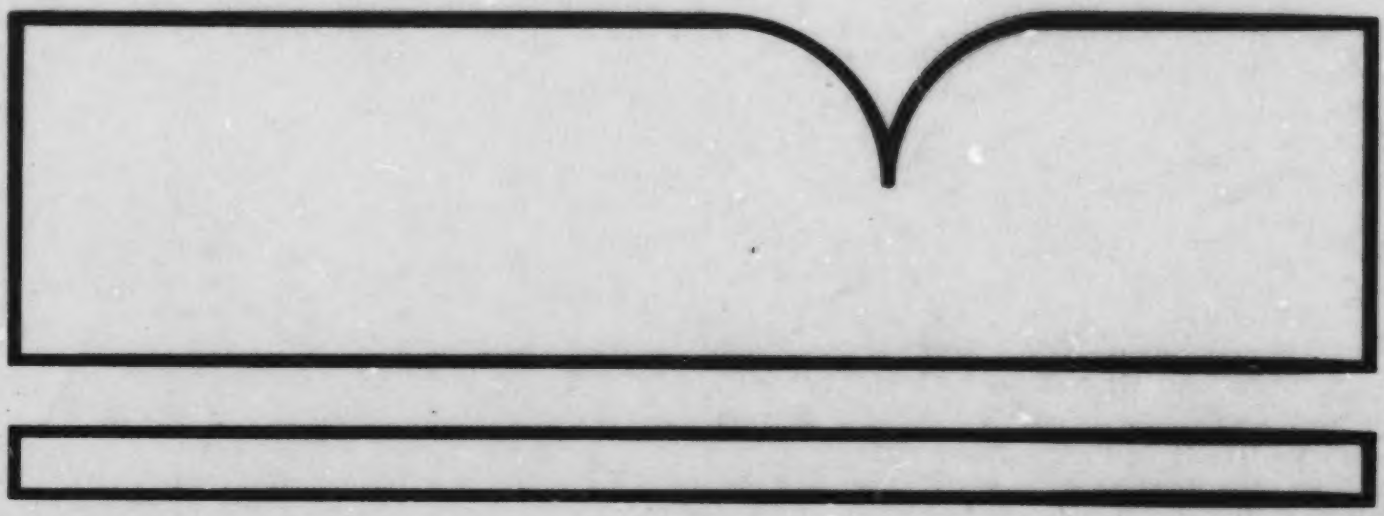

U.S. Department of Commerce
National Technical Information Service
NTIS

NOAA FORM 25-13 (1-78)

BIBLIOGRAPHIC DATA SHEET

U. S. DEPARTMENT OF COMMERCE
NATIONAL OCEANIC AND ATMOSPHERIC ADMINISTRATION

1. NOAA ACCESSION NUMBER	2.	3. RECIPIENT'S ACCESSION NUMBER
NOAA-80082606		PB81 104499

4. TITLE AND SUBTITLE
A Study of Visibility in Carbon and Emery Counties, Utah

5. REPORT DATE
July 1980

6.

7. AUTHOR(S) Paul A. Allee and Rudolf F. Pueschel (Both ERL, Atmospheric Chemistry Program, Boulder, CO)

8. REPORT NO.
NOAA-DR-ERL-ARL-1

9. PERFORMING ORGANIZATION NAME AND ADDRESS
NOAA, Environmental Research Laboratories,
Silver Spring, MD, 20910
Air Resources Laboratories

10. PROJECT/TASK NO.

11. CONTRACT/GRANT NO.

12. SPONSORING ORGANIZATION NAME AND ADDRESS
Same; and
U.S. Dept. Interior Bureau of Land Management; and
U.S. Environmental Protection Agency

13. TYPE OF REPORT AND PERIOD COVERED
Data Rept.

14.

15. PUBLICATION REFERENCE
NOAA Data Report ERL ARL-1, July 1980. 112 p, 59 fig, 23 tab, 32 ref.

16. ABSTRACT Visibilities were measured at Cedar Mountain, Utah (39°11'N; 110°37'W; 2336 m MSL), during 10 non-consecutive periods of 4 weeks each between November 1976 and October 1978. Annual means of 128 kilometers from the photographic method and of 160 kilometers from telephotometry with a phototopic filter were derived. Except for the unusually clear period from November 1976 to January 1977 the average visual range had remained unaltered within one sigma standard deviation for seasonally comparable periods. No effects of local or regional power plants on visibility could be delineated. Visibilities varied by as much as 3.5 times during individual observation periods in response to changes in mesometeorology. In support of the visibility study, aerosols were collected on filters for size, shape, and elemental composition analyses. X-ray fluorescence, induced by alpha-particles for bulk analysis, and by electrons for single-particle analysis, was used to determine the elemental composition of the aerosol. No statistically significant correlation between visibility and aerosol elemental composition could be established. One case of low visibility, however, coincided with the advection of moist, lead-laden air from southern California to the observation site. (Author modified)

17. KEY WORDS AND DOCUMENT ANALYSIS

17A. DESCRIPTORS
*Visibility, *Air pollution, Clouds, Cloud cover, Power plants, Lead, data

17B. IDENTIFIERS/OPEN-ENDED TERMS
Utah, California

17C. COSATI FIELD/GROUP
4B

18. AVAILABILITY STATEMENT
Released for distribution:
Elaine S. Downs

19. SECURITY CLASS (This report)	21. NO. OF PAGES
UNCLASSIFIED	113 p.
20. SECURITY CLASS (This report)	**22. PRICE**
UNCLASSIFIED	

NOAA FORM 25-13 (1-78) SUPERSEDES ALL PREVIOUS EDITIONS.

80082606

PB81-104499

NOAA Data Report ERL ARL-1

A STUDY OF VISIBILITY IN CARBON AND EMERY COUNTIES, UTAH

Paul A. Allee
Rudolf F. Pueschel

Air Resources Laboratories
Silver Spring, Maryland
July 1980

REPRODUCED BY
NATIONAL TECHNICAL
INFORMATION SERVICE
U.S. DEPARTMENT OF COMMERCE
SPRINGFIELD, VA 22161

noaa NATIONAL OCEANIC AND ATMOSPHERIC ADMINISTRATION / Environmental Research Laboratories

NOAA Data Report ERL ARL-1

A STUDY OF VISIBILITY IN CARBON AND EMERY COUNTIES, UTAH

Paul A. Allee
Rudolf F. Pueschel

Atmospheric Chemistry Program
Boulder, Colorado

Air Resources Laboratories
Silver Spring, Maryland
July 1980

UNITED STATES DEPARTMENT OF COMMERCE
Philip M. Klutznick, Secretary

NATIONAL OCEANIC AND ATMOSPHERIC ADMINISTRATION
Richard A. Frank, Administrator

Environmental Research Laboratories
Wilmot N. Hess, Director

NOTICE

Mention of a commercial company or product does not constitute an endorsement by NOAA Environmental Research Laboratories. Use for publicity or advertising purposes of information from this publication concerning proprietary products or the tests of such products is not authorized.

FOREWORD

The visual range studies summarized herein were performed by the U.S. Department of Commerce National Oceanic and Atmospheric Administration under an interagency agreement with the U.S. Department of the Interior Bureau of Land Management and the U.S. Environmental Protection Agency.

Sections 2.1, 2.2.1, 2.2, and 2.2.2 have appeared in NOAA Data Reports ERL APCL-3, -4, -5, and -6.

CONTENTS

		Page
ABSTRACT		vi
1.	INTRODUCTION	1
2.	HORIZONTAL VISUAL RANGE	9
	2.1 The Concept of Visual Range	9
	2.2 The Theory of Visual Range	11
	2.2.1 The Photographic Method	13
	2.2.2 The Telephotometric Method	13
	2.2.3 The Light Scattering Method (Nephelometer)	14
	2.2.4 Turbidity Method	14
	2.2.5 Solar Radiation Method	17
	2.2.6 National Park Service Program Method	18
	2.2.7 Color Photography Method	19
3.	DISCUSSION AND RESULTS	19
	3.1 Meteorological Parameters and Their Effect on Visibility	19
	3.1.1 Temperature	58
	3.1.2 Relative Humidity	58
	3.1.3 Wind	59
	3.1.4 Particulates	66
	3.1.5 Pressure	66
	3.1.6 Instability	83
	3.2 Aircraft Measurements	83
	3.2.1 Horizontal Atmospheric Homogeneity	87
	3.2.2 Vertical Temperature Profiles	87
	3.2.3 Aerosol Dynamics	89
	3.2.4 Aerosol Chemistry	94
4.	SUMMARY AND CONCLUSIONS	102
5.	ACKNOWLEDGMENTS	104
6.	REFERENCES	104

ABSTRACT

Visibilities were measured at Cedar Mountain, Utah (39°11'N; 110°37'W; 2336 m MSL), during 10 non-consecutive periods of 4 weeks each between November 1976 and October 1978. Annual means of 128 kilometers from the photographic method and of 160 kilometers from telephotometry with a phototopic filter were derived. Except for the unusually clear period from November 1976 to January 1977 the average visual range had remained unaltered within one sigma standard deviation for seasonally comparable periods. No effects of local or regional power plants on visibility could be delineated.

Visibilities varied by as much as 3.5 times during individual observation periods in response to changes in mesometeorology. Visibility had a correlation coefficient of -0.93 with southerly 500-mb winds. This correlation with southerly wind direction is a result of the distribution of high- and low-pressure centers that determine the character of air flow patterns. In a region of prevailing westerlies, a low to the west results in a southerly trajectory of an air mass that has been in contact with land surfaces over long distances, gathering moisture and surface-generated particulates. In contrast, a high to the west results in the subsidence to the surface of clean, dry upper air with resultant increased visual range.

In support of the visibility study, aerosols were collected on filters for size, shape, and elemental composition analyses. X-ray fluorescence, induced by alpha-particles for bulk analysis, and by electrons for single-particle analysis, was used to determine the elemental composition of the aerosol. Scanning and transmission electron-microscopy provided information on size and shape of individual particles. It was found that the optically important size range from 0.1- to 1.0-μm particle radius is dominated by spheres that are made up of elements of atomic weight smaller than that of sodium. The elements silicon and sulfur dominate the inorganic portion of the aerosol at concentrations of a few micrograms per cubic meter. It is worth noting that, occasionally, spherical silicon particles dominate the submicron portion of the aerosol. No statistically significant correlation between visibility and aerosol elemental composition could be established. One case of low visibility, however, coincided with the advection of moist, lead-laden air from southern California to the observation site.

A STUDY OF VISIBILITY IN CARBON AND EMERY COUNTIES, UTAH

Paul A. Allee and Rudolf F. Pueschel

1. INTRODUCTION

The Southwest has historically enjoyed exceptionally high air quality, with visibilities commonly exceeding 50 miles (80 kilometers). The Southwest Energy Study of 1972 states: "The scenic beauty of the rugged southwest landscape coupled with unique clarity of the air have been widely acclaimed as natural assets, worthy of protection for the enjoyment of future generations of Americans."

Section 169A of the Clean Air Act Amendment of 1977 provides a legislative mandate for the protection of visibility in and near mandatory Class I areas. The Environmental Protection Agency (EPA) must provide reports to Congress on monitoring methodology, predictive techniques, and cause/effect relationships associated with visibility degradation. Regulations that provide guidance to states on methods to prevent future and remedy existing visibility degradation are to be promulgated by EPA. The Bureau of Land Management (BLM), for purposes of land use planning, management, and environmental impact analysis, needs information to define more adequately the atmospheric visibility effects resulting from natural phenomena and from energy-development activities. The National Oceanic and Atmospheric Administration's Environmental Research Laboratories climatic research programs require information about the aerosol burden and the proportions of natural to anthropogenic cloud droplet and ice nuclei in order to assess the potential impact of energy development activities on weather and climate. These requirements resulted in the formulation of an interagency agreement among BLM, EPA, and NOAA to initiate a visibility study in the Western United States. The purpose of the study was to (1) establish existing baseline visibilities and (2) if possible, delineate the effects on visibility of accelerated power generation utilizing local coal reserves.

The potential impact of local coal-fueled power plants on visibility is of concern throughout the West. A unique opportunity for investigation of power plant impact existed in the Castle Valley of Utah (approximately 100 miles (160 kilometers) southeast of Salt Lake City) before 1977 because there was relatively little air pollution from coal-fired sources and from the low population. The only coal-fired electric power plant in the area was the Utah Power and Light power plant (160 MW) constructed in 1953 in Price River Canyon, a few miles upstream from Helper, Utah.

The Castle Valley, however, is surrounded on the west, north, and east by mountains containing coal deposits that are scheduled to be exploited and, in part, utilized locally for energy generation. Beginning in the spring of 1977, more power plant activity occurred with a consequent population increase. A 415-MW coal-fired power plant was activated in April 1977, a 415-MW in July 1977 (the Huntington power plant), a 415-MW in July 1978, and a projected 415-MW in March 1980 (the Emery power plant) for a total of 1820 MW from the power plants located in the Castle Valley region. Construction of another power plant (IPP) near Hanksville, Utah, is proposed for 1980, and 16 new mines have been proposed for southeastern Utah, development to start about 1980. Each power plant requires about 600 employees, and each coal mine about 260 employees. Population growth during the next decade will be about 6,000 families plus the families of organizations that furnish services to these families. The population of the two counties and nearby region is anticipated to increase by at least another 25,000 by the year 1990.

This report summarizes data of ten monthly study periods, from November 1976 through March 1979, carried out by the Atmospheric Chemistry Program group of the Atmospheric Physics and Chemistry Laboratory, NOAA.

The measurements of visibility, or visual range, and atmospheric parameters associated with visibility were made at Cedar Mountain, overlooking Castle Valley (Allee and Cozad, 1979; Allee and Lowery, 1979; Allee et al., 1979; Williams and Allee, 1979; Martin Marietta Corporation, 1976-1979).

Horizontal visibilities were measured by means of the photographic technique (Middleton, 1952). This involves photographing a distant mountain range target

against the horizon sky. A measurement of the contrast ratio of the film densities of the target and sky was used to calculate visual range. The photographic technique was used during nine of the monthly investigative periods. A telephotometer was used during the last four periods to measure the illuminance of the target and horizon sky directly. The contrast ratio of the illuminance values was used to calculate the visual range. Table 1 lists the parameters that were measured in the visibility study in a mobile laboratory at Cedar Mountain.

Figure 1 is a schematic map of the area where the measurements were taken, showing the observing point at Cedar Mountain, location and distance of the photographic targets, and other pertinent geographical features. The targets were photographed once every hour from 0800 to 1600 MST with a 35-mm SLR camera equipped with a 2000-mm telephoto Schmidt lens. When available, a telephotometer was used to obtain data at approximately the same time. When the telephotometer was being used, supplementary measurements of visual range were obtained with the Henry Mountains and the Abajo Mountains as targets. Table 2 records altitude, latitude, longitude, true and magnetic bearings, and distance from Cedar Mountain (CM) and the six mountain peaks used as visual range targets. Figures 2, 3, 4 and 5 are photographs of the north, east, south and west targets, respectively, and the location on the target at which the illuminance of the target was measured. The illuminance of the horizon sky was measured directly above the target.

In order to increase both the data base and the history of visibility-related measurements, solar radiation was measured with a Volz sunphotometer and Eppley pyrheliometers and pyranometers. An MRI integrating nephelometer was operated continuously at the observing point at Cedar Mountain during each observational period except July 1977. The light scattering coefficients measured with this instrument were converted to visual ranges by the Koschmieder relationship. The rest of the parameters listed in table 1 are an aid to data interpretation.

The results show that visibilities are primarily affected by regional and global, rather than local, climatology. Secondary factors that cause variabilities are clouds behind the target, cloud cover, and hourly, daily, and seasonal changes in target illuminations. The existing industrial and urban activities could not be identified as causes for visibility variations.

Table 1.--Parameters measured at Cedar Mountain during the Utah visibility study

Parameter	Units	Method of recording	Frequency of recording	Instruments	Precision	Sensitivity
Contrast		Photography	Hourly	Telescopic camera		
Turbidity	μA	Log	Preselected times	Volz Sunphotometer	10%	0.1
Color photographs		Color photography	Hourly	Camera		
Light scattering coefficient	m^{-1}	Strip chart, mag tape	Continuous	Integrating nephelometer	5%	0.15×10^{-4}
Solar energy direct, total	Cal $cm^{-2}min^{-1}$	Strip chart, mag tape	Continuous	Pyrheliometer	5%	0.01
Solar energy direct, spectral	Cal $cm^{-2}min^{-1}$	Strip chart, mag tape	Continuous	Pyheliometer plus filter	5%	0.01
Solar energy diffuse, total	Cal $cm^{-2}min^{-1}$	Strip chart, mag tape	Continuous	Pyranometer	5%	0.01
Solar energy diffuse, spectral	Cal $cm^{-2}min^{-1}$	Strip chart, mag tape	Continuous	Pyranometer plus filter	5%	0.01
Temperature	°C	Strip chart	Continuous	Thermistor	2%	0.25
Relative humidity	%	Strip chart, mag tape	Continuous	Hygrometer	3%	0.5
Wind direction	Degrees	Strip chart, mag tape	Continuous	Aerovane	10%	5
Wind speed	$m\ s^{-1}$	Strip chart	Continuous	Anemometer	10%	0.5
Vertical wind profile	$m\ s^{-1}$, degrees	Log	Preselected times	Pilot balloon Theodolite	10%	
Cloud cover	%	Log	Hourly	Visual observation		
Atmospheric pressure	mbar	Log	Hourly	Precision barometer	1 bm	
Aerosol elemental composition		Visual count, log, mag tape	Preselected times	Scanning EM, X-ray energy spectrometry		
Cloud condensation nuclei	m^{-3}	Photography	Preselected times	Thermal diffusion chamber	5%	2×10^{-6}
Aitken nuclei	m^{-3}	Strip chart, mag tape	Continuous	Expansion chamber	10%	5×10^{-5}
Aitken nuclei	m^{-3}	Light attenuation, log	Preselected times	Expansion chamber	10%	2×10^{-4}
Ice nuclei	m^{-3}	Visual crystal counts, log	Preselected times	Thermal diffusion chamber	50%	1×10^{-5}

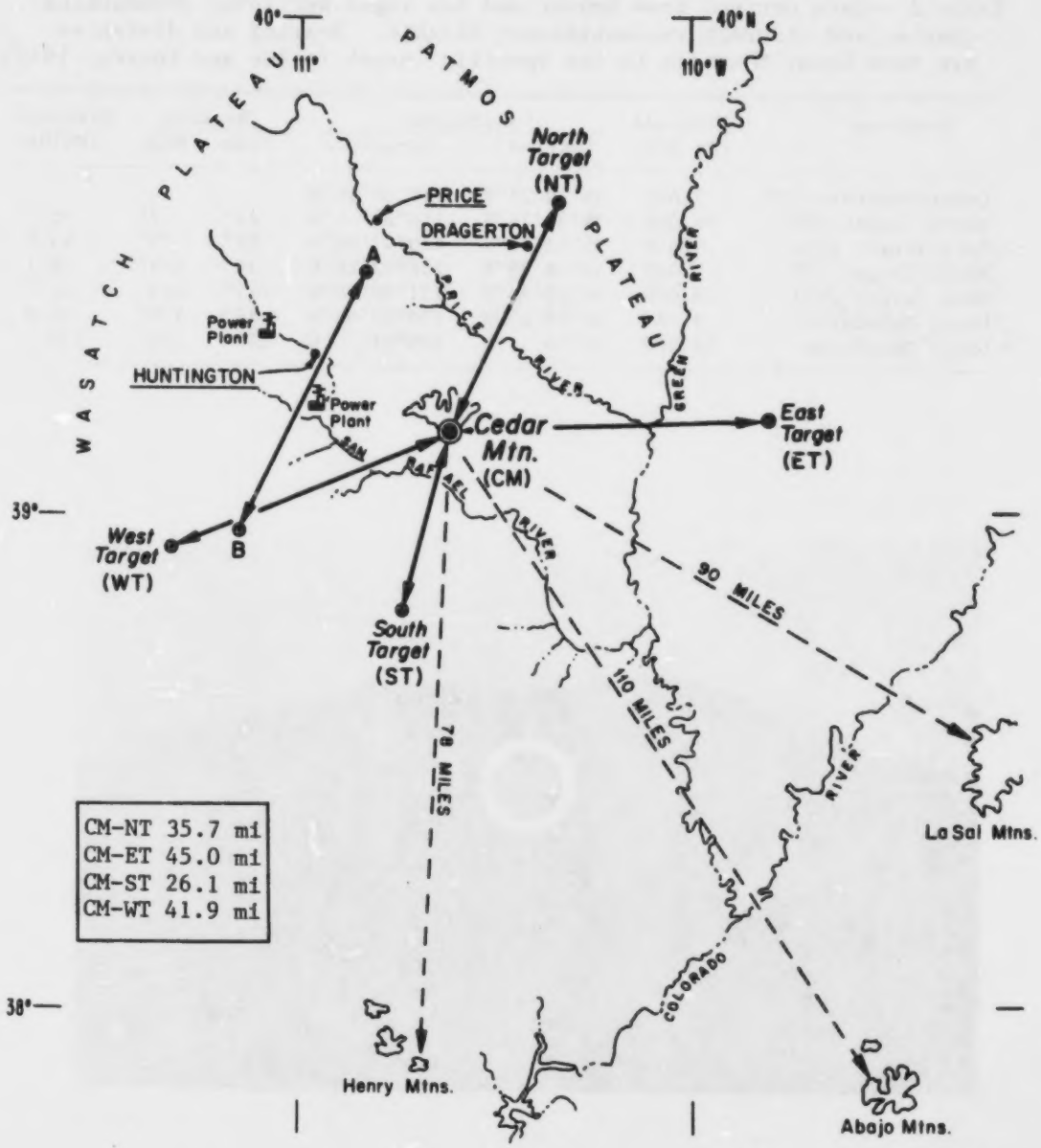

Figure 1.--Topography in the vicinity of Cedar Mountain, Emery County, Utah, showing the location of the four mountain peaks, the Henry Mountains, and the Abajo Mountains that were used as targets to determine the visual range (Allee and Lowery, 1979).

Table 2.--Data derived from Denver and Las Vegas sectional aeronautical charts, and aircraft reconnaissance flights. Bearing and distances are from Cedar Mountain to the specific target (Allee and Lowrey, 1979)

Location	Altitude (ft MSL)	Coordinates		Bearing		Distance (Miles)
		Latitude	Longitude	True	Mag.	
Cedar Mountain (CM)	7,655	39°10'25"N	110°37'10"W			
North Target (NT)	10,000	39°39'25"N	110°22' 5"W	22°	7°	35.7
East Target (ET)	9,510	39°11'25"N	110°47'00"W	88°	73°	45.0
South Target (ST)	7,425	38°48'25"N	110°43'20"W	194°	179°	26.1
West Target (WT)	8,600	38°55'25"N	111°20'30"W	246°	231°	41.9
Henry Mountains	9,187	38° 8'25"N	110°13'45"W	184°	170°	72.0
Abajo Mountains	10,500	37°50' N	109°31' W	147°	132°	110

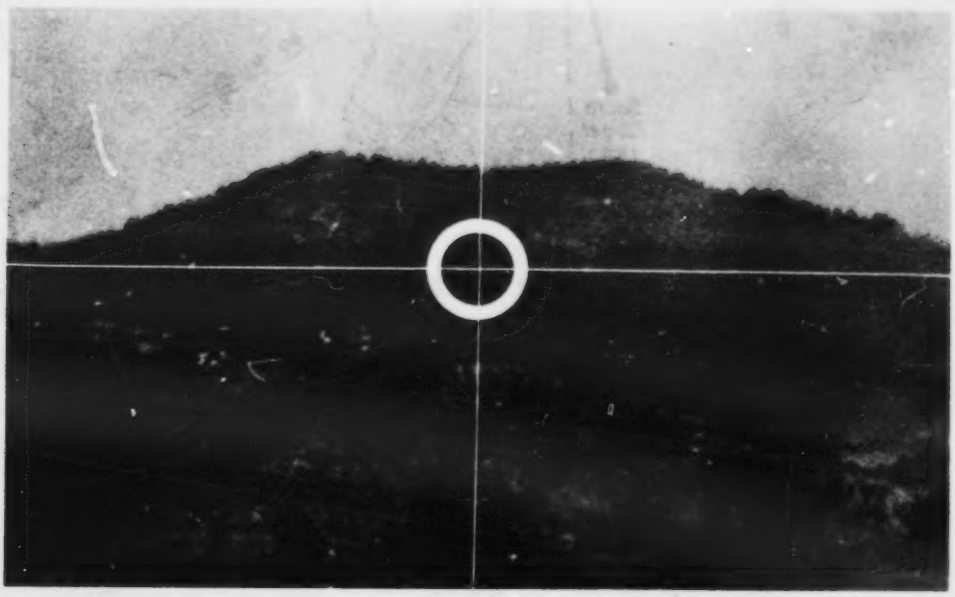

Figure 2.--North target.

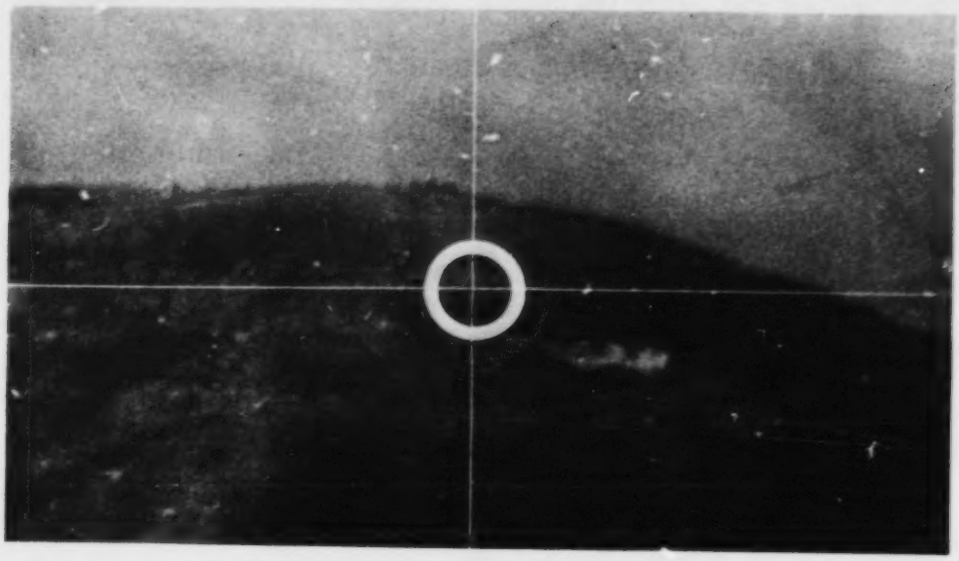

Figure 3.--East target.

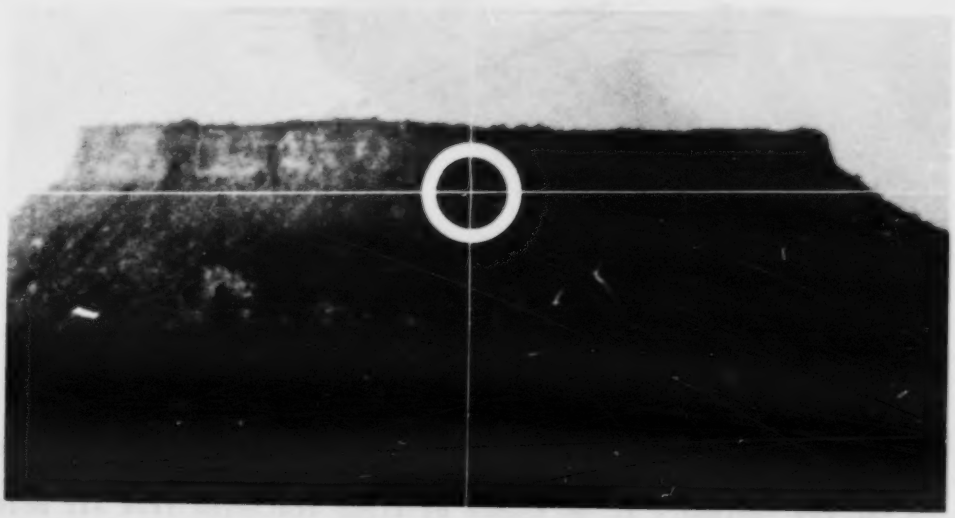

Figure 4.--South target.

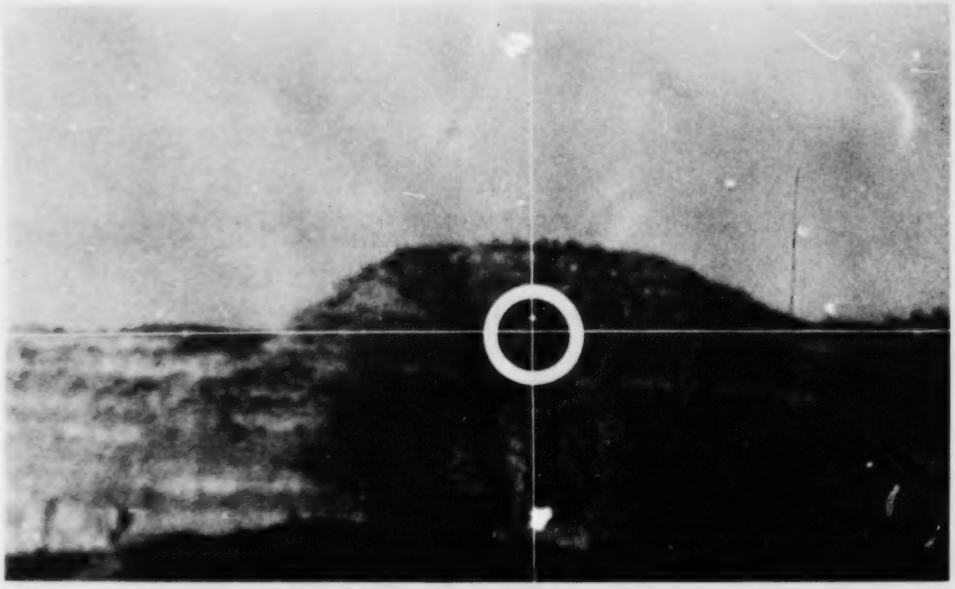

Figure 5.--West target.

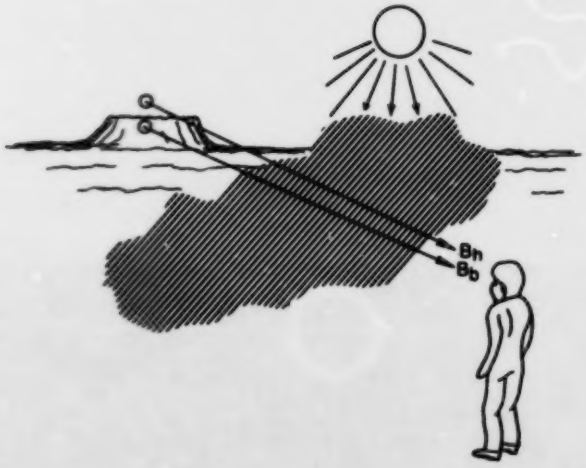

Figure 6.--Observations for determining the visual range. B_b is the luminance of the target mountain, B_h the luminance of the horizon sky above the target. The contrast ratio between the target luminance and the sky luminance is decreased by light scattered from air molecules and particles suspended in the atmosphere between the observer and the target.

2. HORIZONTAL VISUAL RANGE

2.1 The Concept of Visual Range

The measurements and discussion of horizontal visual range in this data report are restricted to daytime values of the visual range. It is defined (Glossary of Meteorology, 1959) as the distance under daylight conditions, at which the contrast between a specified type of target and its background becomes just equal to the threshold contrast of an observer. Contrast is the ratio of the apparent luminance of the target, minus that of its background, to the apparent luminance of the background. This is expressed as

$$C' = \frac{B_b - B_h}{B_h} \qquad (1)$$

where C' is the contrast, B_b is illuminance of the target, and B_h is illuminance of the background, or, in this study, the illuminance of the horizon sky directly above the target. The contrast is negative if the target is darker than its background, positive if the target is lighter. Figure 6 is an illustration of the relationship between the observer, the target, and atmospheric conditions relating to the visual range. Threshold contrast is the smallest contrast (or liminal contrast) of luminance (or brightness) that is perceptible to the human eye under specified conditions of adaptation of the eye to the luminance of nearby objects and of the angle subtended by the target. Objects either so close or so large, or both, that they shade an appreciable portion of the observer's vision decrease the amount of light entering the eye and increase its brightness contrast, thereby increasing the visual range. Large targets (>10°) can be seen farther away than small targets (<2°). Objects subtending visual angles of less than 0.5° are more difficult to detect because of the increased threshold contrast required for detection. Targets used in this study subtended angles of about 0.5°.

Threshold contrast varies from one observer to another under fixed external conditions. It tends to increase with decreasing adaptation illuminance, and with decreasing target visual angle below about 1°. An overall absolute value of the threshold contrast range is from about 0.005 to 5.0 for all observing conditions. A value of 0.02 is used in this study as being the approximate

contrast value to be found during daylight when a mountain target is viewed with a visual angle of about 0.5°. The contrast value of 0.02 was usually confirmed with photopic telephotometric measurements of visual range when mountain ranges at 72 and 110 miles were barely visible under daylight conditions.

Middleton (1952) lists simplifying assumptions attributed to Gruner and Koschmieder that are necessary to develop the theory of visual range of a black target against a lighter background:

(1) The atmosphere is considered a turbid medium, containing a large number of small particles.

(2) Each element of volume contains a very large number of particles, each of a much smaller order of magnitude than the element itself.

(3) The scattering action of each particle is independent of the presence of all the others.

(4) The light scattered from an element of volume originates from a point source of which the intensity is proportional to the number of particles.

(5) Light rays are considered rectilinear, i.e., atmospheric refraction is neglected.

(6) A cloudless sky is assumed.

(7) The coefficient of attenuation by scattering, b, is constant in a horizontal plane, in particular near the surface of the earth, where it takes the value b_o.

(8) The curvature of the Earth is neglected, and its surface is considered to be a diffusely reflecting horizontal plane.

(9) The linear dimensions of the whole observed object are small in comparison to its distance from the observer.

Some of these assumptions need additional comment with respect to the field site conditions at Cedar Mountain, Utah. The targets are not true blackbody objects. The north target (NT) is mostly covered with evergreen trees and its albedo changes little with the seasons. The east target (ET) luminance is measured on an area covered with aspen trees that are leaf-covered in summer and during winter the slope of the target is so shallow that the tree trunks block a view of the snow-covered ground; therefore, the albedo does not change much with the seasons. The south target (ST) and west target (WT) have very steep slopes,

sparsely covered with juniper and piñon pine trees. Heavy snowfall accumulates on these steep slopes and the albedo changes in winter. The albedo of the ST and WT, being greater than for the NT and ET, would lead to less contrast between the target and the sky and would tend to give lower values of visual range when the target is sunlit.

The other assumptions are well met in Utah. The coefficient of attentuation by scattering (item 7) has been measured with a nephelometer in an aircraft flying along the line of sight and no significant variation of the coefficient of attenuation has been found along that line of sight (see Section 3.2.1).

Not all parts of the atmosphere in the horizontal plane along the line of sight are equally illuminated in the presence of clouds. The effect of this on visual range has been investigated (Allee and Lowery, 1979). Visual range is increased when the target is in the shadow of a cloud, increasing the contrast between target and background. The phenomenon has been observed to occur during movement of cloud shadows across the target, but no quantitative assessment of the effect has been studied during a short time interval. Clouds behind the target affect visual range. Summer clouds, turrets of white clouds behind the targets, increase the contrast and visual range. Winter clouds, dull gray stratus, lower the contrast and decrease the visual range.

2.2 The Theory of Visual Range

By referring to Middleton (1952) and Harrison (1945) the relationship depicted in fig. 6 between visual range and the illuminance of the target, B_b, and the horizon sky, B_h, can be derived.

If i is the daylight flux on a unit volume of the column of air between the target and the observer, and σ is the attenuation coefficient of the air, considered to be homogeneous, then a fraction a of the energy passing a unit volume is scattered toward the observer. The flux of illumination from an element dx toward the observer will be aidx, and the amount reaching the observer will be $ai \exp(-\sigma x)dx$. The brightness b of a black body at a distance d will be the total flux reaching the observer from all elements of the column from distance d to the observer, or

$$b = \int_0^d ai \exp(-\sigma x)dx = ai(1-\exp(-\sigma d)). \quad (2)$$

Similarly for the brightness of the horizon sky, h, above the target

$$h = \int_0^\infty ai \exp(-\sigma x)dx = \frac{ai}{\sigma} \quad . \quad (3)$$

Putting this value of h into Eq. 2,

$$b = h\ (1-\exp(-\sigma d)). \quad (4)$$

This can be written

$$\ln\ [\frac{1}{1-b/h}] = \sigma d \quad . \quad (5)$$

If a liminal contrast ratio of 0.02 is assumed, then from Eq. 1

$$C' = 0.02 = \frac{B_b - B_h}{B_h} \quad ,$$

and if $B_h = 1$,
then $B_b = 0.98B_h$.
Since $b = B_b$ and $h = B_h$,
from Eq. 4 we have

$$\ln\ [\frac{1}{1 - 0.98B_h/B_h}] = \sigma d, \text{ or} \quad (6)$$

$$d = \frac{\ln 50}{\sigma} = \frac{3.912}{\sigma} \quad . \quad (7)$$

If a target viewed at distance r has the illuminance B_b, and the sky above has the illuminance of B_h, then from Eq. 5

$$\sigma r = [\frac{1}{1 - B_b/B_h}] \ ,$$

$$\text{or} \quad \sigma = \frac{1}{r} \ln\ [\frac{1}{1 - B_b/B_h}] \quad . \quad (8)$$

Putting the value of σ from Eq. 8 into Eq. 7, assuming σ is the same over distance d and r,

$$d = \frac{-3.912r}{\ln(1 - B_b/B_h)}$$

In this report the visual range is denoted as V_r, where r is the distance to the respective target, and

$$V_r = \frac{-3.912r}{\ln(1 - B_b/B_h)} \quad . \tag{9}$$

2.2.1 Photographic Method

The photographic method of determining V_r used an Olympus OM-1 camera coupled to a Celestron 8 lens, focal length 2000 mm, f10, Schmid-Cassegrain type construction. The film used was Kodak Panatomic X, black and white, ASA 32. A densitometer was used to measure the density of the target and horizon sky images on the developed negative. From densitometric calibration of the film and its characteristic curve the relative illuminance of the target and sky can be determined. Visual range can then be calculated from Eq. 9.

2.2.2 Telephotometric Method

B_b and B_h were measured directly with a Gamma Scientific, Inc., Model 2009 Auto-telephotometer. The optical head used a 200-mm objective lens with a viewing eyepiece to locate the target. A fiber optic with a 6-min aperture was placed on the target image at locations shown in figs. 2, 3, 4, and 5. These figures show the location at which densitometer readings on the film were taken when the photographic method for determining V_r was used. The telephotometer readings were made on the same location. The 6-min fiber optic is set in the equipment so that there appears to be a ring around the fiber of approximately twice the fiber diameter. This ring was set tangent to the horizon above and below to measure B_h and B_b, respectively. When tested with a cardboard mock-up of field conditions and illuminated with sunlight, tne telephotometer gave the same reading above and below the cardboard "horizon," simulating field measurements, when compared to measurements when the field of view of the eyepiece was completely filled with the "sky" or "target." The test indicates that any light scattering within the telephotometer lens system is negligible. The fiber optic transmits the light to a photomultiplier tube. The detector has an S11 photosurface spectral response that is corrected by a filter to a photopic (human eye) response. Three values of B_b and B_h were measured; readings were always

taken without changing scale. When necessary a neutral filter was introduced into the detector system so that B_b and B_h would be read on the same readout scale. Visual range can then be calculated from Eq. 9.

2.2.3 Light Scattering Method

A nephelometer was operated during each period of observation on Cedar Mountain, except July 1977. The output of the nephelometer is a value of σ in units of m x 10^{-4}. Visual range in meters can be derived directly from Eq. 7. The nephelometer-derived value of σ is a point measurement, and is assumed to be constant along the line of sight in any direction from the observation site. Aircraft measurements of σ along the line of sight from Cedar Mountain to the various visibility targets indicate that σ varies within ±10 percent limits of the mean value of σ along the flight path.

2.2.4 Turbidity

In 1960-61 a network of sunphotometers was established in the United States (Flowers et al., 1969). Results of this study show that Cedar Mountain is near the center of a region that has the lowest average turbidity in the United States. On Cedar Mountain, attenuation of shortwave solar radiation (turbidity) caused by suspended particulates, molecular scattering, and gaseous absorption was measured with a Volz sunphotometer.

The turbidity of the atmosphere, B_λ, was determined at 380 nm and 500 nm. From B_λ, a value of the horizontal visual range can be determined from a simple model, derived as follows. The atmospheric turbidity coefficient, B_λ, is the extinction at wavelength λ, considering vertical transmission, for aerosols in the size range from r = 0.1 μm to 1.0 μm. It is defined by the decadic equation

$$I_\lambda \cdot s = I_{0\lambda} \cdot 10^{-(\tau_{r\lambda} + \tau_{3\lambda} + B_\lambda)M} ,$$

where I_λ is the irradiance at wavelength λ at the observing point,
$I_{0\lambda}$ is the extraterrestrial irradiance at wavelength λ at the mean Sun-Earth distance,

s is the correction factor for mean Sun-Earth distance,

$\tau_{r\lambda}$ is the scattering coefficient for air molecules,

$\tau_{3\lambda}$ is the absorption coefficient for ozone,

B_λ is the turbidity coefficient, and

M is the absolute air mass (optical path length in the atmosphere).

The sunphotometer does not measure the spectral irradiance I_λ; it provides a meter deflection J_λ in microamperes that is directly proportional to I_λ. Similarly $J_{0\lambda}$ is the meter reading when the irradiance is $I_{0\lambda}$. The absolute air mass M is related to the relative optical air mass M_h (which is a function of the solar elevation angle above the horizon) by

$$M = M_h\,(P/P_0), \qquad (10)$$

where P is the station pressure and P_0 is the standard pressure at sea level.

The relative air mass value as read from the instrument diopter is used in the calculation of the turbidity coefficient, and the extinction coefficients $\tau_{r\lambda}$ and $\tau_{3\lambda}$ are adjusted for the elevation of the observation site. The following values were obtained from Elterman (1968):

Elevation	λ = 380 nm		λ = 500 nm	
(km)	τ_r	τ_3	τ_r	τ_3
0	0.1954	0	0.0630	0.005
1	.1733	0	.0560	.005
2	.1533	0	.0495	.005
3	.1355	0	.0434	.005
4	.1190	0	.0382	.005

The value of $\tau_{r\lambda}$ for Cedar Mountain, elevation 2.33 kilometers, was interpolated as $\tau_{r380} = 0.1468$, $\tau_{r500} = 0.0475$, $\tau_{3\ 380} = 0$, $\tau_{3\ 500} = 0.005$.

M was calculated from the expression derived by Kasten (1964).

$$M = \{\sin E + 0.1500(E + 3.885)^{-1.253}\}^{-1},$$

where E is the solar elevation angle. E was derived from the time of observation from the expression

$$\sin E = \sin\phi \sin\delta + \cos\phi \cos\delta \cos t,$$

where

ϕ = latitude,

δ = solar declination, and

t = hour angle (Greenwich Hour Angle (or GHA) - longitude)

GHA and δ are available from the Nautical Almanac (U.S. Naval Observatory, Washington, D.C.) for the appropriate year.

The sunphotometer was calibrated June 21-28, 1976, before the project began, and again on April 26, 1979, after completion of the project. For the earlier calibration $J_{0\ 380} = 67.6$, and $J_{0\ 500} = 47.7$. For the latter calibration $J_{0\ 380} = 70.4$, and $J_{0\ 500} = 46.3$.

One of the results that can be derived from Eq. 4 (Middleton, 1952) is

$$C_R = C_o e^{-\sigma r} , \tag{11}$$

where C_R is the contrast ratio of distant objects, and C_0 is the contrast ratio of the same objects nearby.

Under limiting visual range conditions

$$C_R/C_0 = 0.02,$$

so that for V_r, the limit of visual range can be written

$$0.02 = e^{\sigma V r} \tag{12}$$

or

$$V_r = \frac{3.912}{\sigma} . \tag{13}$$

By analogy the equation for sunphotometer

$$\frac{J_o}{J_{o\lambda}} = 10^{-(\tau_{r\lambda} + \tau_{3\lambda} + B_\lambda)\ M}$$

can be written as

$$0.02 = 10^{-(\tau_{r\lambda} = \tau_{3\lambda} + B_\lambda)M} \tag{15}$$

or, taking $\log_{10}$ of both sides,

$$M = \frac{1.699}{(\tau_{r\lambda}+\tau_{3\lambda}+B_{\lambda})} \quad . \tag{16}$$

For an elevation of 2336 meters at Cedar Mountain, $\tau_{r\lambda} = 0.0475$, $\tau_{3\lambda} = 0.0005$ ($\lambda = 500$ nm). $\lambda = 500$ nm is used since it is close to the wave length of light to which the human eye is most sensitive.

If the approximate number of air molecules in the atmosphere above 2336 meters is determined for a unit column, and then that number of molecules is used to determine the equivalent length of a horizontal unit conduit at 2336 meters, M can be expressed in terms of a horizontal distance. In terms of kilometers this length is

$$V_{rB} = 8.145 \text{ M km} = 5.062 \text{ mi} \tag{17}$$

where V_{rB} is the visual range. Substituting the value of M from Eq. 17 in Eq. 16 and neglecting $\tau_{3\lambda}$, the visual range V_{rB} can be derived as a function of B_{λ}:

$$V_{rB} = \frac{13.838}{(0.0475 + B_{\lambda})} \text{ km} = \frac{8.600}{(0.0475 + B_{\lambda})} \text{ mi} \quad . \tag{18}$$

If there were no particulates in the atmosphere, $B_{\lambda} = 0$ and V_r would be 180 miles. This is short of the maximum possible visual range of about 278 miles at $\lambda = 560$ nanometers (Harrison, 1945).

The sunphotometer measures atmospheric transmission to 0.5 percent standard deviation, with derived turbidity values of ±0.005 with B_{500} between 0.025 and 0.100 (Flowers et al., 1974). This would give a visual range variation of $V_{rB} = 60 \pm 1$ km, 120 ± 6 km, 160 ± 16 km, and 200 ± 20 km.

2.2.5 Solar Radiation

One of the programs on Cedar Mountain is the measurement of the direct solar intensity with a normal incidence pyrheliometer. Direct radiation to the

pyrheliometer is through a filter that has a 50 percent cutoff at about 295 nanometers. The response of the pyrheliometer can be expressed as

$$I = I_o e^{-\sigma m} , \qquad (19)$$

where I is the direct solar radiation at the observing point,

I_0 is the extraterrestrial solar radiation,

σ is the attenuation coefficient, and

M is the relative optical air mass.

When the values of lnI (cal cm^{-2} min^{-1}) are plotted as a function of M, the resulting Langley plot for a day of data gives σ as the slope of a straight line. For clear days during the operation periods on Cedar Mountain the best fit of an exponential function was used to derive a value of σ for that day.

A visual range model similar to that used for the turbidity visual range model was used to calculate a V_{rSR} derived from solar radiation. Eq. 13 is applicable when σ has the units of M^{-1}. V_{rSR} is then derived for each day in terms of M, and with the same derivation as used for V_{rB}, M = 5.06 mi, an average visual range V_{rSR} for a given day can be obtained.

2.2.6 National Park Service Method

We learned that a subjective and qualitative program was being pursued by the National Park Service (NPS) of the U.S. Department of Interior. It was decided that we would also make subjective assessment of the visibility of the photographic visibility targets.

Unfortunately, APCL did not have this written description of the NPS program at the start of its program, and during all of the periods of observation on Cedar Mountain a system was used that although similar, consisted of the following categories: 0 not visible, 1 barely visible, 2 no details visible,

3 details visible, 4 very clear. In use, for each target it can be determined whether the visual range is less, equal to, or greater than the target distance. If greater, upper and lower limits of the visual range for each category for each target can be determined by comparison to telephotometric measurements of visual range. With a number of targets at varying known distances the probable visual range of any vista could be determined.

2.2.7 Color Photography Method

During the Utah Visibility Project a color photograph was taken of the target at the same time data measurements were taken to obtain V'_{rP} and V_{rT}. By projecting the color photograph on a screen it is possible to calculate a value of visual range (V_{rCP}) using a telephotometer to measure the illuminance of a vista as depicted by a projection of the slide on a screen.

3. DISCUSSION AND RESULTS

3.1 Meteorological Parameters and Their Effect on Visibility

Figures 7 through 21 are a graphical representation of the observation period average visual ranges, according to the method used, target observed, sky conditions behind target, and combinations of these data that are of interest. V'_{rP} is the visual range derived from photography as reported by Martin Marietta (1976-79), but calculated by the method reported by Allee and Lowery (1979). V_{rT} is the visual range derived from telephotometric measurements. V_{rP} is the visual range reported by Martin Marietta. The number of observations, average visual range, and standard deviation for data shown on the figures is given in tables 3 through 17.

A discussion of the results is best served by referring first to the graph that incorporates all of the data, fig. 21, before discussing its component

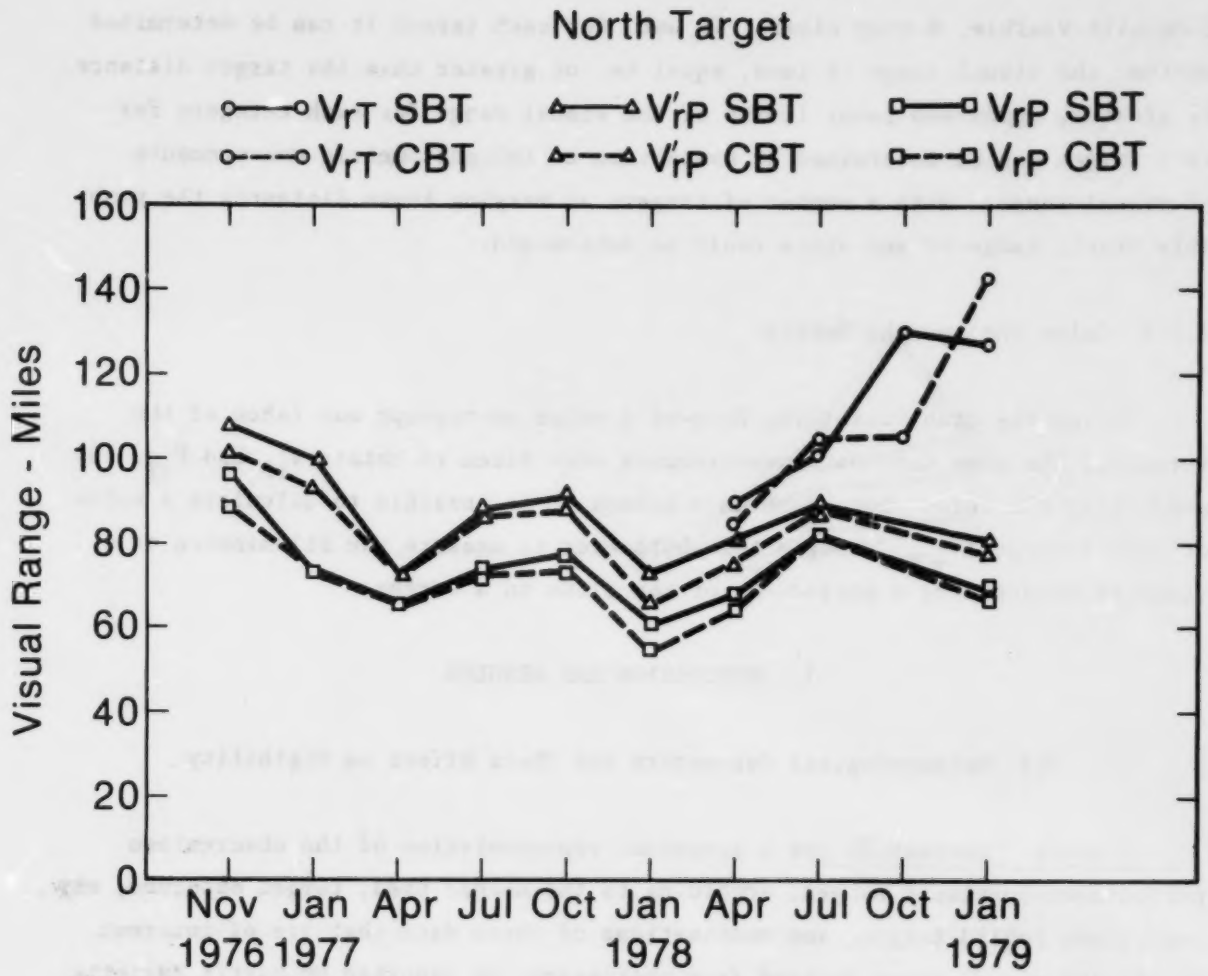

Figure 7.--Average monthly visual range for north target with sky behind target (SBT) and clouds behind target (CBT). V_{rT} = telephotometric visual range, V_{rP} = photographic visual range (Martin Marietta), and V'_{rP} = photographic visual range (NOAA).

Table 3.--Data derived from fig. 7, north target (NT) observations

Observation period		V_{rP}		V'_{rP}		V_{rT}	
		SBT[1]	CBT[2]	SBT	CBT	SBT	CBT
1976							
Nov-Dec	N	138	84	139	82		
	V_r av.	96.6	86.3	108.4	101.4		
	σ	11.3	10.8	16.4	18.9		
1977							
Jan	N	44	68	44	68		
	V_r av.	73.5	73.0	99.5	93.0		
	σ	15.3	14.3	22.9	21.0		
Apr	N	50	127	50	127		
	V_r av.	65.7	65.5	72.4	72.4		
	σ	4.7	10.1	6.9	11.1		
Jul	N	114	110	114	110		
	V_r av.	73.6	72.5	87.7	86.3		
	σ	6.9	5.8	9.0	7.0		
Oct	N	101	89	100	89		
	V_r av.	77.1	73.7	90.9	88.0		
	σ	7.2	80	7.5	10.9		
1978							
Jan	N	38	65	38	65		
	V_r av.	61.1	54.7	72.9	65.2		
	σ	12.4	7.4	15.9	7.8		
Apr	N	47	128	47	125	24	108
	V_r av.	67.8	64.0	80.9	75.8	89.8	84.6
	σ	4.9	9.2	7.5	14.5	5.0	16.4
Jul	N	82	138	80	139	85	130
	V_r av.	72.2	72.1	89.2	87.7	101.2	104.8
	σ	4.1	8.1	5.4	10.1	6.3	15.3
Oct	N					93	98
	V_r av.					130.3	105.2
	σ					23.1	10.9
1979							
Jan	N	70	97	70	96	91	99
	V_r av.	67.8	67.0	80.4	77.9	126.9	142.8
	σ	12.1	12.7	14.6	14.0	34.8	39.4

[1]Sky behind target

[2]Clouds behind target

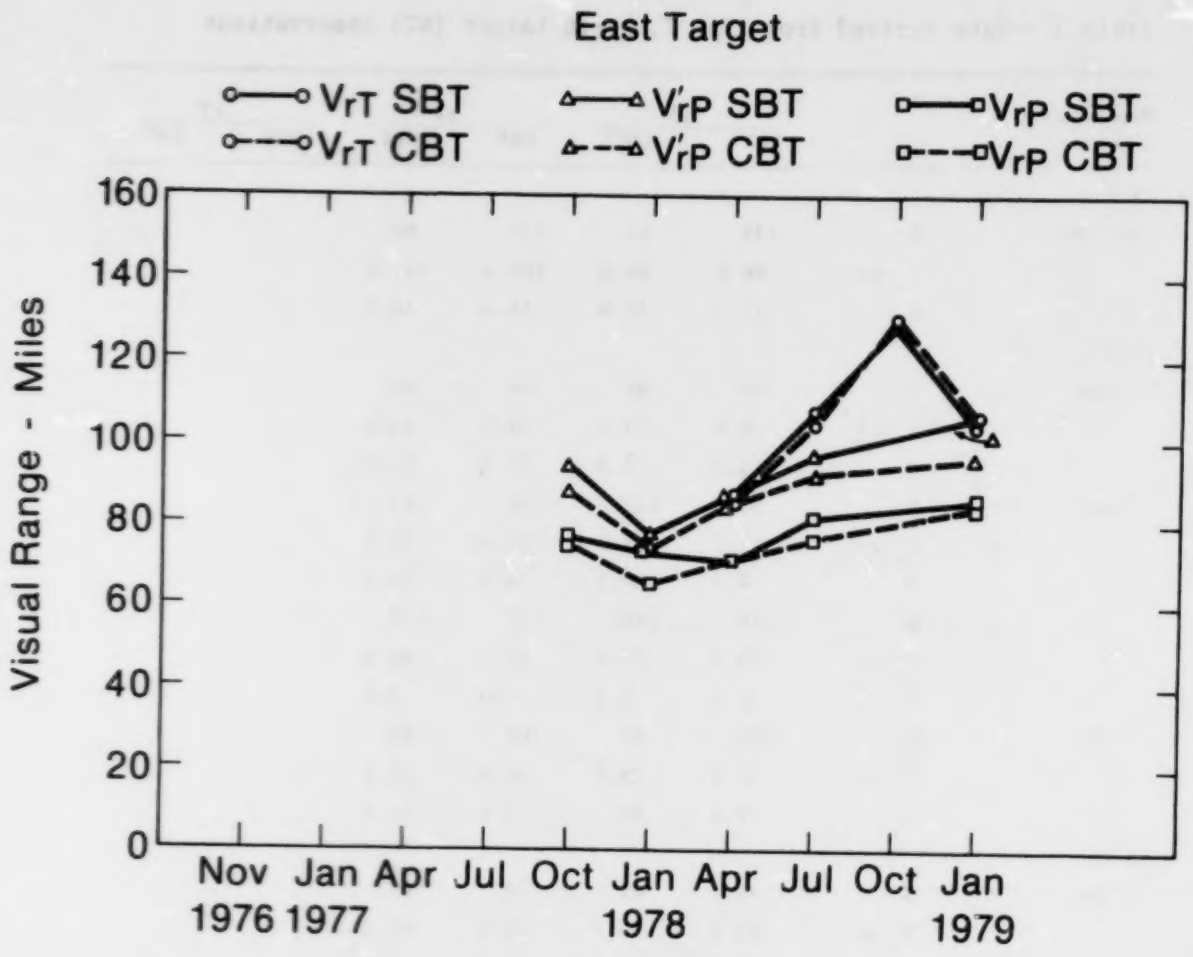

Figure 8.--Average monthly visual range for east target, as in fig. 7.

Table 4.--Data derived from fig. 8, east target (ET) observations

Observation period		V_{rP}		V'_{rP}		V_{rT}	
		SBT[1]	CBT[2]	SBT	CBT	SBT	CBT
1976							
Nov-Dec	N						
	V_r av.						
	σ						
1977							
Jan	N						
	V_r av.						
	σ						
Apr-May	N						
	V_r av.						
	σ						
Jul-Aug	N						
	V_r av.						
	σ						
Oct-Nov	N	105	67	105	67		
	V_r av.	76.5	74.7	93.4	87.7		
	σ	6.2	11.2	13.4	14.9		
1978							
Jan-Feb	N	31	70	31	66		
	V_r av.	73.3	65.2	77.3	73.6		
	σ	5.9	9.0	7.9	12.9		
Apr-May	N	56	129	56	129	31	108
	V_r av.	71.1	71.3	86.5	84.3	87.4	85.4
	σ	8.5	9.1	14.3	14.8	7.0	16.8
Jul-Aug	N	122	99	121	99	123	95
	V_r av.	81.5	76.2	96.7	92.6	106.9	104.2
	σ	4.9	8.9	10.0	11.9	10.0	12.2
Oct-Nov	N					94	96
	V_r av.					128.0	129.7
	σ					11.3	15.5
1979							
Jan-Mar	N	67	87	62	92	86	108
	V_r av.	85.4	84.5	106.4	95.7	103.8	105.5
	σ	11.3	15.5	12.6	16.0	29.7	32.3

[1]Sky behind target

[2]Clouds behind target

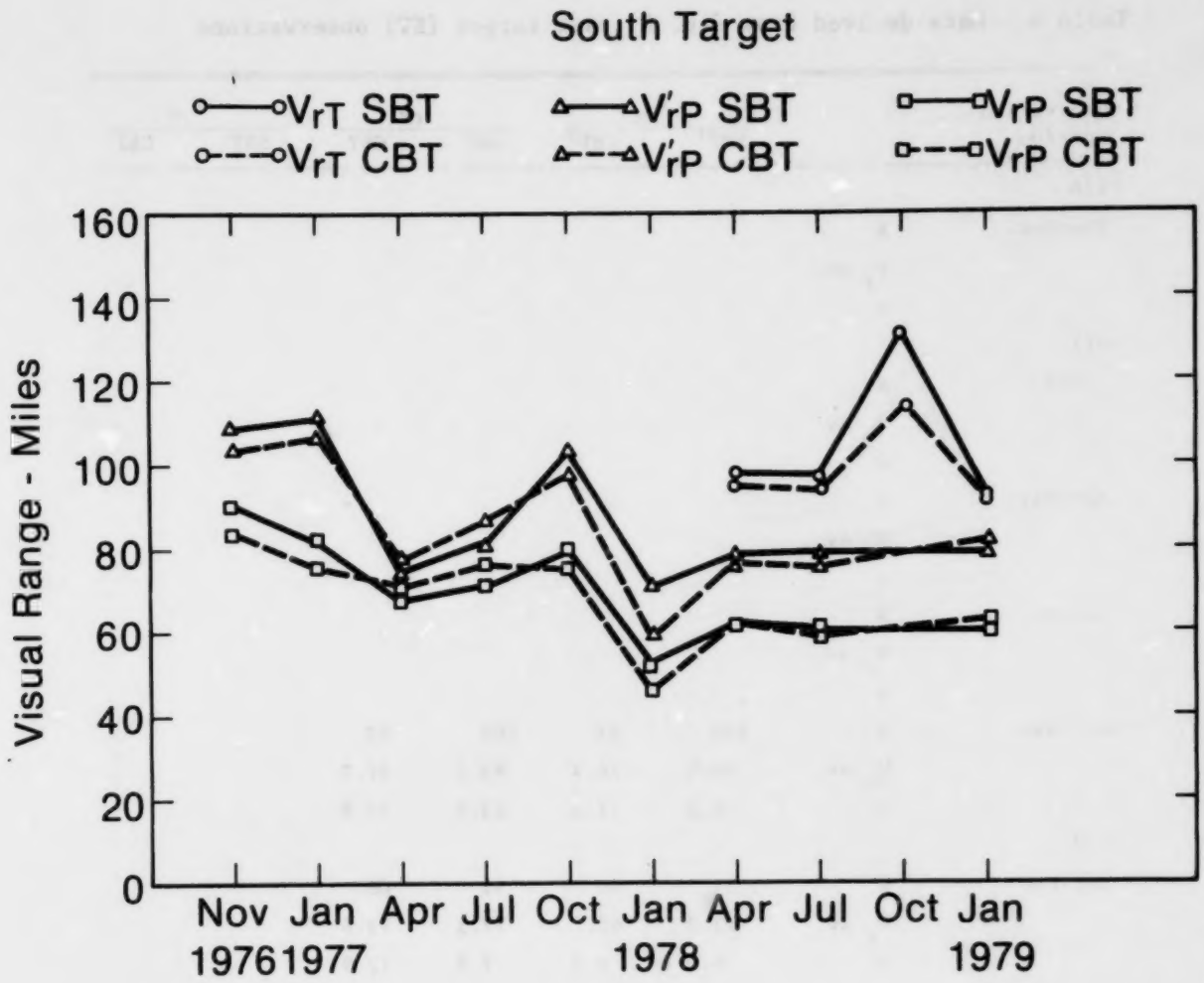

Figure 9.--Average monthly visual range for south target, as in fig. 7.

Table 5.--Data derived from fig. 9, south target (ST) observations

Observation period		V_{rP}		V'_{rP}		V_{rT}	
		SBT[1]	CBT[2]	SBT	CBT	SBT	CBT
1976							
Nov-Dec	N	158	70	158	70		
	V_r av.	90.2	83.9	108.4	103.5		
	σ	10.6	12.3	17.9	17.3		
1977							
Jan	N	56	57	56	57		
	V_r av.	81.8	75.6	111.8	106.6		
	σ	13.3	7.6	12.8	12.6		
Apr-May	N	58	124	58	48.1		
	V_r av.	67.6	71.1	74.2	76.9		
	σ	4.2	6.2	6.1	7.9		
Jul-Aug	N	164	62	164	62		
	V_r av.	71.1	76.4	81.4	86.7		
	σ	7.0	5.5	8.9	6.4		
Oct-Nov	N	139	61	140	61		
	V_r av.	79.5	75.1	103.1	97.1		
	σ	6.7	10.9	13.1	12.2		
1978							
Jan-Feb	N	27	75	27	73		
	V_r av.	52.4	46.2	71.0	58.5		
	σ	6.9	7.6	5.3	10.1		
Apr-May	N	71	112	72	112	47	90
	V_r av.	61.5	62.0	78.1	76.7	98.0	94.9
	σ	9.2	8.0	8.6	10.1	16.0	11.4
Jul-Aug	N	129	88	129	88	117	97
	V_r av.	60.5	59.3	78.5	75.7	97.3	93.8
	σ	3.9	8.2	6.5	11.1	8.6	15.8
Oct-Nov	N					96	98
	V_r av.					131.1	113.8
	σ					12.0	21.9
1979							
Jan-Mar	N	70	111	68	109	103	99
	V_r av.	60.2	61.5	78.8	80.9	92.2	91.6
	σ	7.3	12.6	12.7	10.6	11.6	14.6

[1]Sky behind target

[2]Clouds behind target

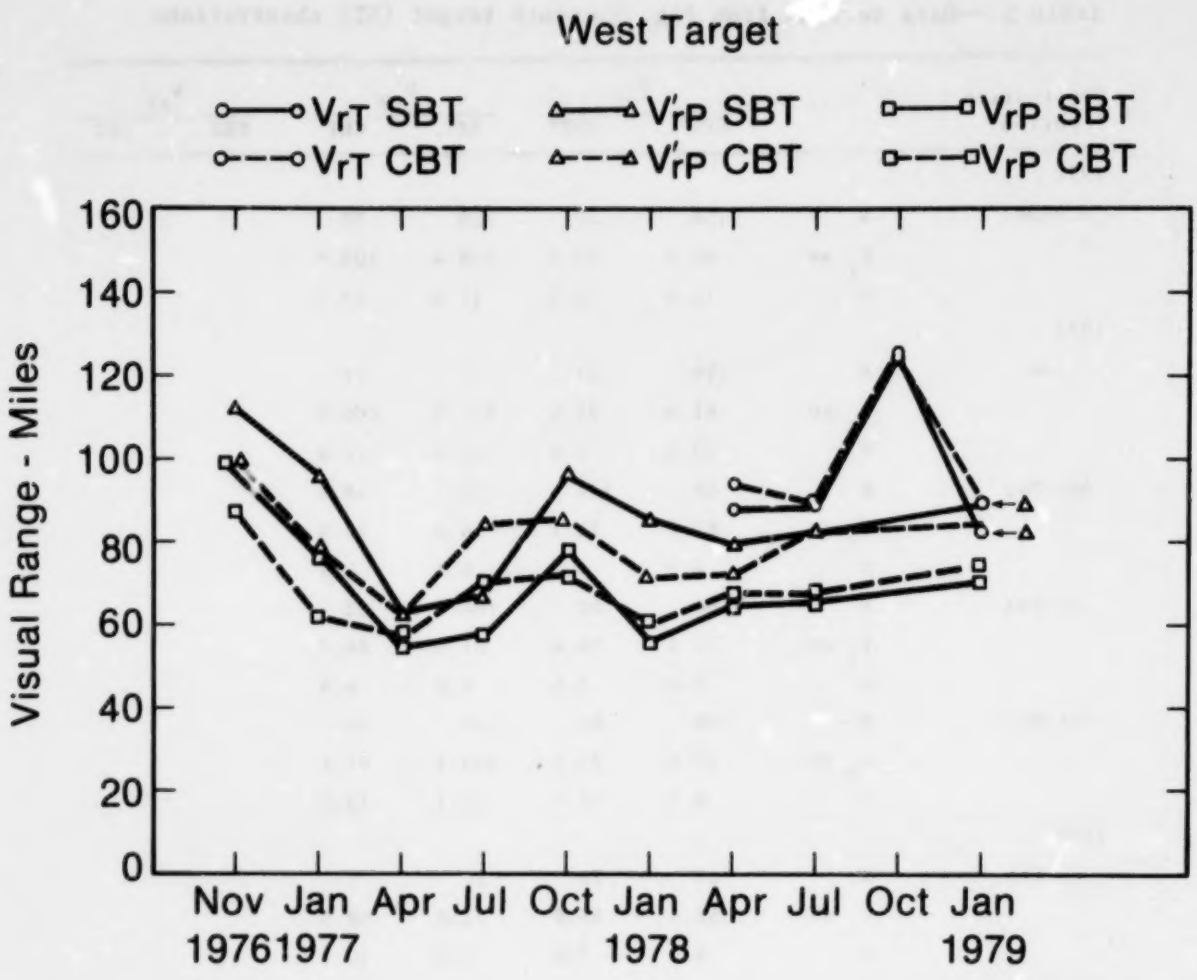

Figure 10.--Average monthly visual range for west target, as in fig. 7.

Table 6.--Data derived from fig. 10, west target (WT) observations

Observation period		V_{rP}		V'_{rP}		V_{rT}	
		SBT[1]	CBT[2]	SBT	CBT	SBT	CBT
1976							
Nov-Dec	N	138	89	137	89		
	V_r av.	98.5	86.9	112.1	99.4		
	σ	11.0	11.2	21.5	12.8		
1977							
Jan	N	64	35	64	36		
	V_r av.	76.8	61.7	95.6	78.0		
	σ	12.9	11.9	16.7	20.0		
Apr-May	N	50	124	50	124		
	V_r av.	54.6	56.2	62.4	62.6		
	σ	5.6	8.4	8.8	9.4		
Jul-Aug	N	164	54	164	54		
	V_r av.	58.1	69.9	67.9	84.0		
	σ	7.9	10.1	11.1	12.9		
Oct-Nov	N	126	62	126	62		
	V_r av.	78	71.5	96.2	85.7		
	σ	5.9	8.4	13.4	10.5		
1978							
Jan-Feb	N	12	88	12	91		
	V_r av.	55.9	60.2	85.6	71.1		
	σ	15.0	8.2	22.4	13.1		
Apr-May	N	48	126	48	126	20	104
	V_r av.	64.4	67.4	79.2	72.3	87.6	93.8
	σ	5.1	10.2	8.0	12.7	13.7	16.3
Jul-Aug	N	99	116	99	116	109	101
	V_r av.	65.9	67.4	82.8	83.2	88.4	88.9
	σ	5.3	12.1	10.3	15.3	13.0	14.5
Oct-Nov	N					102.0	72
	V_r av.					124.7	125.0
	σ					10.0	18.3
1979							
Jan-Mar	N	27	145	27	142	47	135
	V_r av.	74.4	70.0	89.5	85.7	82.5	89.6
	σ	8.4	11.0	11.0	16.6	27.3	31.2

[1]Sky behind target

[2]Clouds behind target

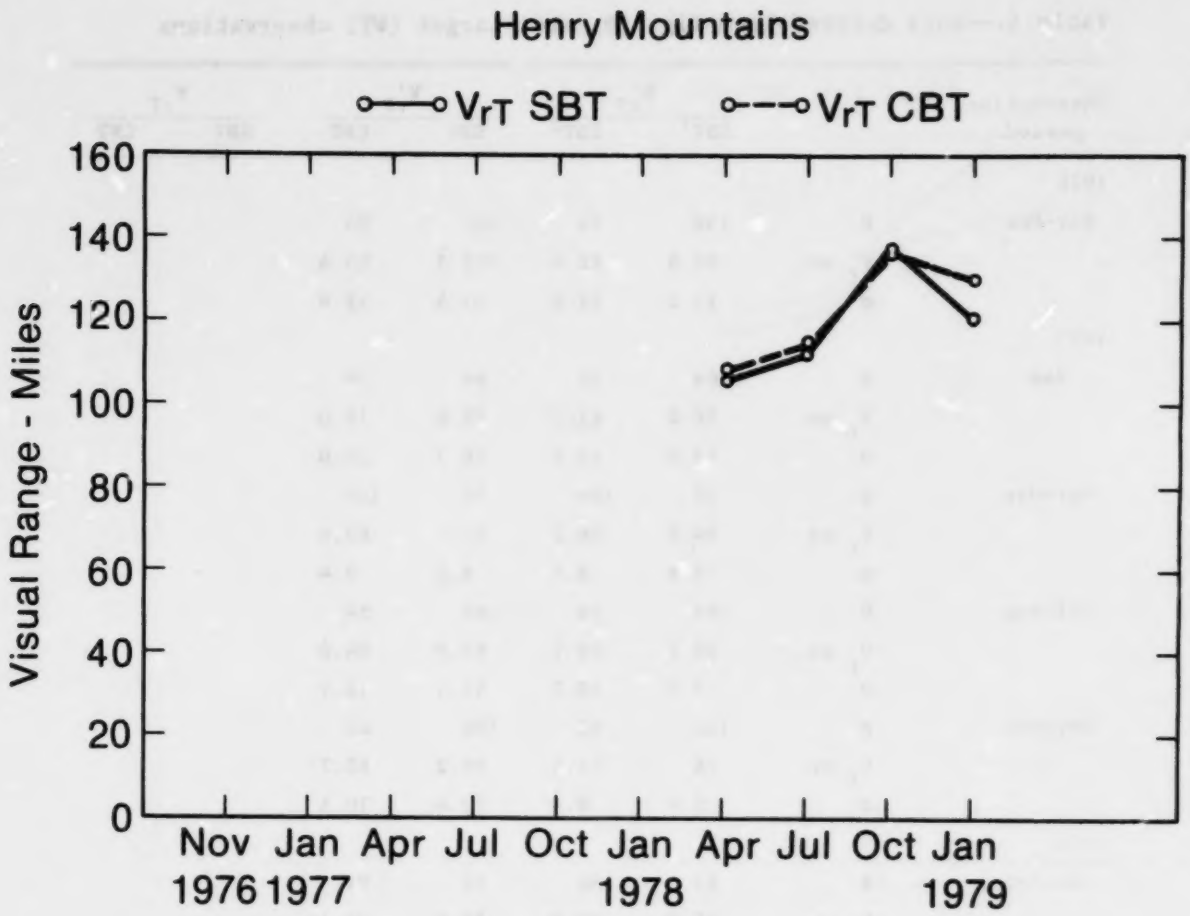

Figure 11.--Average monthly telephotometric visual range for Henry Mountains, as in fig. 7.

Table 7.--Data derived from fig. 11, Henry Mountains observations

Observation period		V_{rT} SBT[1]	V_{rT} CBT[2]
1976			
Nov-Dec	N		
	V_r av.		
	σ		
1977			
Jan	N		
	V_r av.		
	σ		
Apr-May	N		
	V_r av.		
	σ		
Jul-Aug	N		
	V_r av.		
	σ		
Oct-Nov	N		
	V_r av.		
	σ		
1978			
Jan-Feb	N		
	V_r av.		
	σ		
Apr-May	N	36	66
	V_r av.	105.5	108.0
	σ	11.2	8.0
Jul-Aug	N	109	103
	V_r av.	112.4	104.1
	σ	11.5	16.6
Oct-Nov	N	102	59
	V_r av.	137.7	136.3
	σ	10.3	21.9
1979			
Jan-Mar	N	83	97
	V_r av.	120.9	129.8
	σ	19.6	22.0

[1]Sky behind target

[2]Clouds behind target

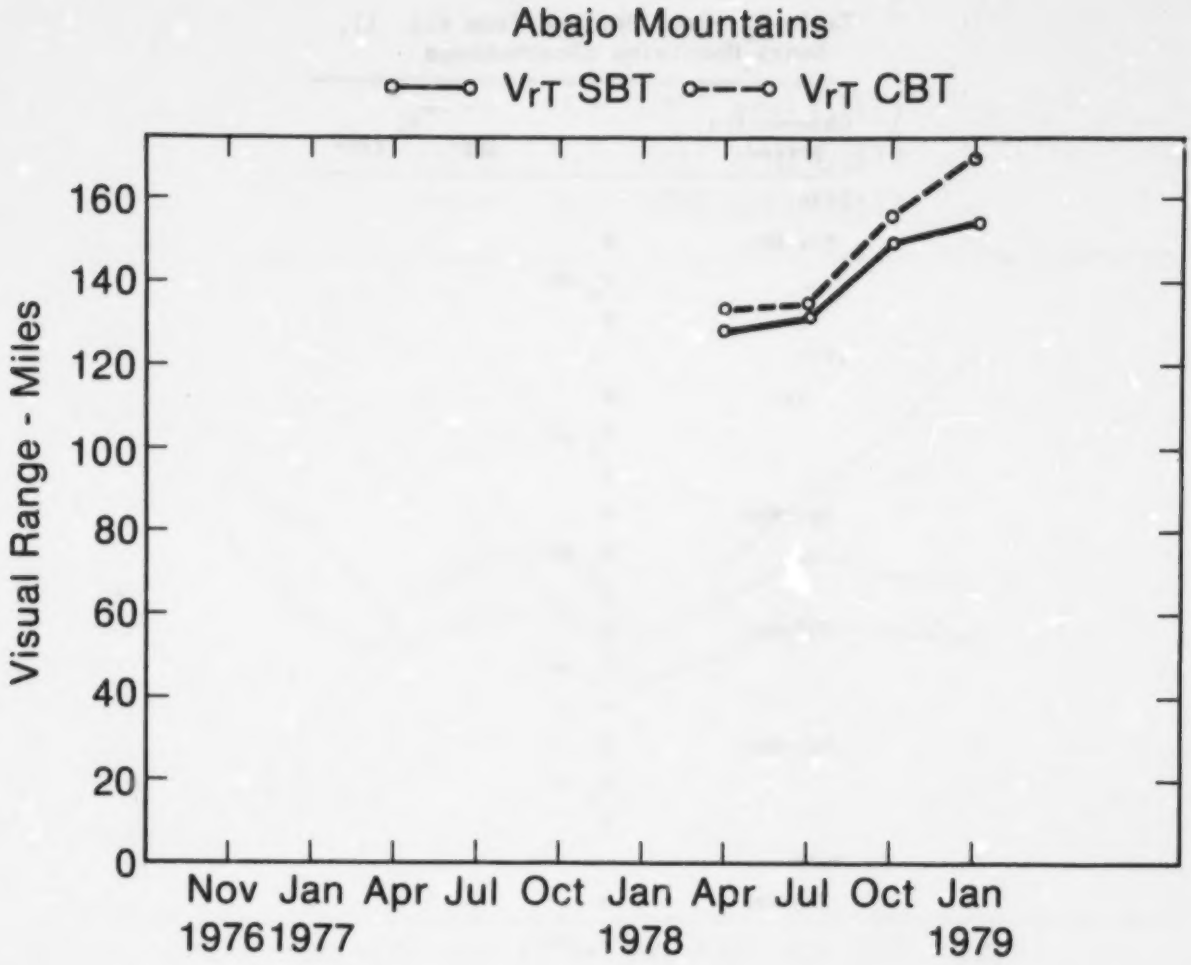

Figure 12.--Average monthly telephotometric visual range for Abajo Mountains, as in fig. 7.

Table 8.--Data derived from fig. 12, Abajo Mountains observations

Observation period		V_{rT} SBT[1]	V_{rT} CBT[2]
1976			
Nov-Dec	N		
	V_r av.		
	σ		
1977			
Jan	N		
	V_r av.		
	σ		
Apr-May	N		
	V_r av.		
	σ		
Jul-Aug	N		
	V_r av.		
	σ		
Oct-Nov	N		
	V_r av.		
	σ		
1978			
Jan-Feb	N		
	V_r av.		
	σ		
Apr-May	N	30	18
	V_r	128.1	133.4
	σ	13.5	8.5
Jul-Aug	N	125	57
	V_r av.	131.1	134.6
	σ	10.7	14.3
Oct-Nov	N	74	31
	V_r av.	149.1	155.2
	σ		
1979			
Jan-Mar	N	46	40
	V_r av.	153.7	169.5
	σ	13.4	15.0

[1]Sky behind target

[2]Clouds behind target

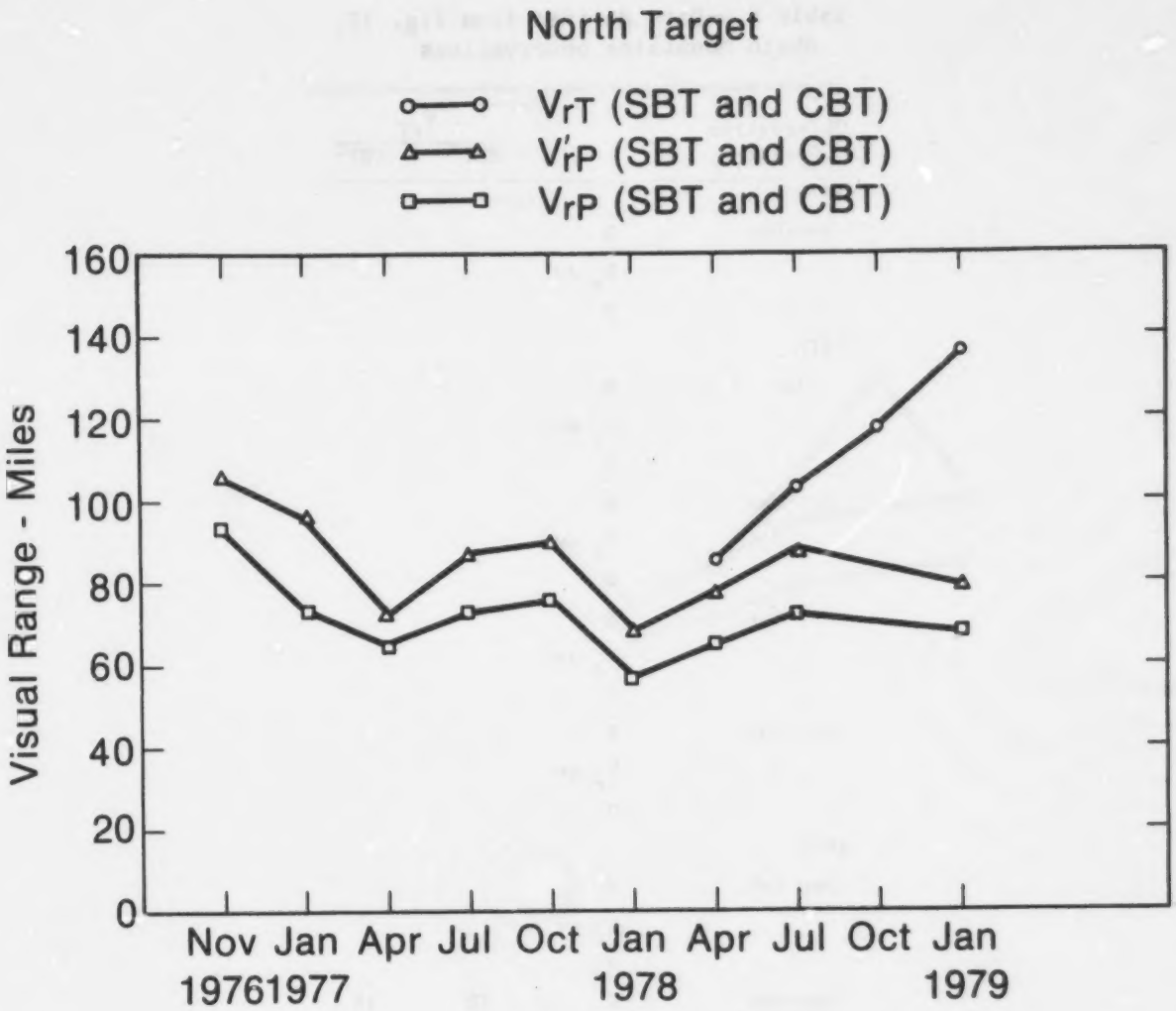

Figure 13.--Average monthly visual range for north target, combining data for clouds behind target(CBT) and sky behind target (SBT) conditions. V_{rT} = telephotometric visual range, V_{rP} = photographic visual range (Martin Marietta), V'_{rP} = photographic visual range (NOAA).

Table 9.--Data derived from fig. 13, north target (NT) observations

Observation period		V_{rP}	V'_{rP}	V_{rT}
1976				
Nov-Dec	N	222	221	
	V_r av.	92.7	105.8	
	σ	11.1	17.3	
1977				
Jan	N	112	112	
Jan	V_r av.	73.2	95.6	
	σ	14.6	21.7	
Apr-May	N	177	177	
	V_r av.	65.6	72.4	
	σ	8.9	10.1	
Jul-Aug	N	224	224	
	V_r av.	73.1	87.0	
	σ	6.4	8.1	
Oct-Nov	N	190	189	
	V_r av.	75.5	89.5	
	σ	7.6	9.2	
1978				
Jan-Feb	N	103	103	
	V_r av.	57.1	68.0	
	σ	9.5	11.4	
Apr-May	N	175	172	132
	V_r av.	65.0	77.2	85.5
	σ	8.3	12.9	15.0
Jul-Aug	N	220	219	215
	V_r av.	72.1	88.2	103.4
	σ	6.9	8.7	12.5
Oct-Nov	N			191
	V_r av.			117.4
	σ			30.2
1979				
Jan-Mar	N	167	166	190
	V_r av.	67.8	79.0	135.2
	σ	12.1	14.2	37.2

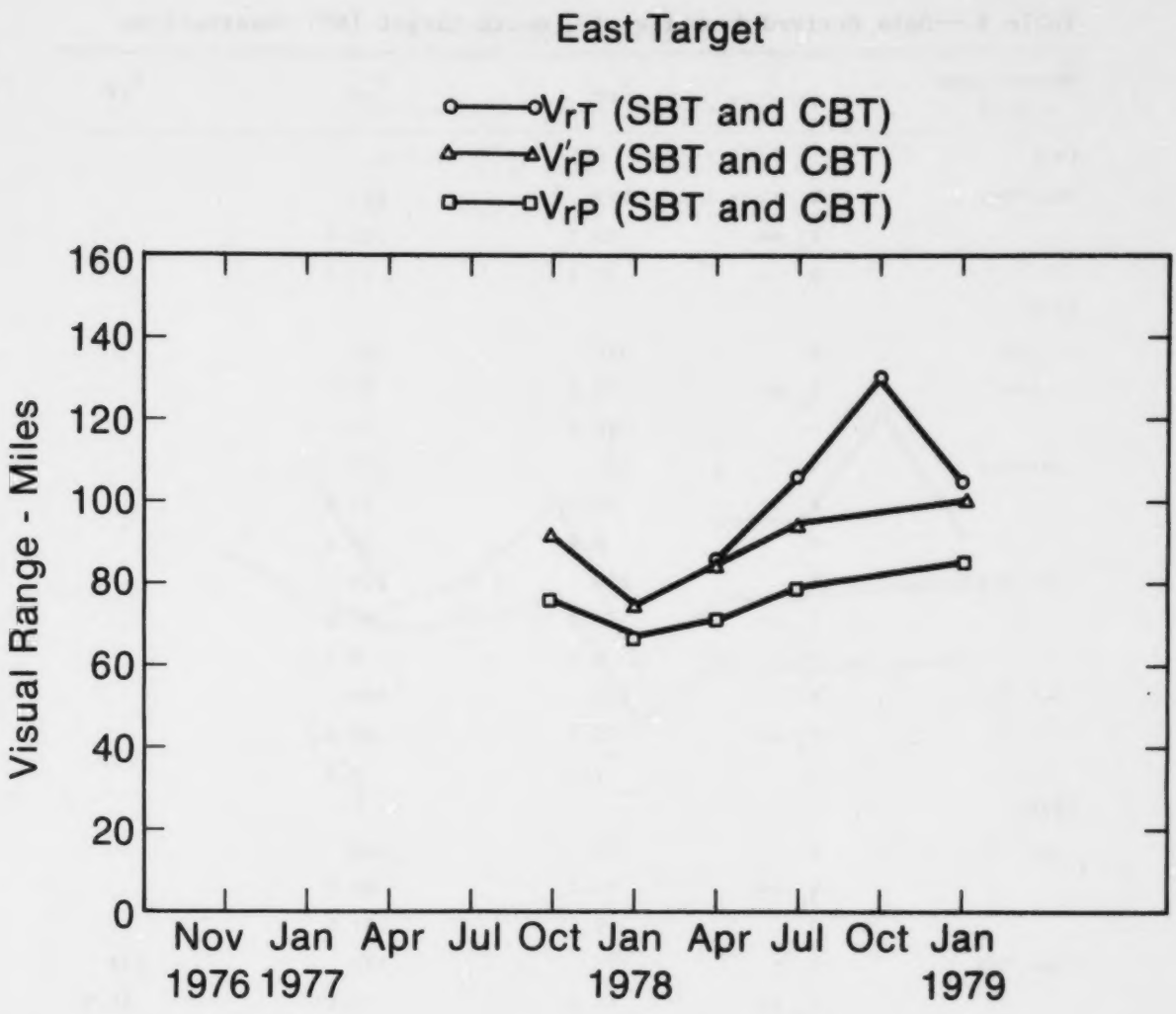

Figure 14.--Average monthly visual range for east target, as in fig. 13.

Table 10.--Data derived from fig. 14, east target (ET) observations

Observation period		V_{rP}	V'_{rP}	V_{rT}
1976				
Nov-Dec	N			
	V_r			
	σ			
1977				
Jan	N			
	V_r av.			
	σ			
Apr-May	N			
	V_r av.			
	σ			
Jul-Aug	N			
	V_r av.			
	σ			
Oct-Nov	N	172	172	
	V_r av.	75.8	91.2	
	σ	8.5	14.0	
1978				
Jan-Feb	N	101	97	
	V_r av.	67.7	74.8	
	σ	8.1	11.5	
Apr-May	N	185	185	139
	V_r av.	71.2	85.0	85.8
	σ	8.9	14.6	15.1
Jul-Aug	N	221	220	218
	V_r av.	79.1	94.9	105.7
	σ	7.0	10.9	11.0
Oct-Nov	N			190
	V_r av.			117.3
	σ			26.4
1979				
Jan-Mar	N	154	154	194
	V_r av.	84.9	100.0	104.7
	σ	13.8	14.7	31.1

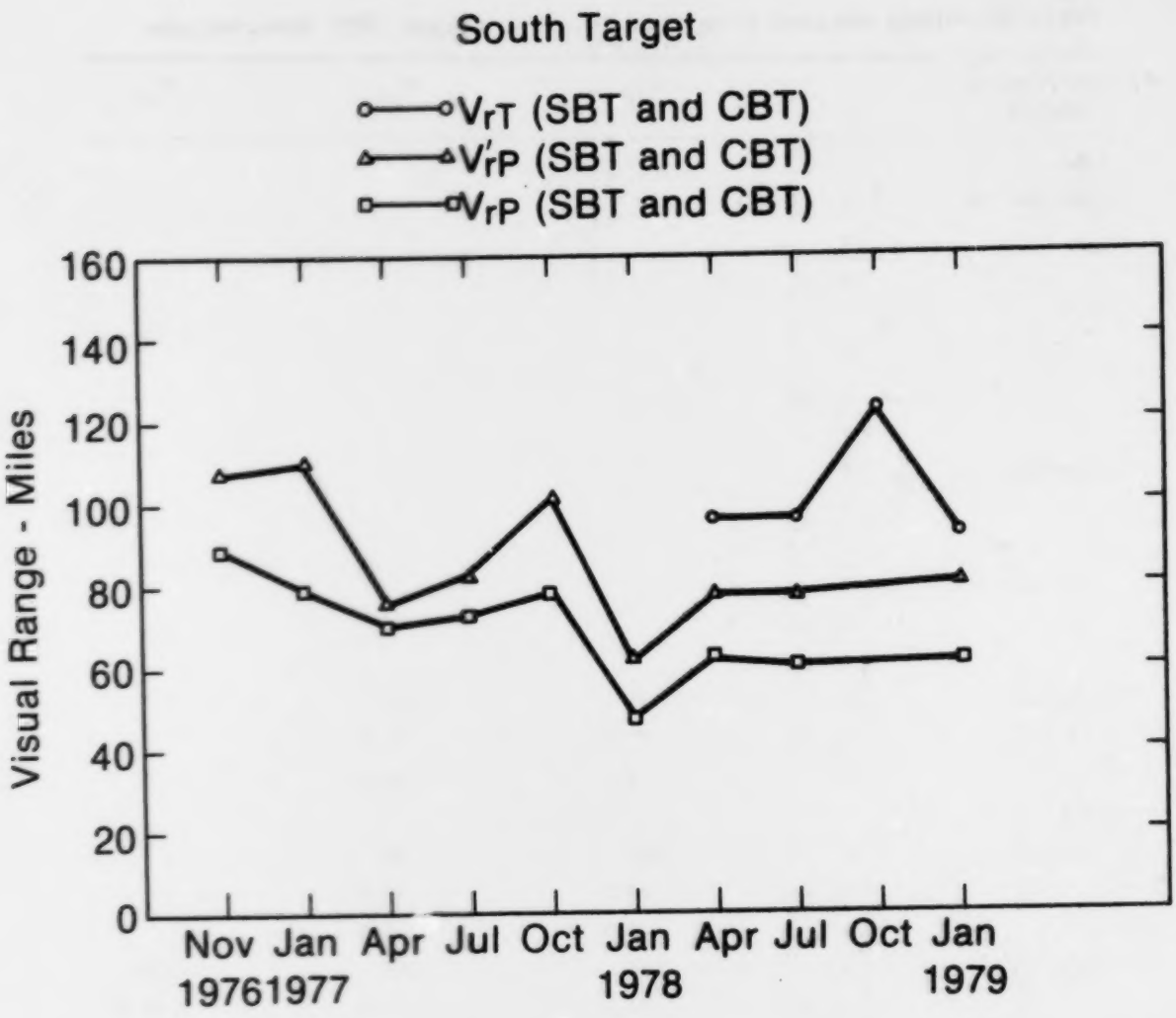

Figure 15.--Average monthly visual range for south target, as in fig. 13.

Table 11.--Data derived from fig. 15, south target (ST) observations

Observation period		V_{rP}	V'_{rP}	V_{rT}
1976				
Nov-Dec	N	228	228	
	V_r av.	88.3	106.9	
	σ	11.1	17.7	
1977				
Jan	N	113	113	
	V_r av.	78.7	109.2	
	σ	10.8	12.6	
Apr-May	N	182	106	
	V_r av.	70.0	75.4	
	σ	5.6	6.9	
Jul-Aug	N	226	226	
	V_r av.	72.6	82.9	
	σ	6.6	8.3	
Oct-Nov	N	200	201	
	V_r av.	78.2	101.3	
	σ	8.2	12.8	
1978				
Jan-Feb	N	102	100	
	V_r av.	47.8	61.9	
	σ	7.4	9.0	
Apr-May	N	183	184	137
	V_r av.	61.8	77.2	96.0
	σ	8.5	9.5	13.1
Jul-Aug	N	217	217	214
	V_r av.	60.0	77.4	95.7
	σ	6.0	8.6	12.4
Oct-Nov	N			194
	V_r av.			122.5
	σ			29.4
1979				
Jan-Mar	N	181	177	202
	V_r av.	61.0	80.1	91.9
	σ	10.8	11.4	13.1

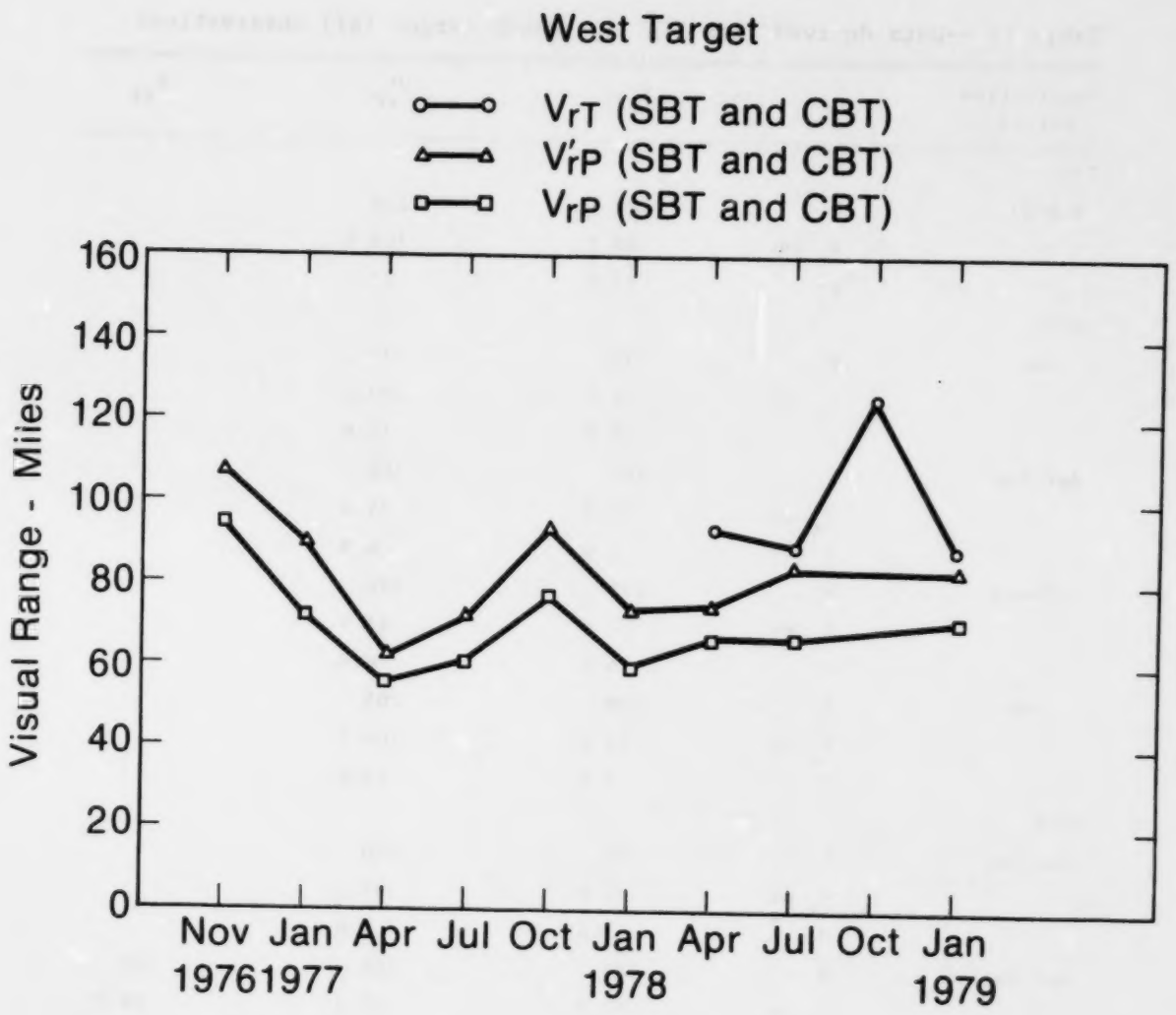

Figure 16.--Average monthly visual range for west target, as in fig. 13.

Table 12.--Data derived from fig. 16, west target (WT) observations

Observation period		V_{rP}	V'_{rP}	V_{rT}
1976				
Nov-Dec	N	227	226	
	V_r av.	94.0	107.1	
	σ	11.1	18.5	
1977				
Jan	N	99	100	
	V_r av.	71.5	89.3	
	σ	12.5	17.9	
Apr-May	N	174	174	
	V_r av.	55.7	62.5	
	σ	7.7	9.2	
Jul-Aug	N	218	218	
	V_r av.	61.0	71.9	
	σ	8.5	11.5	
Oct-Nov	N	188	188	
	V_r av.	75.9	92.7	
	σ	6.8	12.5	
1978				
Jan-Feb	N	100	103	
	V_r av.	59.7	72.8	
	σ	9.2	143	
Apr-May	N	174	174	124
	V_r av.	66.6	74.2	92.8
	σ	9.1	11.6	15.9
Jul-Aug	N	215	215	210
	V_r av.	66.7	83.0	88.6
	σ	9.6	13.2	13.7
Oct-Nov	N			174
	V_r av.			124.8
	σ			28.9
1979				
Jan-Mar	N	172	169	182
	V_r av.	70.7	82.7	87.8
	σ	10.6	15.0	30.2

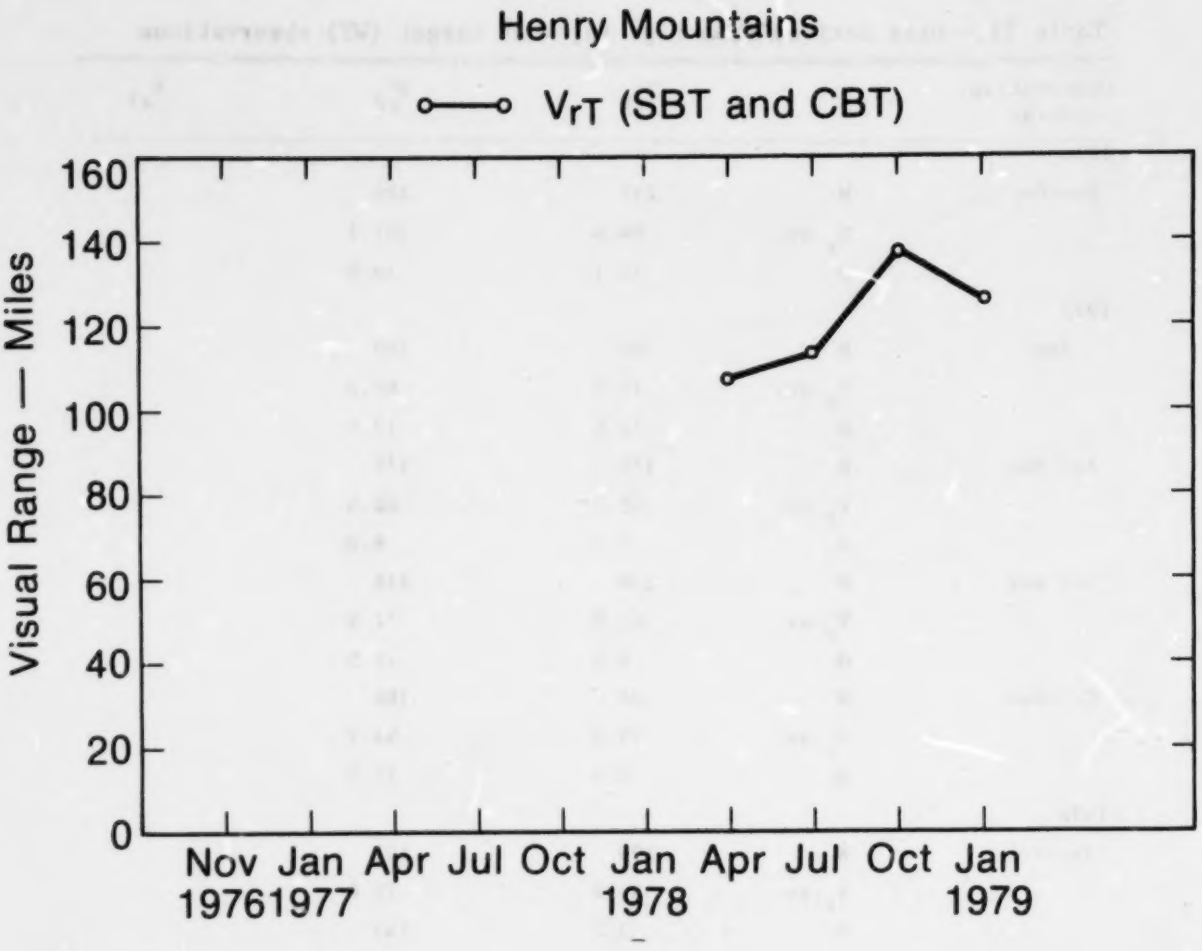

Figure 17.--Average monthly telephotometric visual range for Henry Mountains, as in fig. 13.

Table 13.--Data derived from fig. 17, Henry Mountains observations

Observation period		V_{rT}
1976		
Nov-Dec	N	
	V_r av.	
	σ	
1977		
Jan	N	
	V_r av.	
	σ	
Apr-May	N	
	V_r av.	
	σ	
Jul-Aug	N	
	V_r av.	
	σ	
Oct-Nov	N	
	V_r av.	
	σ	
1978		
Jan-Feb	N	
	V_r av.	
	σ	
Apr-May	N	102
	V_r	107.1
	σ	9.2
Jul-Aug	N	212
	V_r av.	113.2
	σ	14.2
Oct-Nov	N	161
	V_r av.	137.2
	σ	31.4
1979		
Jan-Mar	N	180
	V_r av.	125.7
	σ	20.9

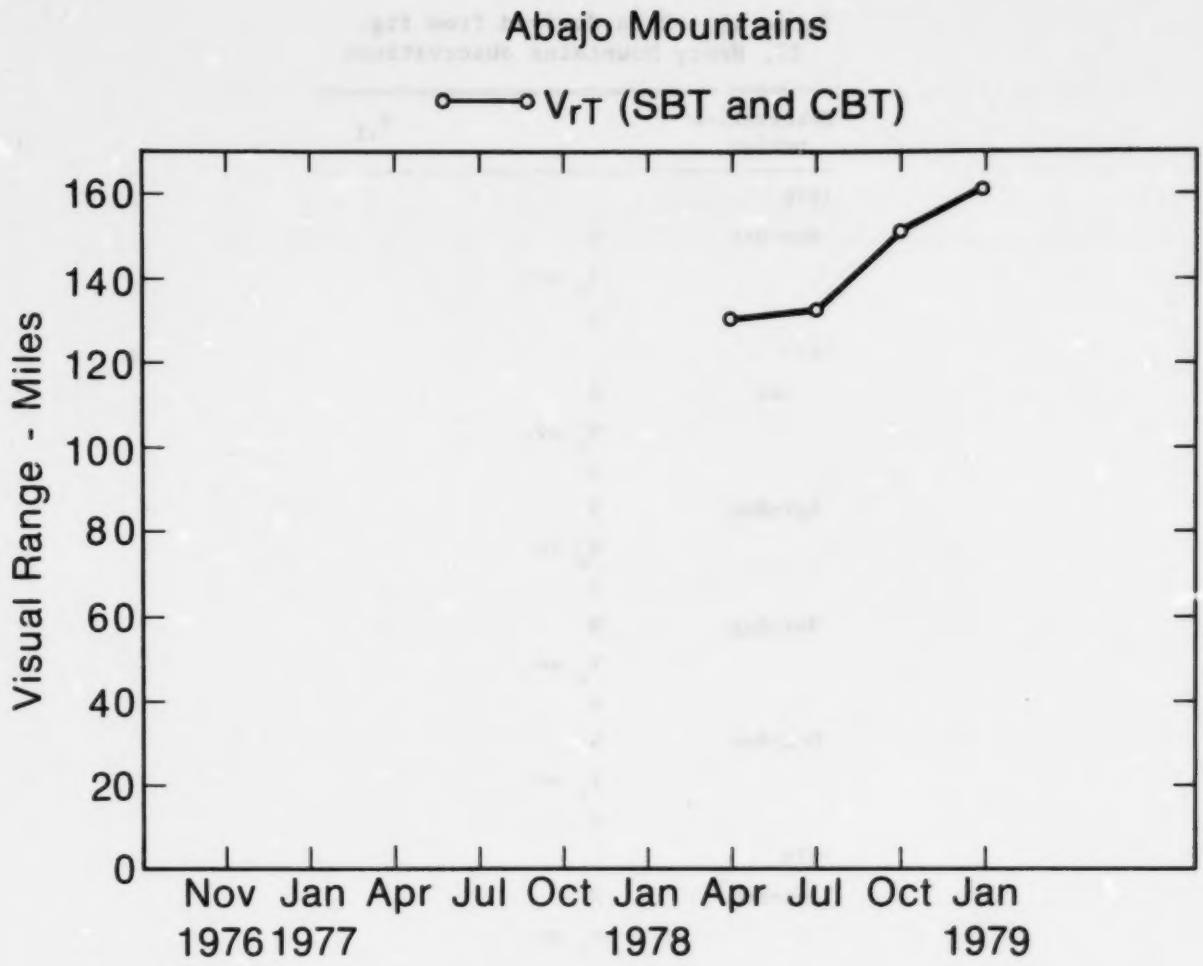

Figure 18.--Average monthly telephotometric visual range for Abajo Mountains, as in fig. 13.

Table 14.--Data derived from fig. 18, Abajo Mountains observations

Observation period		V_{rT}
1976		
Nov-Dec	N	
	V_r av.	
	σ	
1977		
Jan	N	
	V_r av.	
	σ	
Apr-May	N	
	V_r av.	
	σ	
Jul-Aug	N	
	V_r av.	
	σ	
Oct-Nov	N	
	V_r av.	
	σ	
1978		
Jan-Feb	N	
	V_r av.	
	σ	
Apr-May	N	48
	V_r av.	130.1
	σ	11.8
Jul-Aug	N	182
	V_r av.	132.4
	σ	12.1
Oct-Nov	N	105
	V_r av.	151.0
	σ	21.6
1979		
Jan-Mar	N	86
	V_r av.	161.0
	σ	14.1

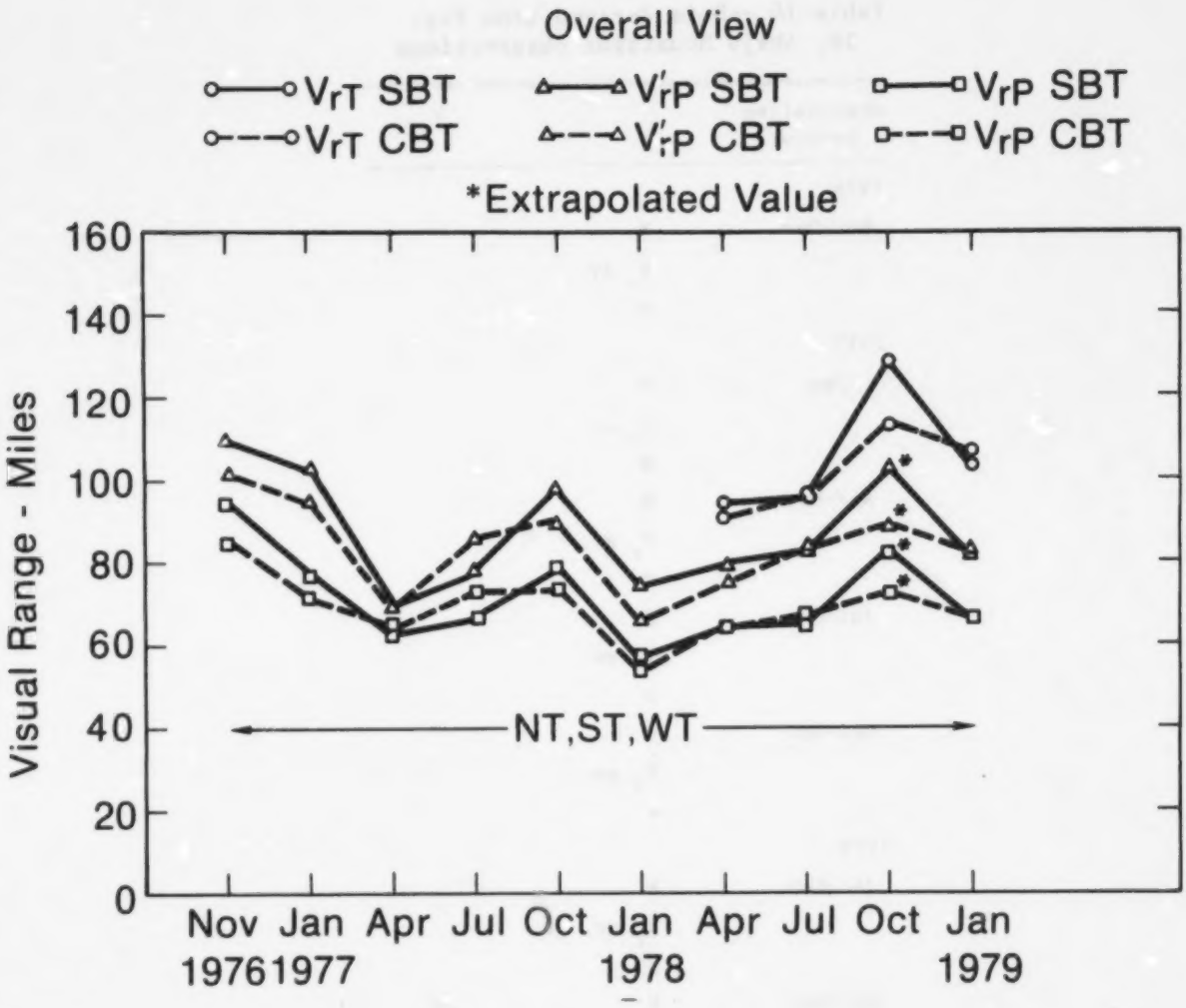

Figure 19.--Overall average monthly visual range for three targets with clouds behind target (CBT) and sky behind target (SBT). V_{rT} = telephotometric visual range, V_{rP} = photographic visual range (Martin Marietta), and V'_{rP} = photographic visual range (NOAA).

Table 15.--Data derived from fig. 19, NT, ST, and WT observations

Observation period and target		V_{rP} SBT[1]	V_{rP} CBT[2]	V'_{rP} SBT	V'_{rP} CBT	V_{rT} SBT	V_{rT} CBT
1976							
Nov-Dec	N	434	243	434	241		
	V_r av.	94.9	85.8	109.6	101.3		
	σ	10.9	11.3	186	16.3		
1977							
Jan	N	164	160	164	161		
	V_r av.	77.6	71.5	102.2	94.5		
	σ	13.6	11.7	17.4	18.1		
Apr-May	N	158	375	158	375		
	V_r av.	62.9	64.3	69.9	71.4		
	σ	4.8	8.4	7.2	9.4		
Jul-Aug	N	442	226	442	226		
	V_r av.	66.9	72.9	78.0	85.9		
	σ	7.3	7.0	9.8	8.6		
Oct-Nov	N	366	212	366	212		
	V_r av.	78.3	73.5	97.4	89.9		
	σ	6.6	9.0	11.9	11.1		
1978							
Jan-Feb	N	77	228	77	229		
	V_r av.	57.2	54.0	74.2	65.4		
	σ	11.1	7.7	14.3	10.8		
Apr-May	N	166	366	167	363	91	302
	V_r av.	64.1	64.6	79.2	74.9	93.6	90.8
	σ	7.1	9.2	8.1	12.6	13.3	15.0
Jul-Aug	N	310	342	308	343	311	328
	V_r av.	65.3	67.2	82.7	83.1	95.2	96.7
	σ	4.4	9.6	7.7	12.3	9.9	15.0
Oct-Nov	N					291	268
	V_r av.	69.0*	67.8*	102.3*	89.3*	128.6	113.7
	σ					15.9	17.5
1979							
Jan-Mar	N	167	353	165	347	241	333
	V_r av.	65.7	66.5	81.2	82.0	103.4	106.0
	σ	9.7	12.0	13.2	14.2	25.6	20.2

[1]Sky behind target

[2]Clouds behind target

*Extrapolated values

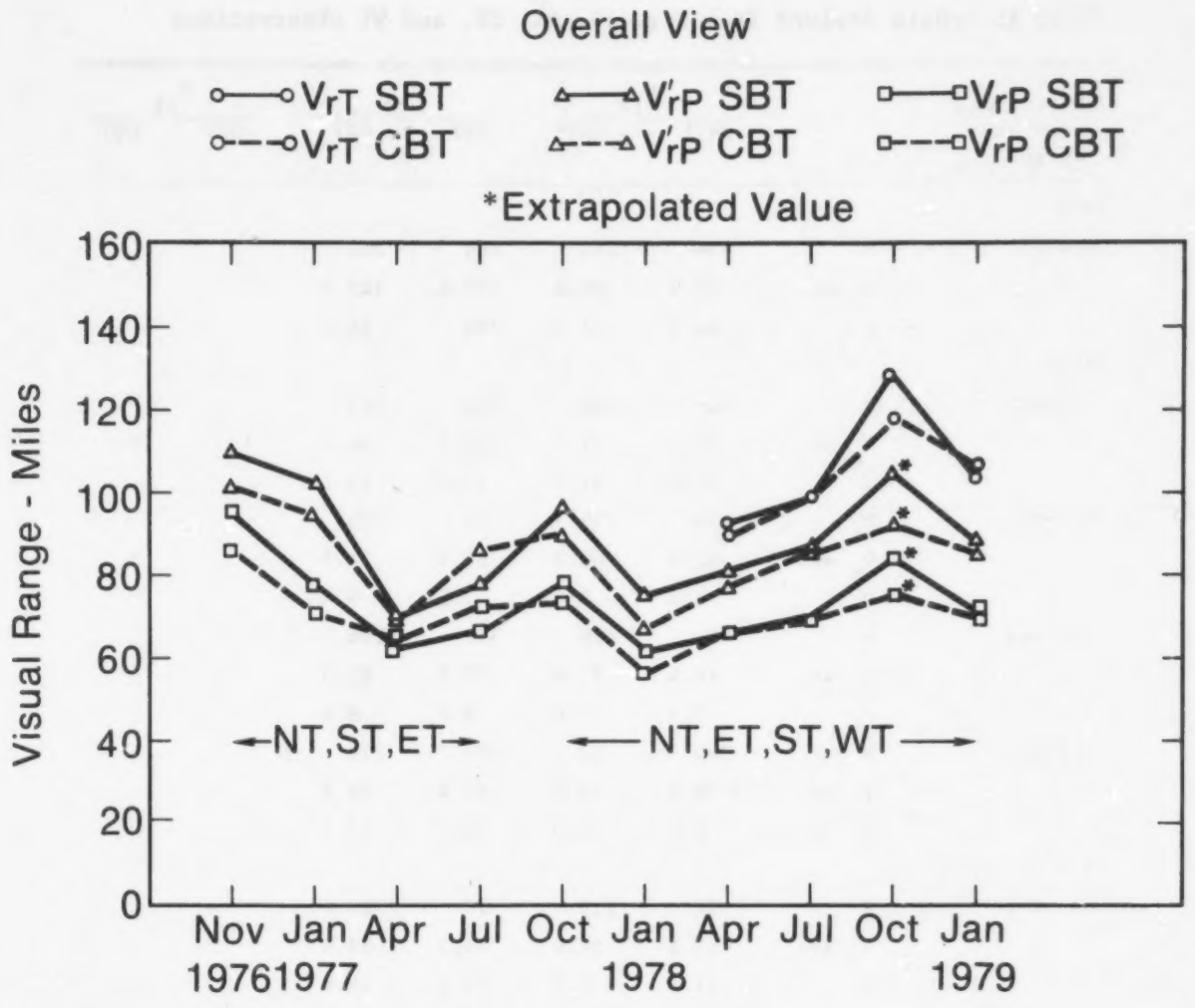

Figure 20.--Overall average monthly visual range for three targets, Nov. 1976 to Jul. 1977, and for four targets, Oct. 1977 to Jan. 1979.

Table 16.--Data derived from fig. 20

Observation period and target		V_{rP} SBT**	V_{rP} CBT**	V'_{rP} SBT	V'_{rP} CBT	V_{rT} SBT	V_{rT} CBT
1976							
Nov-Dec[1]	N	434	243	434	241		
	V_r av.	94.9	85.8	109.6	101.3		
	σ		11.3	18.6	16.3		
1977							
Jan[1]	N	164	160	164	161		
	V_r av.	77.6	71.5	102.2	94.5		
	σ	13.6	11.7	17.4	18.1		
Apr-May[1]	N	158	375	158	375		
	V_r av.	62.9	64.3	69.9	71.4		
	σ	4.8	8.4	7.2	9.4		
Jul-Aug[1]	N	442	226	442	226		
	V_r av.	66.9	72.9	78.0	85.9		
	σ	7.3	7.0	9.8	8.6		
Oct-Nov[2]	N	471	279	471	279		
	V_r av.	77.9	73.7	96.5	89.4		
	σ	6.5	9.5	12.2	12.1		
1978							
Jan-Feb[2]	N	108	298	108	295		
	V_r av.	61.8	56.7	75.1	67.2		
	σ	9.9	8.0	12.8	11.3		
Apr-May[2]	N	222	495	223	492	122	410
	V_r av.	65.9	66.3	81.0	77.4	92.0	89.4
	σ	7.4	9.2	10.0	13.2	12.0	15.5
Jul-Aug[2]	N	432	441	429	442	434	423
	V_r av.	69.9	69.2	86.6	85.2	98.5	98.3
	σ	4.6	9.5	8.4	12.2	9.9	14.4
Oct-Nov[2]	N					385	364
	V_r av.	83.6*	73.2*	104.4*	91.6*	128.5	117.9
	σ					14.9	15.4
1979							
Jan-Mar[2]	N	234	440	227	439	327	441
	V_r av.	71.3	70.1	88.1	84.9	103.5	105.9
	σ	10.2	12.7	13.0	14.6	26.7	25.4

[1]NT, ST, WT
[2]NT, ET, ST, WT

*Extrapolated values

**Sky behind target
Clouds behind target

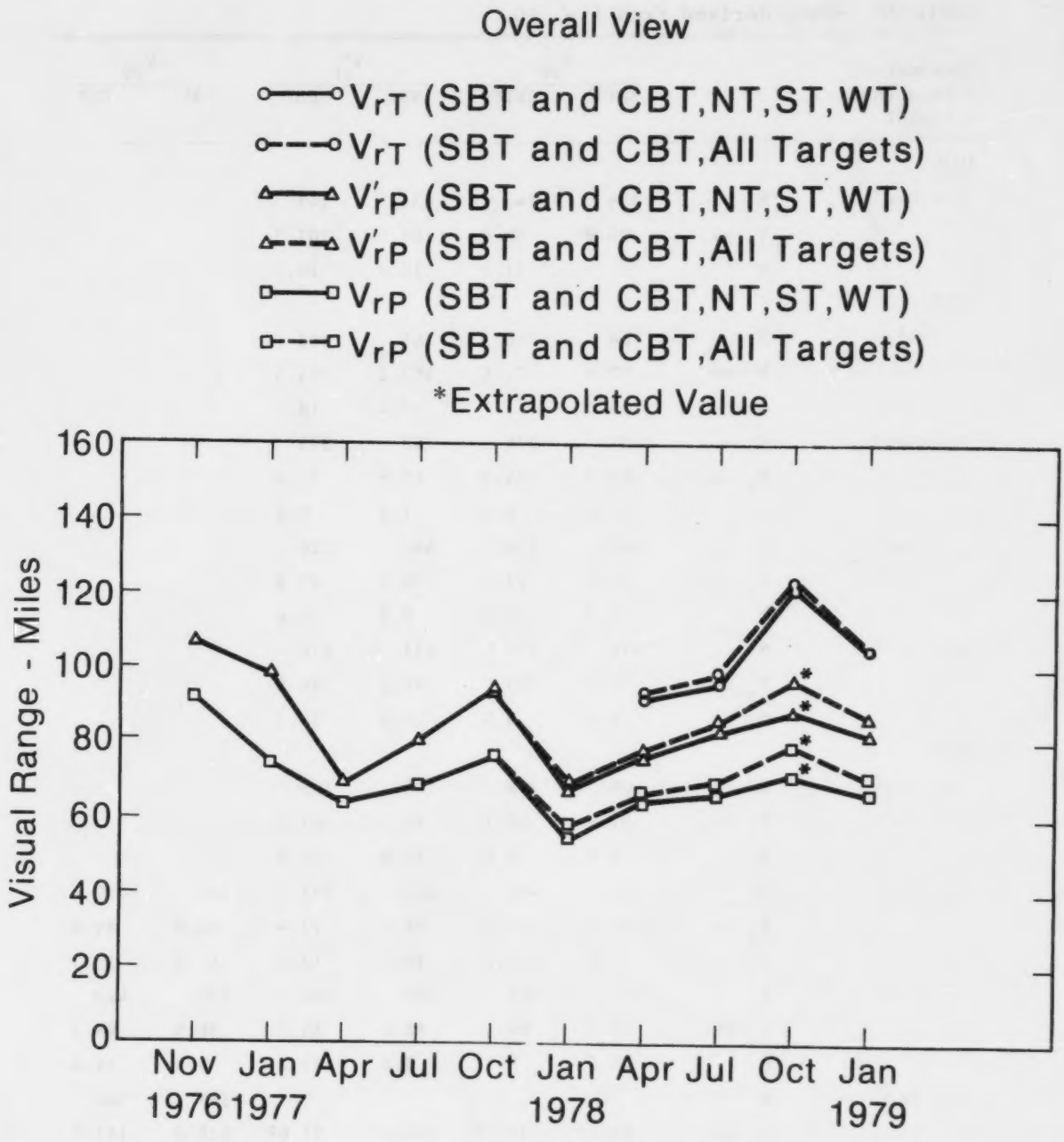

Figure 21.--Overall average monthly visual range, combining data for sky behind target and clouds behind target conditions.

Table 17.--Data derived from fig. 21

Observation period		V_{rP}		V'_{rP}		V_{rT}	
		NT, ST, WT	NT, ET ST, WT	NT ST, WT	NT, ET ST, WT	NT ST, WT	NT, ET ST, WT
1976							
Nov-Dec	N	677		675			
	V_r av.	91.6		106.6			
	σ	11.0		17.8			
1977							
Jan	N	324		325			
	V_r av.	74.6		98.4			
	σ	12.7		17.7			
Apr-May	N	533		533			
	V_r av.	63.9		71.0			
	σ	7.5		8.8			
Jul-Aug	N	668		668			
	V_r av.	68.9		80.7			
	σ	7.2		9.4			
Oct-Nov	N	578	750	578	750		
	V_r av.	76.5	76.3	94.6	93.9		
	σ	7.6	7.7	11.6	12.2		
1978							
Jan-Feb	N	305	406	306	403		
	V_r av.	54.8	58.1	67.6	69.3		
	σ	6.7	8.5	11.8	11.7		
Apr-May	N	532	717	530	715	393	532
	V_r av.	64.4	66.2	76.3	78.5	91.4	90.0
	σ	8.6	8.7	11.4	12.3	14.6	14.8
Jul-Aug	N	632	873	651	871	639	857
	V_r av.	66.3	69.5	82.9	85.9	96.0	98.4
	σ	7.6	7.5	10.4	10.5	12.8	12.3
Oct-Nov	N					559	749
	V_r av.	68.4*	76.2*	88.2*	96.8*	121.5	123.3
	σ					16.7	15.1
1979							
Jan-Mar	N	520	674	512	666	574	768
	V_r av.	66.2	70.5	81.7	86.0	104.9	104.9
	σ	11.3	11.9	13.9	14.1	28.3	25.9

*Extrapolated values

elements. This discussion will be limited to values of V'_{rP}, and considering only three targets, NT, ST, and WT, since these values are available from November 1976 through January 1979. No photographic method values of the visual range were obtained in October 1978. However, extrapolated values were obtained by fitting a linear regression curve to the V'_{rP} and V_{rT} values for April and July 1978 and January 1979, then calculating extrapolated values of V'_{rP} for October 1978.

In retrospect, the observation periods November and December 1976 and January 1977 were so climatologically unusual that they should not be considered in context with the other eight successive observation periods when considering "typical" weather conditions. The late fall of 1976 and the winter of 1976-77 were unusually dry; both the relative humidity (see Section 3.1.2) and snowfall were low. Rarely was the snowfall deep enough to prevent access to Cedar Mountain (unlike the "normal" winters of 1977-78 and 1978-79). There were many clear days, and with a pressure ridge (meteorological) to the west a much greater proportion of the winds aloft (as determined by pibal measurements) had a northerly component when compared with January 1978 and January 1979. (See Section 3.1.3.)

The mountain targets, from November 1976 through January 1977, were not covered by snow nearly as extensively or completely as during January 1978 and January 1979. Since the turbidity (see Section 2.2.4) increased during January 1978 and January 1979, it is probable that the decrease in visual range during this period is due to increased particulate loading. Conversely, when the sequences October 1977 to January 1978 and October 1978 to January 1979 are considered, on both the turbidity decreased and the visual range decreased. Since there were copious amounts of snowfall on the targets, it is probable that the decrease in visual range from October to January can be considered as being partly the result of decreased contrast between the target and sky due to snow on the target increasing the target albedo.

The effect is apparent in January 1979 since the visual range decreased from the October 1978 value, but the decrease is only 6 miles, compared with 27 miles from October 1977 to January 1978. Since turbidity decreased more for

the October 1977 to January 1978 interval than for the October 1978 to January 1979 interval, the effect of decrease in visual range during the January 1978 period is probably due to decreased contrast ratio between the sky and target rather than to a relative increase of particulates.

With the November 1976 to January 1977 data not being considered, a linear regression line fitted to the three targets' (NT, ST, WT) values of V'_{rP} gives a 10.4 percent increase in the visual range from April 1977 to January 1979. (V_{rP} gives a 1.2 percent increase for the same targets and time period.) It is apparent from inspection that from October 1977 to January 1979 that V'_{rP} for a four-target average increased more than for the three-target average. Also, V_{rT} has greater average values of visual range than V'_{rP} for reasons discussed by Allee and Lowery (1979).

In support of the visibility data, corollary measurements of the turbidity coefficients were made for several reasons. First, the history of turbidity measurements goes back further than that of visual range measurements. This is important for establishing trends. Second, sun photometer observations are adopted by the World Meteorological Organization as valid air quality measurements, which opens the possiblity of comparative programs on a worldwide basis. Third, a significant positive correlation will increase the visibility data base and make the results more conclusive because the turbidity is not affected by albedo and other changes.

Figure 22 shows the results of measurement of the observational period turbidity coefficients, B_λ, for λ = 380 nm; fig. 23 is the same information for λ = 500 nm. The value of B_{500} increased from November 1976 to January 1977, decreased from October 1977 to January 1978 and from October 1978 to January 1979. Figure 24 shows V'_{rP} decreased from November 1976 to January 1977, which is expected for an increase in the turbidity coefficient. However, V'_{rP} also decreased from October 1977 to January 1978 and October 1978 to January 1979 even though the turbidity coefficient decreased. The reason is that the snow-covered targets had a higher albedo that resulted in a decrease of contrast between the target and sky, and consequently decreased average visual range for the two January 1978 and 1979 observational periods, qven though the turbidity coefficient decreased.

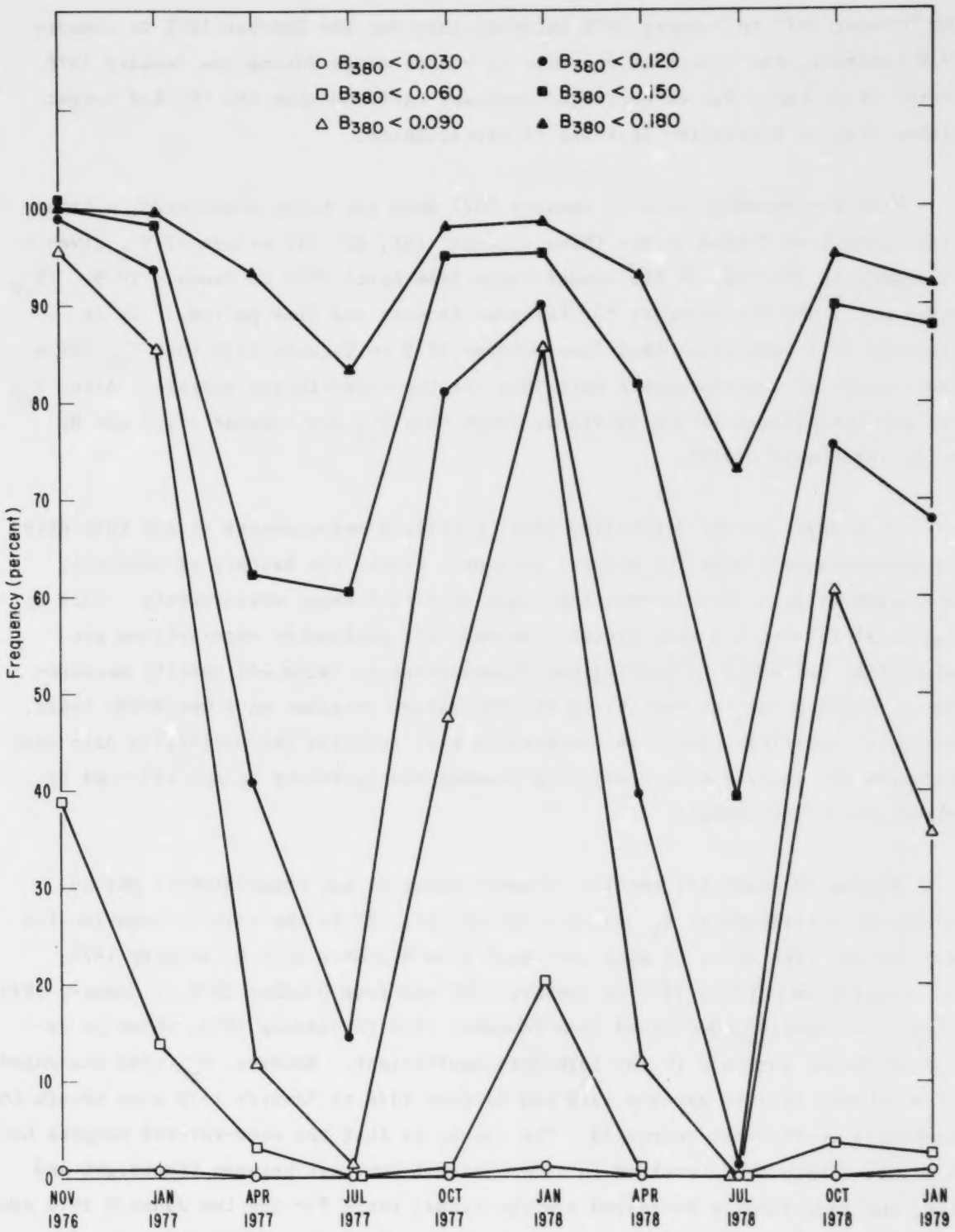

Figure 22.--Monthly average values of turbidity coefficient B_λ for λ = 380 nm (less than a specific threshold value). Low values of B_λ are associated with high visual range.

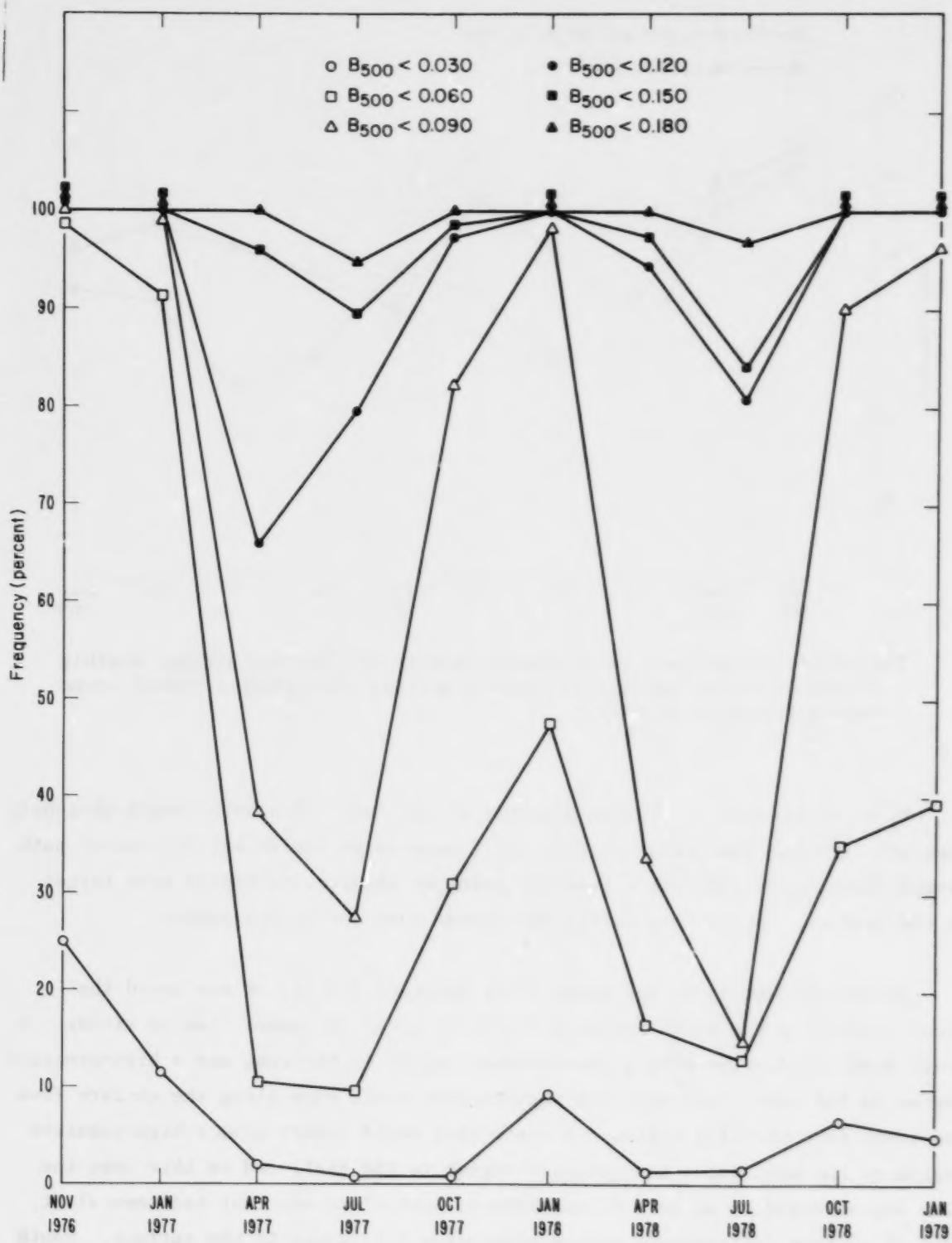

Figure 23.--Monthly average values of turbidity coefficient B_λ for λ = 500 nm (less than a specific threshold value). Low values of B_λ are associated with high visual range.

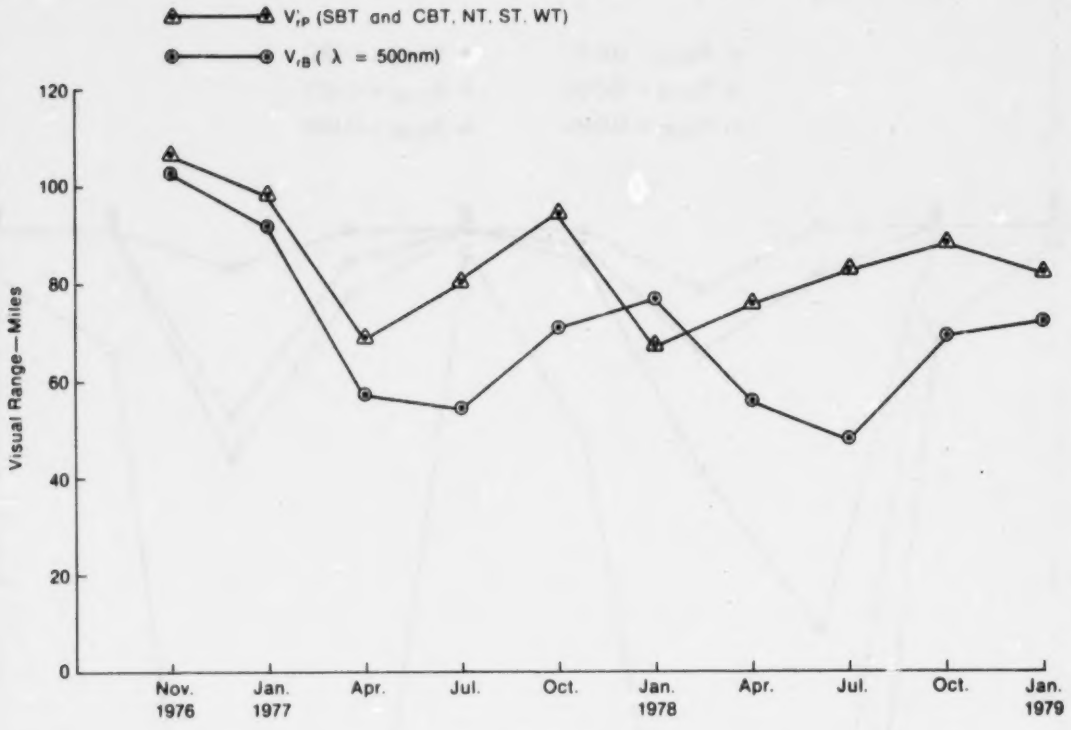

Figure 24.--Comparison of turbidity coefficient-derived average monthly values of visual range with overall monthly photographic visual range values for three targets.

B_λ is determined by looking directly at the Sun. This path length obviously does not have the same value that it would have on an equivalent horizontal path length through the atmosphere from the point of observation toward some target on the horizon. B_λ is less during the winter than during the summer.

In the discussion of the winds aloft (Section 3.1.3), it was noted that winds aloft from the south are more likely to occur in summer than in winter. A south wind would occur with a low-pressure region to the west and a high-pressure region to the east. Air with its particulates would flow along the surface from the south into the Utah region. A north wind would result from a high-pressure region to the west and a low-pressure region to the east, and in this case the Utah region would be an area of subsidence, with clean air that had been aloft, free of surface contaminants before undergoing subsidence to the surface. South winds aloft would result in greater values for the turbidity coefficient; north winds aloft would mean lower values of the turbidity coefficient.

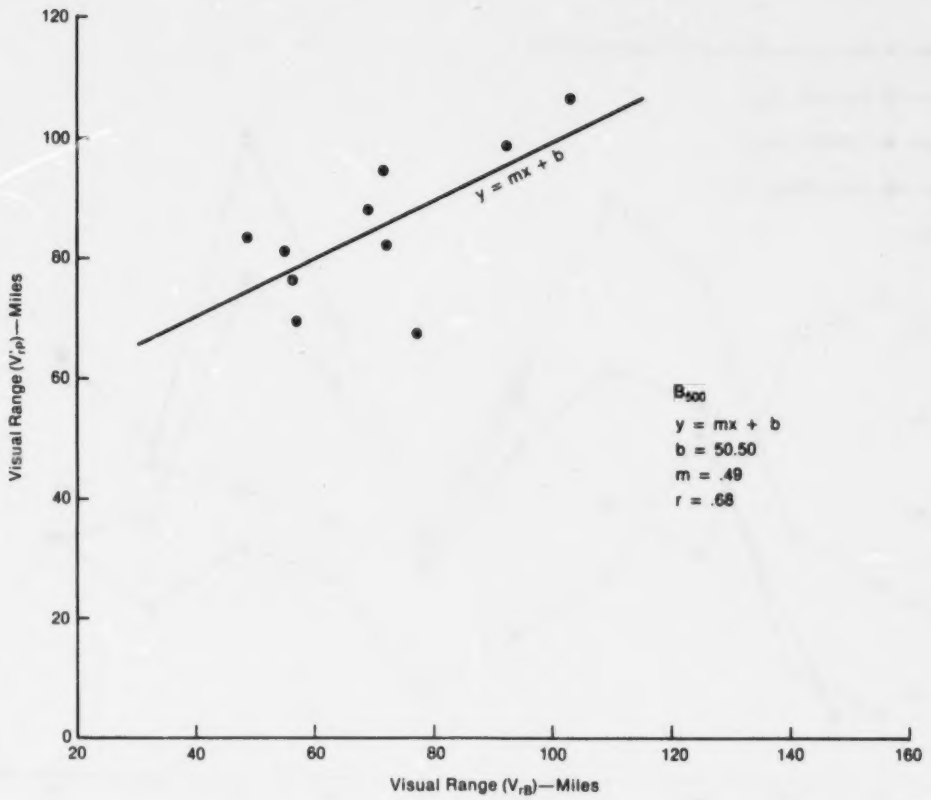

Figure 25.--Comparison of monthly averages of photographic visual range V'_{rP} (derived from fig. 21) with turbidity visual range, V_{rB}.

This seasonal change could be due to the presence or absence of inversion layers above Cedar Mountain during the observation period. In the winter when particulates that result in lower visibility (V'_{rP}) are trapped along the line of sight under an inversion that is a short distance above Cedar Mountain, the visual range (V'_{rP}) can be less than the visual range (V_{rB}) that is a function of the particulate concentration in the air column between the observer and the Sun as in January 1978, although some of the decrease is probably due to increased albedo of the target due to snow on the targets (see fig. 24). In the summer with more daylight hours, a warm land surface, and more vertical mixing, the particulates are not confined under an inversion layer, are mixed to greater height above Cedar Mountain, and V_{rB} is considerably less than V'_{rP}, as shown in fig. 24. The correlation coefficient between V'_{rP} and V_{rB} is r = 0.68 as shown on fig. 25.

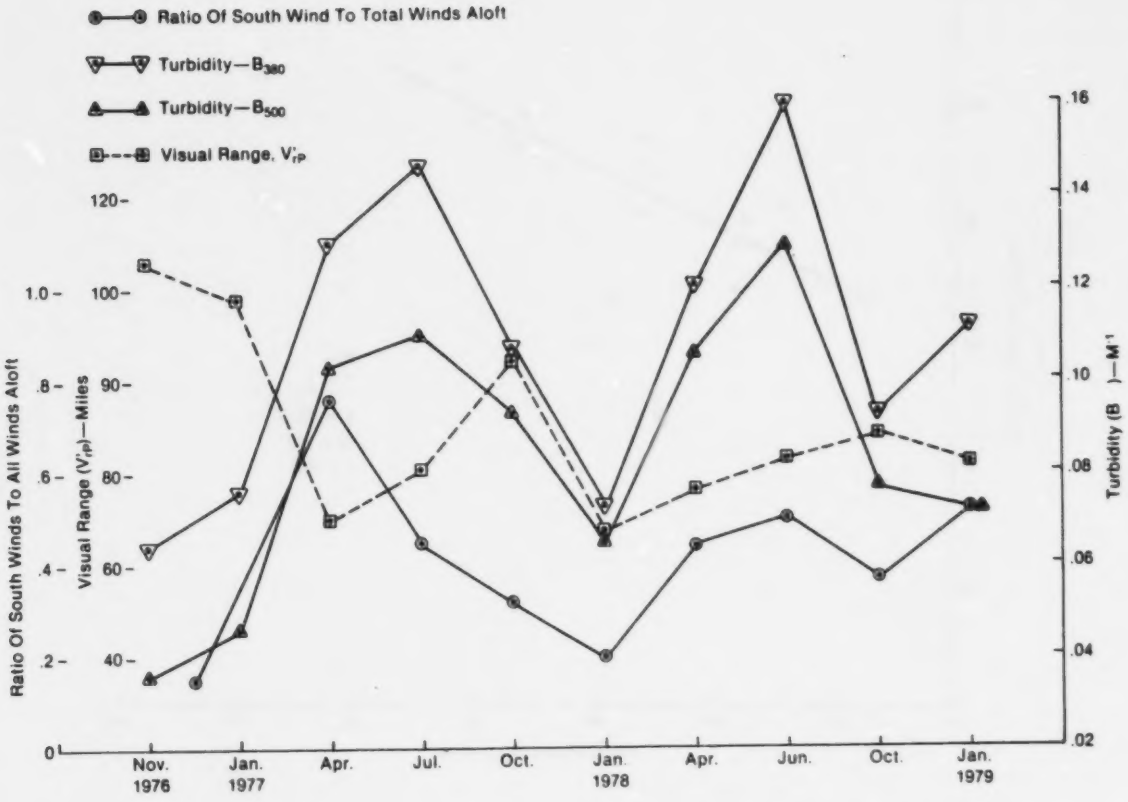

Figure 26.--Comparison of monthly averages of ratio of south winds aloft to all winds aloft, turbidity coefficients B_{380} and B_{500}, and photographic visual range V'_{rP} (derived from fig. 21).

The same as for the visual range V'_{rP}, there is a correlation between the ratio of south wind aloft to all wind directions aloft, to the B_{500} turbidity coefficient of r = 0.69, and to the B_{380} turbidity coefficient of r = 0.74. All four parameters are graphed on fig. 26.

Walther and Malm (1979) noted in their study of air quality at Page, Arizona, 170 miles south-southwest of Cedar Mountain, that the ratio of B_{380}/B_{500} was less than unity before 1974, indicating that the concentrations of particles smaller than 1 micrometer were low. The ratio became and remained greater than unity after the winter of 1975. The ratio B_{380}/B_{500} has always been greater than unity during the time of the Utah Visibility Project, but has approached unity during winter months when advection of south winds aloft transported particulates from the south. An exception, as noted before, is the winter of 1976-77 with its fine clear days and little snow on Cedar Mountain.

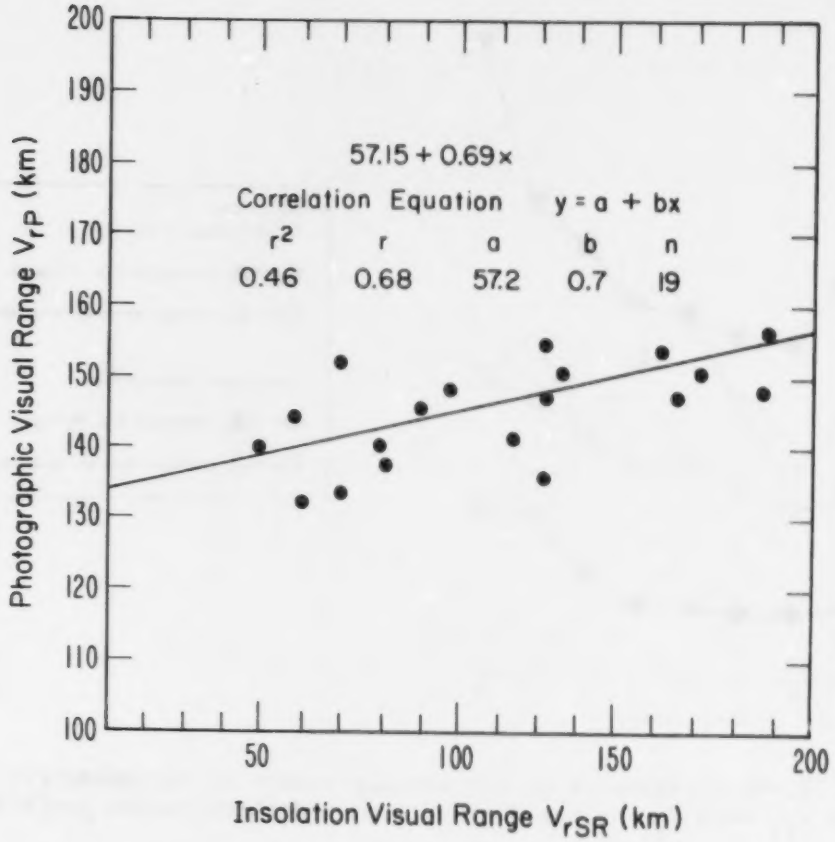

Figure 27.--Comparison of photographic visual range V_{rP} with insolation visual range V_{rSP} for three targets on clear days, Nov. 1976-Jan. 1977.

Figure 27 is a plot of VrP versus VrSR. Correlation between the two methods is good, but data availability is limited, requiring at least a half day to derive one value of V_{rSR}. The data points on fig. 27 represent valid data for V_{rSR} available from November 1976 through July 1977 observation periods. The method is interesting, but not worthy of investment of time for developing a data bank of visual range based on this method.

Figure 28 shows the result of a day's color photography comparison. Plotted are the simultaneous values of V_{rT} for the four primary targets (average distance 37.2 miles) and two distant mountain ranges (average distance 91 miles) and V_{rCP} for the same targets. $V_{rCP} > V_{rT}$ for the four primary targets by at least 50 percent at all times. $V_{rCP} > V_{rT}$ by about 10 to 15 percent for distant targets. Obviously the color film chemists have developed a film that emphasizes

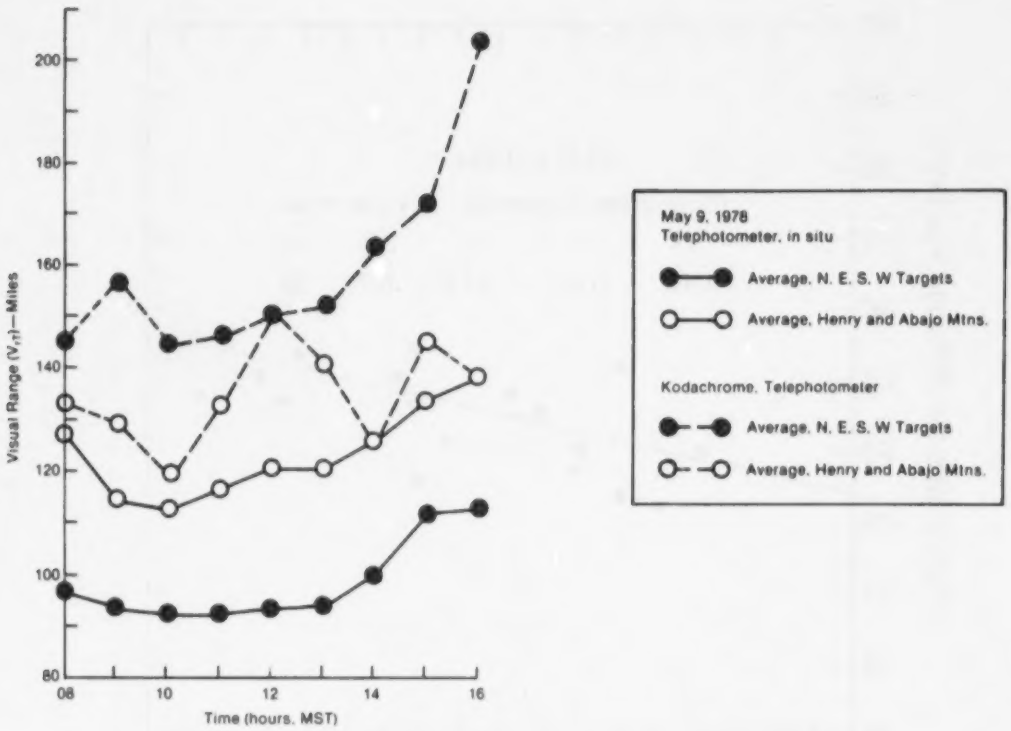

Figure 28.--Comparison of hourly average values of telephometric visual range V_{rT} with V_{rT} values derived from Kodachrome slide projection.

contrast to make their product more pleasing to the casual viewer. The degree of contrast is greater for the high-contrast nearby targets than it is for the distant low-contrast mountain ranges.

3.1.1 Temperature

An analysis has yet to be made of temperature compared with visual range. It would probably have about the same correlation as relative humidity (Section 3.1.2) except of the opposite sign.

3.1.2. Relative Humidity

Figure 29 shows a plot of the average relative humidity of the period from November 1976 to January 1979. Except for the abnormal November 1976 through January 1977 period the relative humidity is highest in January, lowest in July. Figure 30 shows relative humidity versus visual range (V'_{rP}) with the linear

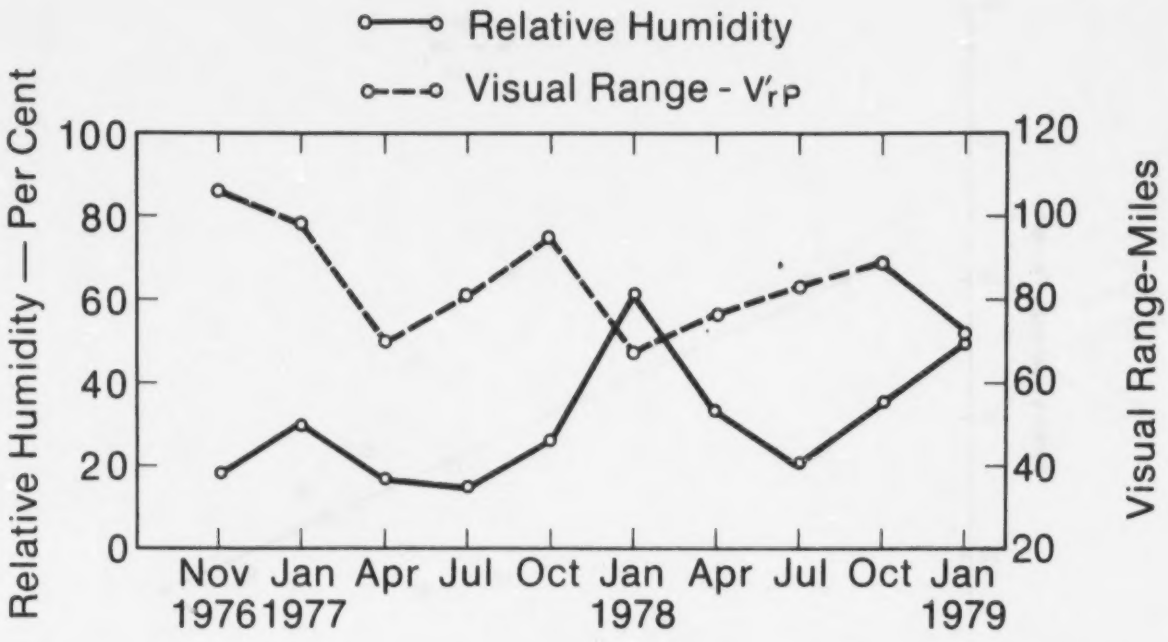

Figure 29.--Comparison of average relative humidity with overall photographic visual range V'_{rP} for three targets combining data for clouds behind target and sky behind target conditions.

regression curve, with coefficient of correlation r = -0.37. A positive coefficient of correlation has been found for the period November 1976 through January 1977 because on days with a high visual range that were associated with a northerly wind aloft that had come across Canada from the Gulf of Alaska, the air was clean, undergoing subsidence, and having been previously over the Pacific Ocean had a higher moisture content than most air masses that go across Cedar Mountain.

3.1.3 Wind

The wind at Cedar Mountain was measured in two ways.

First, the wind direction and speed were measured and recorded continuously about 20 feet above the surface by automatic equipment. The results of these measurements are summarized by wind roses shown in figs. 31 and 32. The winds are categorized according to speed depicted by the thickness of the lines, and by the percentage of the time for which they came from a certain direction. Figure 33 shows the relationship of the percentage of south wind at the surface to the visual range (V'_{rP}); the correlation coefficient is r = 0.016.

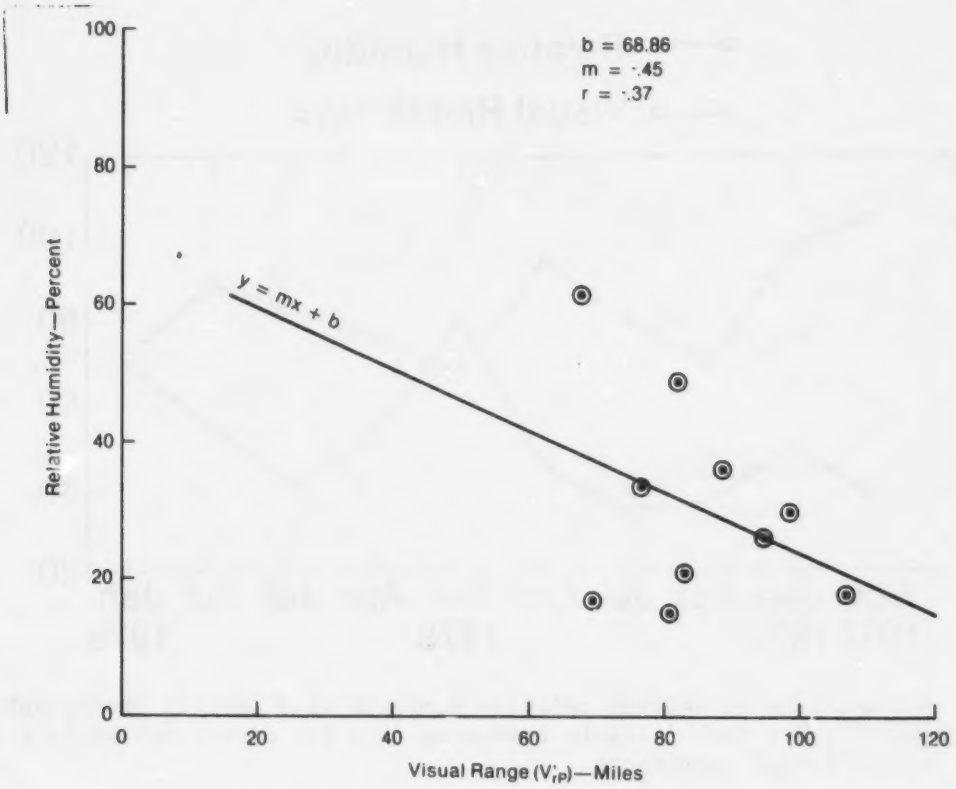

Figure 30.--Comparison of relative humidity daily maximum values with overall monthly average visual range V'_{rP}.

Second, pilot balloons (pibals) were released when weather conditions permitted during all observation periods, for observation of upper air direction and speed. The pibals were terminated at about 20,000 feet MSL after December 13, 1976. Before that date they were terminated at about 16,200 feet. The surface wind directions at the Cedar Mountain site have been classified into five sectors that are definable according to the surface features surrounding the site. Sector I, extending from 340° to 90°, includes the towns of Price, Helper, Wellington, and Dragerton, and the Utah Power and Light Co. coal-fired power plant near Castle Gate. These are located along Price River Valley, which forms the channel for the nocturnal downslope winds (drainage winds).

Sector II, which extends from 90° to 180°, includes Green River, Utah (28 miles), and Grand Junction, Colorado (80 miles), and the Grand River Valley. A drainage wind flows down the broad valley of the Gunnison River in western Colorado and the Colorado River (i.e., the Grand River Valley) into Utah. At

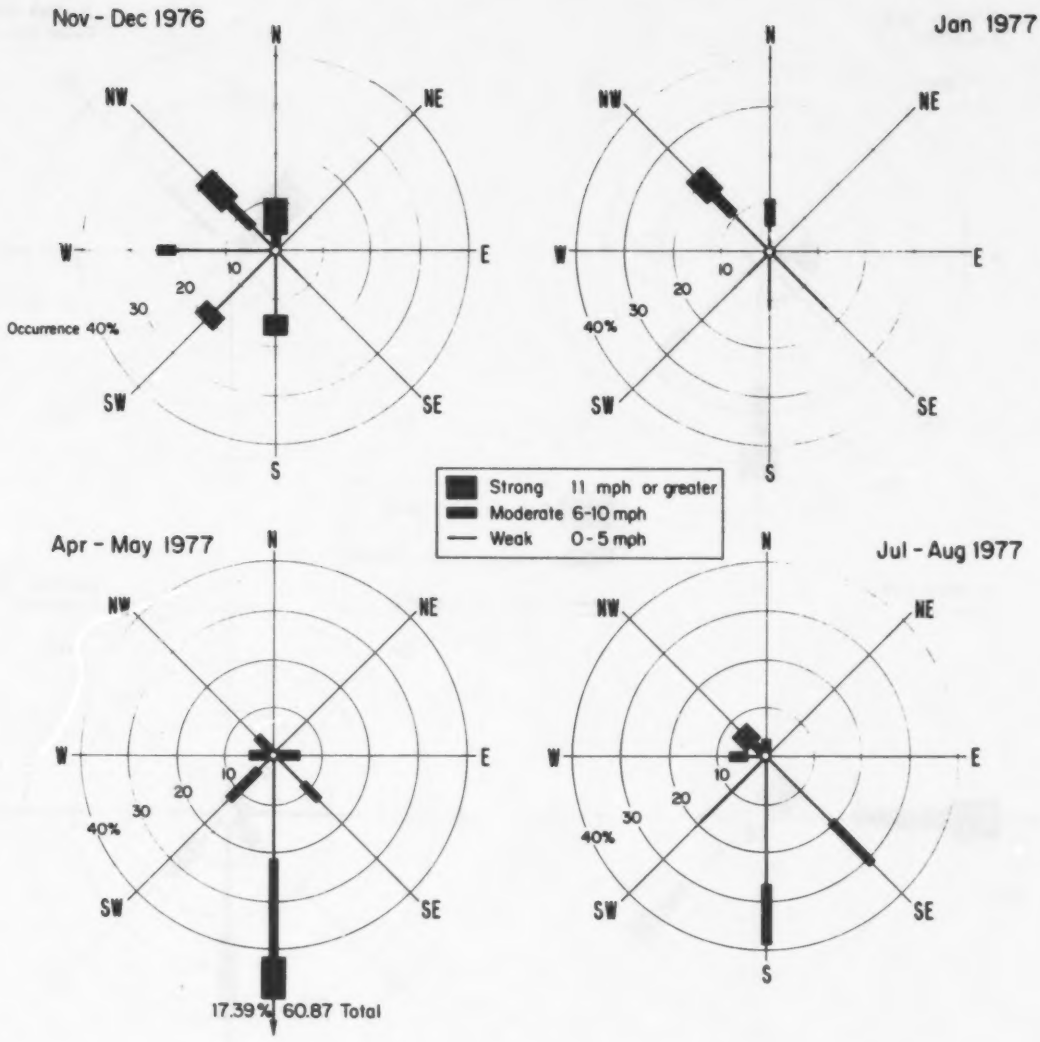

Figure 31.--Surface wind analyses for hourly observations coincident with measurements of photographic visual range for four observation periods between Nov. 1976 and Aug. 1977.

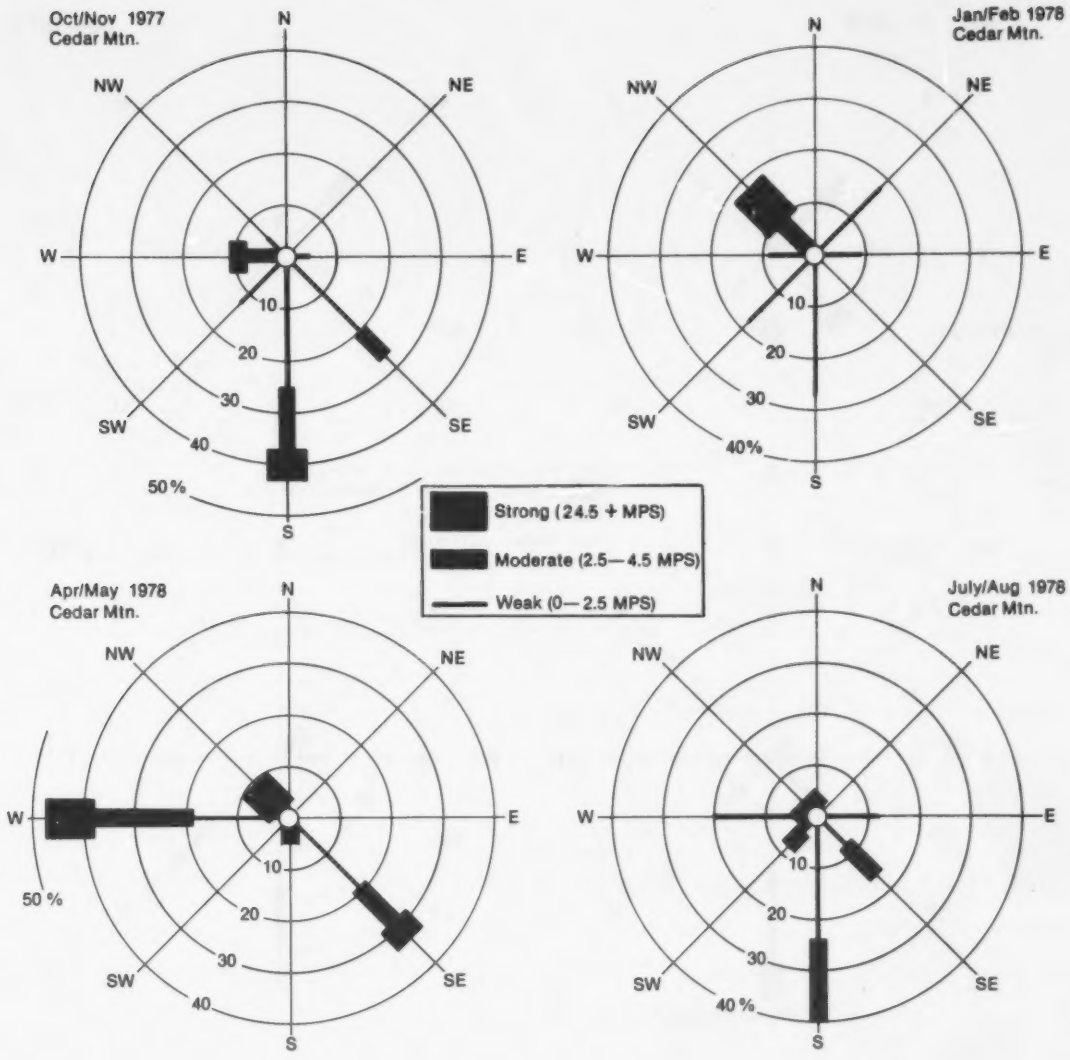

Figure 32.--Surface wind analyses for hourly observations coincident with measurements of photographic visual range for four observation periods between Oct. 1977 and Aug. 1978.

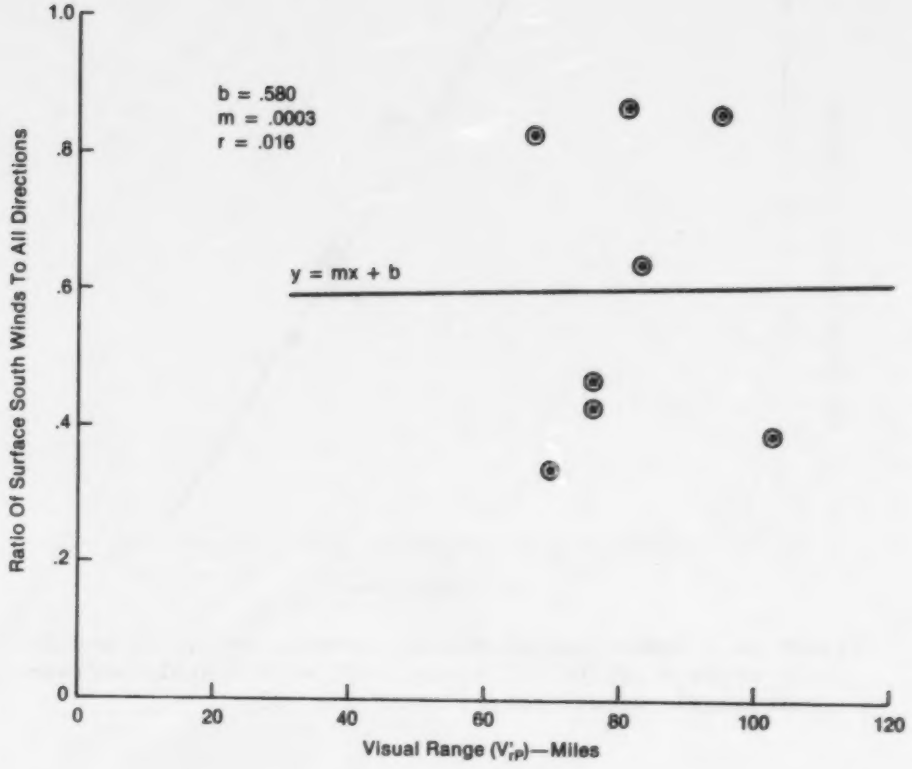

Figure 33.--Comparison of monthly average ratios of south surface winds to all surface winds with monthly average photographic visual range V'_{rp} for three targets, combining data for sky behind target and clouds behind target conditions.

the National Weather Service station at Grand Junction this drainage wind layer is usually between 300 and 600 meters thick and has a velocity of 2 to 5 m s^{-1}. At its closest the region affected by these drainage winds is about 80 kilometers from Cedar Mountain.

Sector III extends from 180° to 250°. There is very little habitation in this sector within a distance of 80 kilometers, and only a few small communities within the next 80 kilometers, but it does include part of the San Rafael River Valley that receives drainage winds from Sector IV.

Sector IV, extending from 250° to 290°, includes the towns of Orangeville, Castle Dale, and Ferrone, and the site of the Emery power plant. These are located in the San Rafael River Valley.

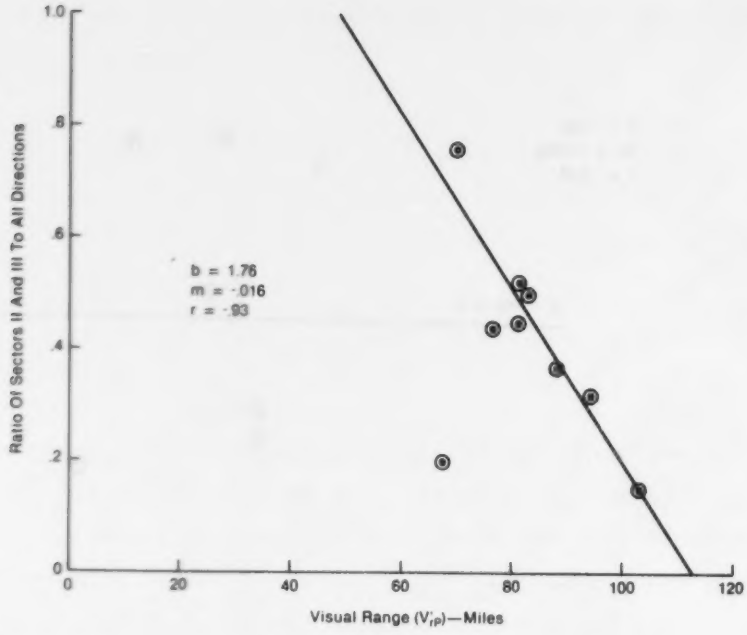

Figure 34.--Comparison of monthly average ratios of southerly winds aloft to all winds aloft with monthly average photographic visual range, as in fig. 33.

Sector V, 290° to 340°, includes the Huntington power plant and the towns of Huntington, Cleveland, and Elmo located in the upper San Rafael River Valley and the associated wind drainage region.

The upper air winds for each minute of pibal flight from 8,000 to 15,000 feet (12 minutes of flight) were classified according to the surface sectors. The modal wind direction was taken to be the wind direction aloft at Cedar Mountain for that day. If there were two equally possible wind directions by this definition, then the lower level was the choice of wind direction.

Figure 34 is a plot of the ratio of the number of days the upper winds came from Sectors II and III, divided by the total number of days in an observation period with valid pibal data, plotted against visual range. One point on the plot has been eliminated from calculation of the linear regression curve, the point at 67.5, 0.20. This point is for January 1978; it has fewer than half the number of pibal flights that the other points have. The period had unusually inclement weather with low-level stratus clouds occasionally covering Cedar Mountain. (Note high relative humidity for January 1978, fig. 29.) Also,

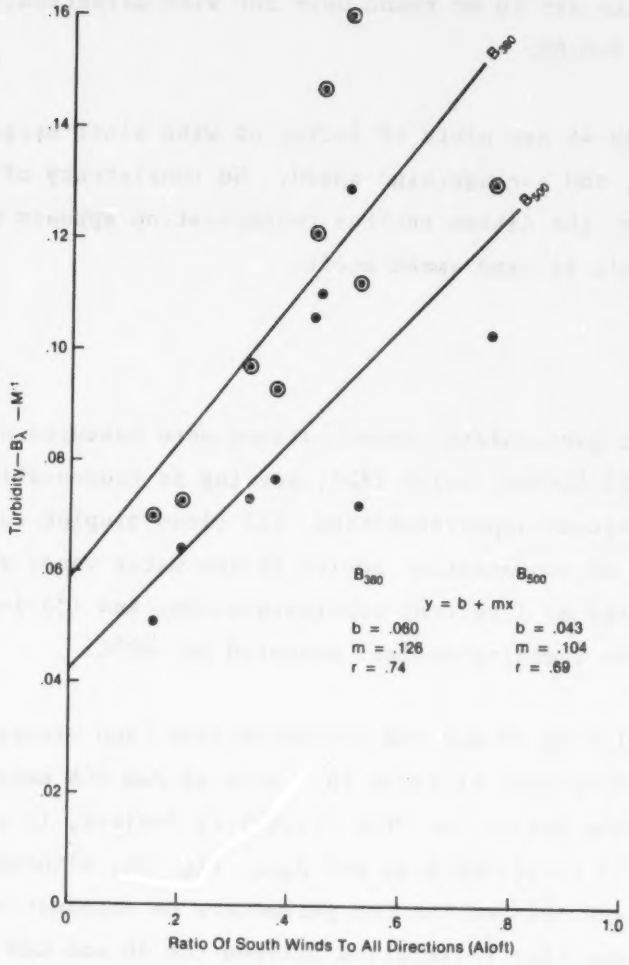

Figure 35.--Comparison of monthly average turbidity coefficients, B_{380} and B_{500}, with monthly average ratios of south winds to all winds aloft, as in fig. 33.

surface winds are predominantly from the south (fig. 32, Oct.-Nov.) even though upper winds are mostly from the northerly direction, so that the lower-level line-of-sight paths to the targets were under the influence of southerly air flows. For these reasons it is justifiable to eliminate the January 1978 point from fig. 34. When this is done the coefficient of correlation is r = 0.93 and explains that the visual range at Cedar Mountain is a regional phenomenon. This is probably the most important meteorological factor that determines the average visual range for a month-long observational period at Cedar Mountain.

Figure 35 is a plot of turbidity B_{380} and B_{500} versus the ratio of the south wind to all directions of wind (aloft). Next to visual range the best

correlation coefficients are to be found here for wind direction, for B_{380}, $r = 0.74$, for B_{500}, $r = 0.69$.

Figures 36 through 44 are plots of sector of wind aloft origin, Aitken nucleus concentration, and average wind speed. No consistency of results is apparent in this study; the Aitken nucleus concentration appears to be independent of sector of wind origin or wind speed aloft.

3.1.4 Particulates

Three atmospheric particulate concentrations were measured during the observation periods: (1) Aitken nuclei (AN), serving as condensation nuclei at greater than 300 percent supersaturation, (2) cloud droplet condensation nuclei (CCN), serving as condensation nuclei at low water vapor supersaturation in nature, measured at 1 percent supersaturation, and (3) ice crystal nuclei (ICN), active as freezing nuclei, measured at -20°C.

Figure 45 is a plot of AN and CCN concentrations (and visual range V'_{rP}) by observational period from data of Table 18. Both AN and CCN concentrations appear to have increased during the Utah Visibility Project, in support of the increasing trend toward turbidity B_{380} and B_{500}, fig. 35, although there appears to be little correlation between the two parameters on examination of monthly values. Figure 46 shows that correlation between the AN and CCN concentrations when visual range is low, for AN, $r = -0.12$ and for CCN, $r = -0.21$.

The correlation coefficient between monthly ICN concentration and monthly average visual range (V_{rP}) for all targets is $r = -0.62$ for seven periods. The good correlation between ICN concentration and V_{rP} indicates the ICN are a portion of the size range of particulates (0.1 to 1.0 μm) that are effective in limiting visual range. Correlation coefficients for daily values within an observational period varied from $r = -0.43$ to $r = 0.45$.

3.1.5 Pressure

Wind direction has the highest direct correlation with visual range, but it is in response to the location of areas of high and low pressure that the wind

direction at the surface and aloft is determined. Reference to the U.S. Department of Commerce daily weather map series shows that high-pressure areas northwest and low-pressure areas northeast can result in events that have higher average values of visual range for the observational period. With areas of low pressure southwest and high pressure southeast, events with lower than average values can occur.

Figure 47 is an example of the variation of visual range (V_T) for the observation period of October-November 1978. The low value of average daily visual range on October 20 is a result of a closed low-pressure area at the 500-mb level at a distance of 1,200 miles southwest of Utah. A study of the movement of air at the surface, on a similar series of days, October 18-20, 1977, (see Section 3.3.4) shows there was a movement of air from the southern California region toward Utah that had decreasing values of visual range and increasing values of humidity and lead particulates. The surface weather map of October 20, 1978, showed a rather flat surface pressure gradient in the vicinity of Utah, although 2 days earlier there was a high-pressure area east-southeast of Utah at 800 miles. A strong low pressure at the 500-mb level southwest of Utah will usually result in low visual range values in Utah, but the effect can be mitigated or even completely overcome as it was on October 23, with a low at 500 mb 800 miles southwest, and with a surface high-pressure area 300 miles to the west.

High-pressure air masses usually originate north of the United States where the general circulation of the atmosphere causes subsidence and cooling at high latitudes. The air cools and becomes more dense; there is time for coagulation and fallout of particulates before such air masses move southward. Such air masses are quite clean and have high visual range values.

When a high-pressure air mass moves southward to a position northwest of Utah and dominates the region, subsidence occurs and the surface is immersed in air that had been aloft and is more free of particulates than air from any other source that can be found at the surface. Since the air is clean and there is little local addition of particulates, the air remains clean and clear for a short time, on the order of a few days, or until replaced by air from another region.

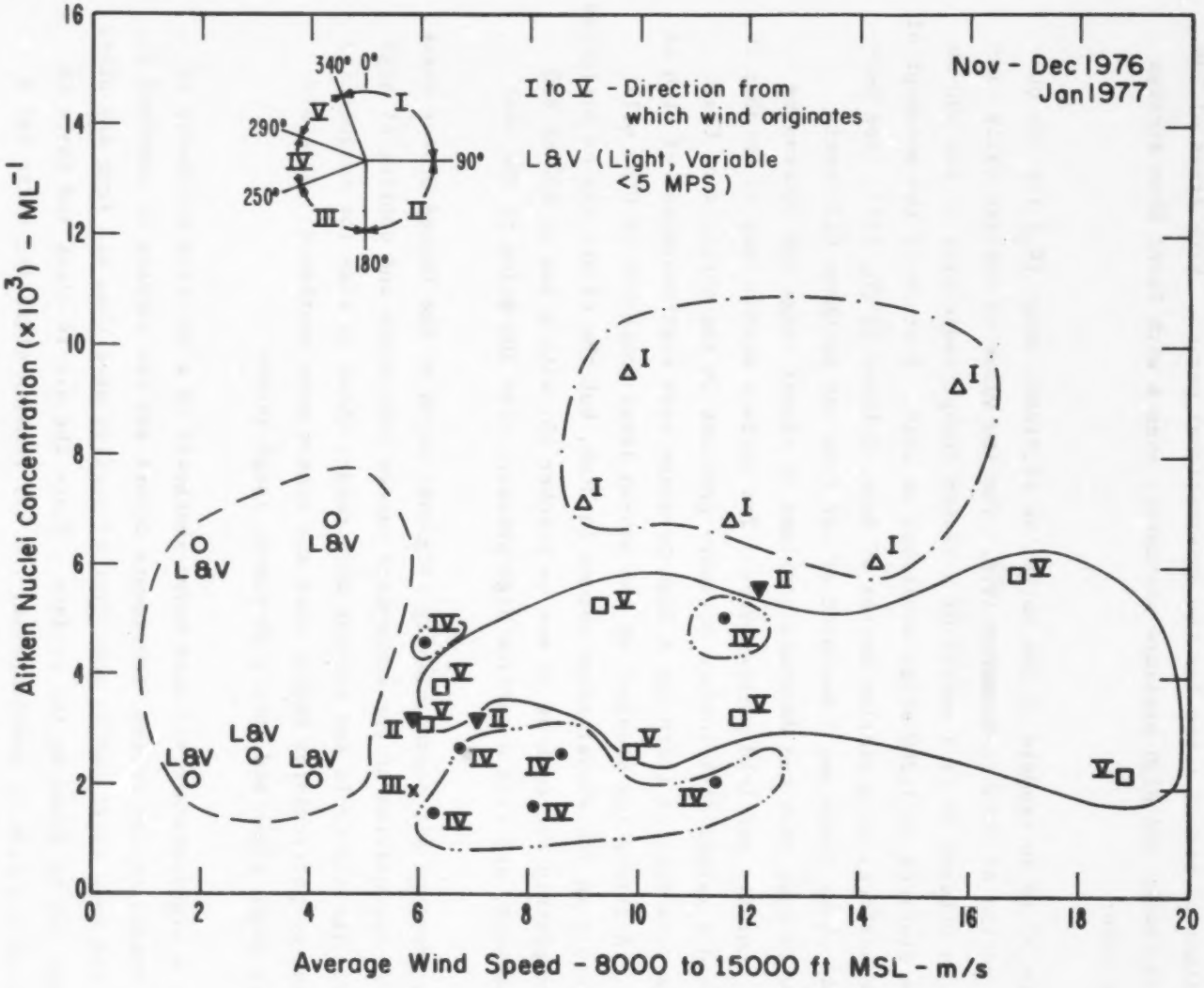

Figure 36.--Comparison of modal wind direction and average wind speed of upper air with surface Aitken nucleus (AN) concentration, Nov.-Dec. 1976, Jan. 1977.

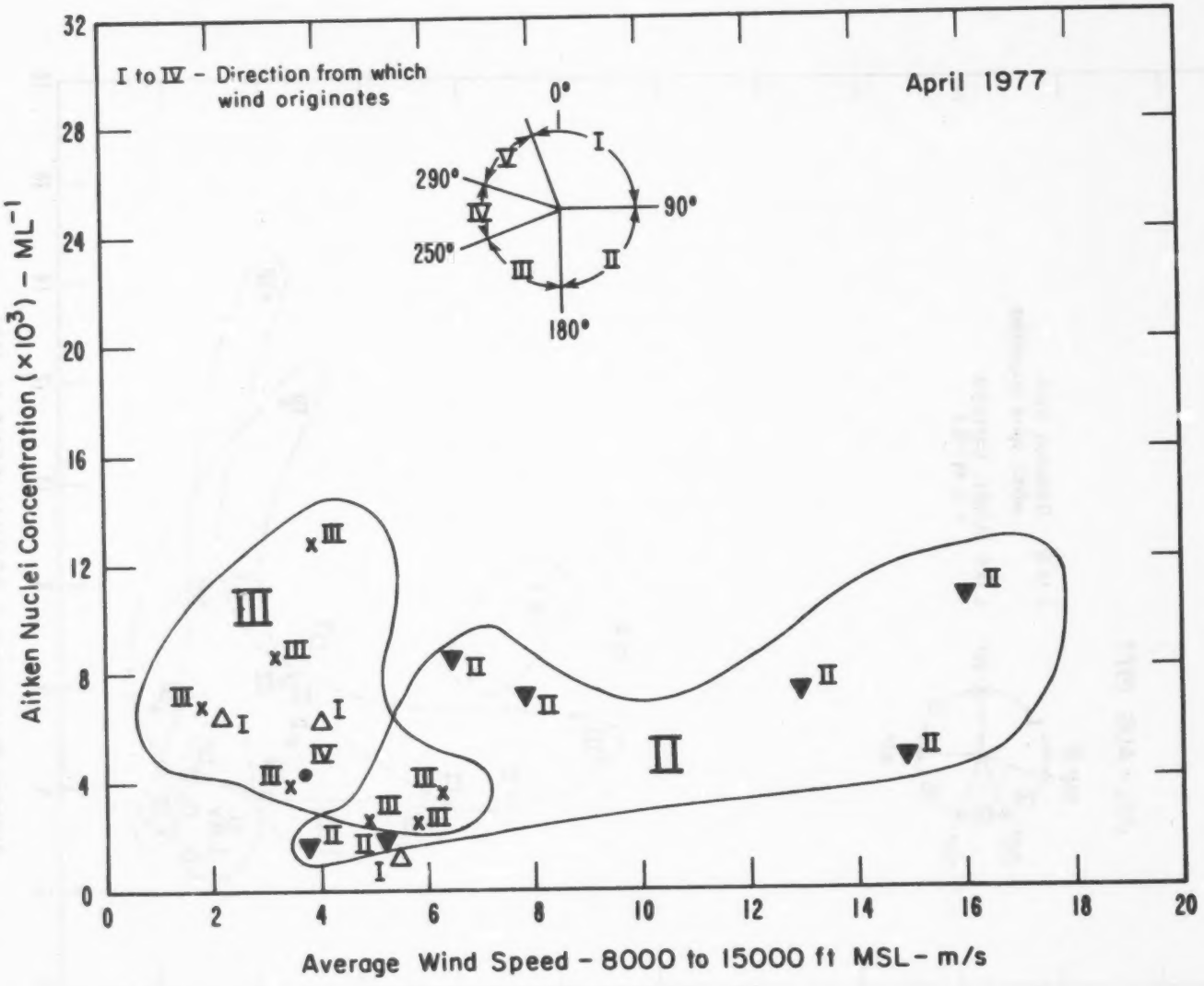

Figure 37.--Comparison of wind observations with AN concentration, Apr. 1977.

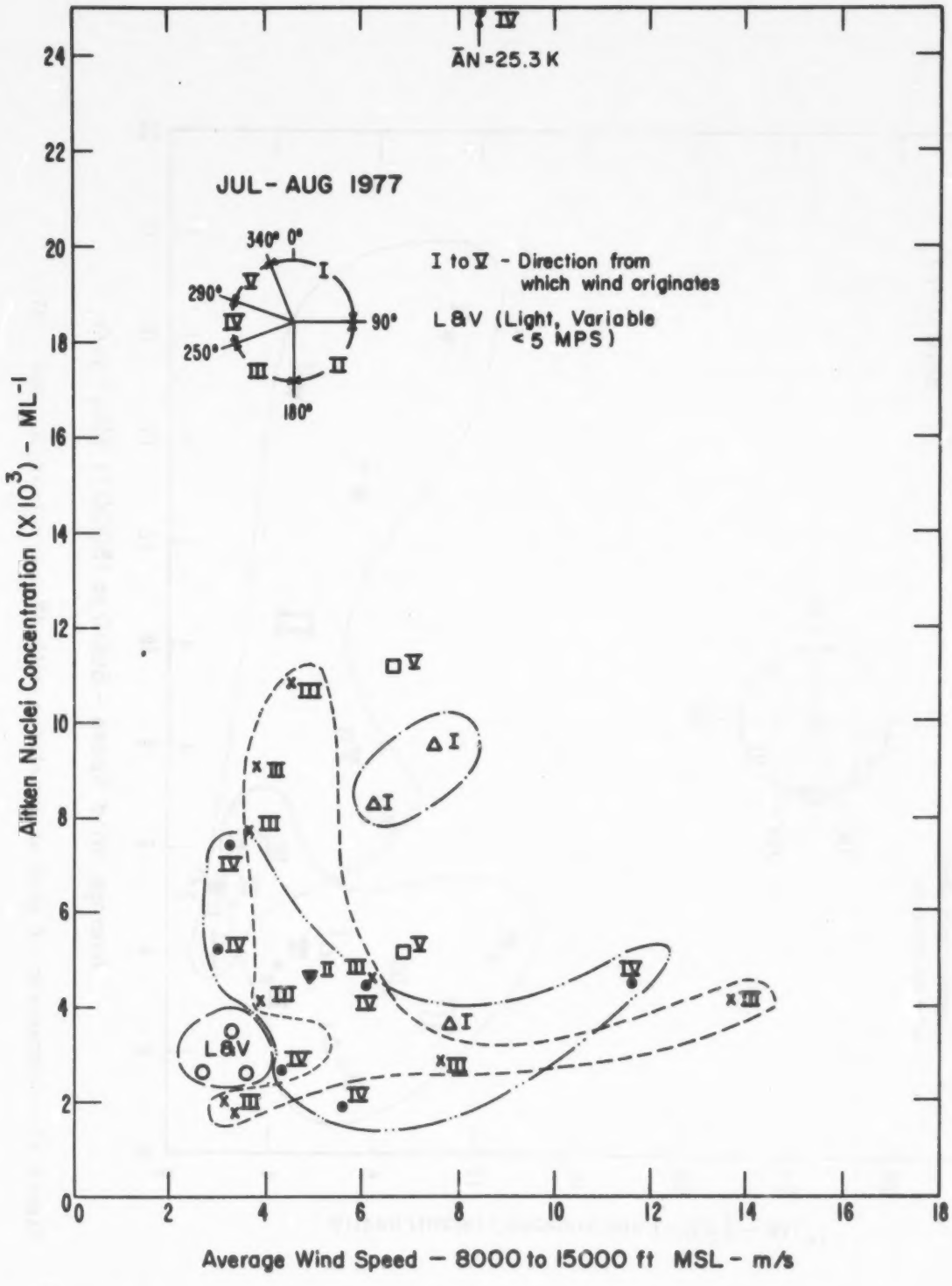

Figure 38.--Comparison of wind observations with AN concentration, Jul.-Aug. 1977.

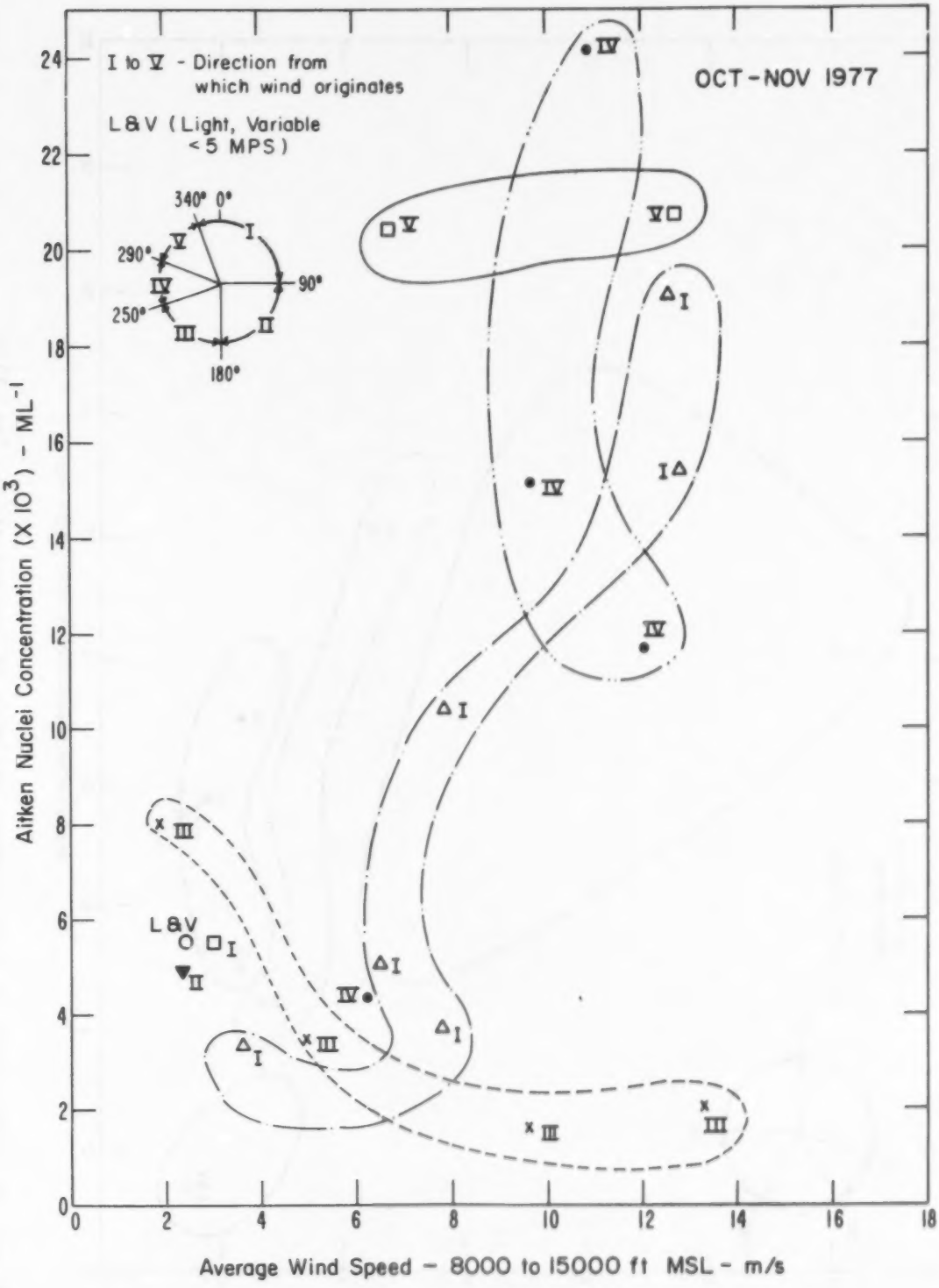

Figure 39.--Comparison of wind observations with AN concentration, Oct.-Nov. 1977.

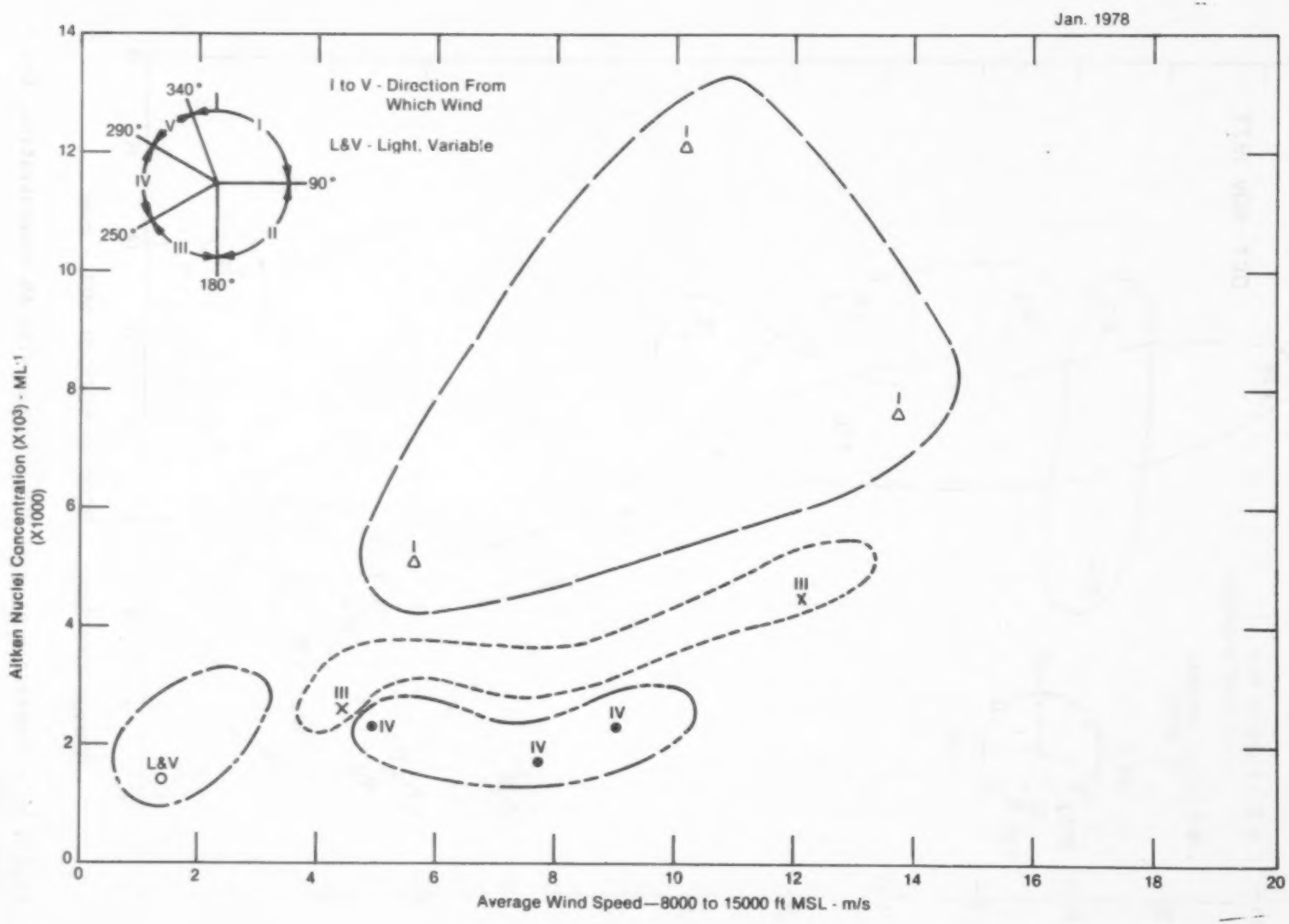

Figure 40.--Comparison of wind observations with AN concentration, Jan. 1978.

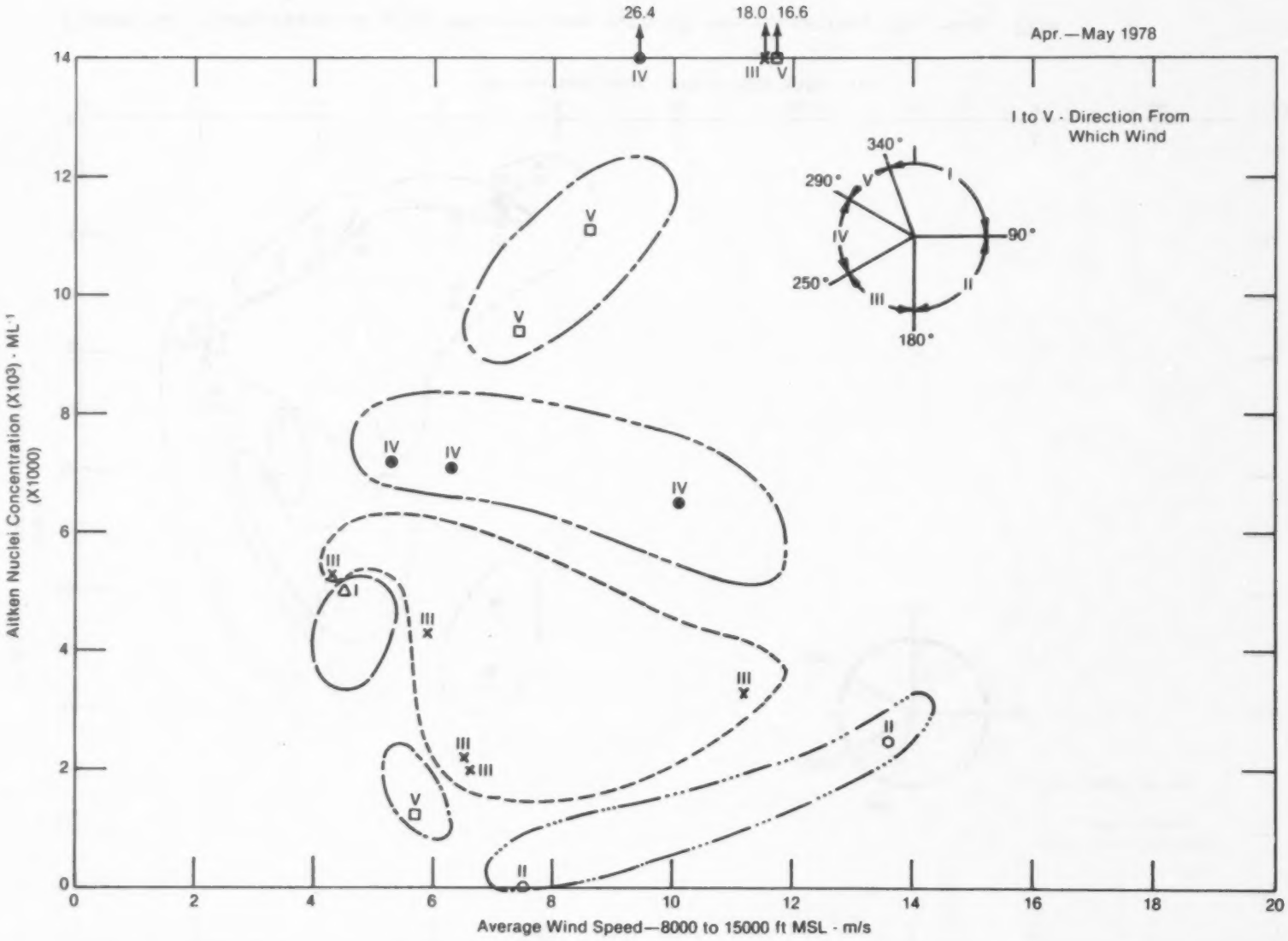

Figure 41.--Comparison of wind observations with AN concentration, Apr.-May 1978.

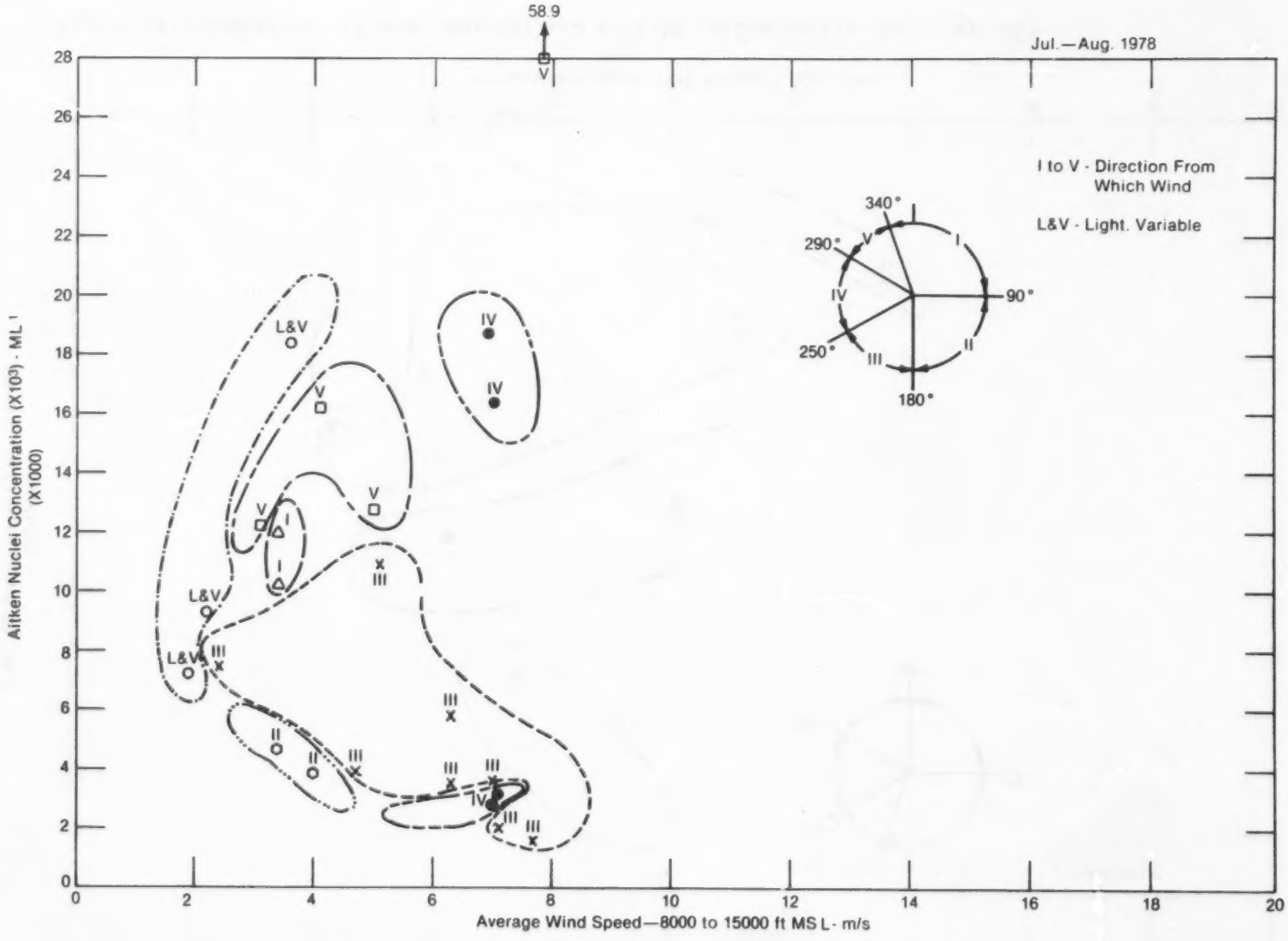

Figure 42.--Comparison of wind observations with AN concentration, Jul.-Aug. 1978.

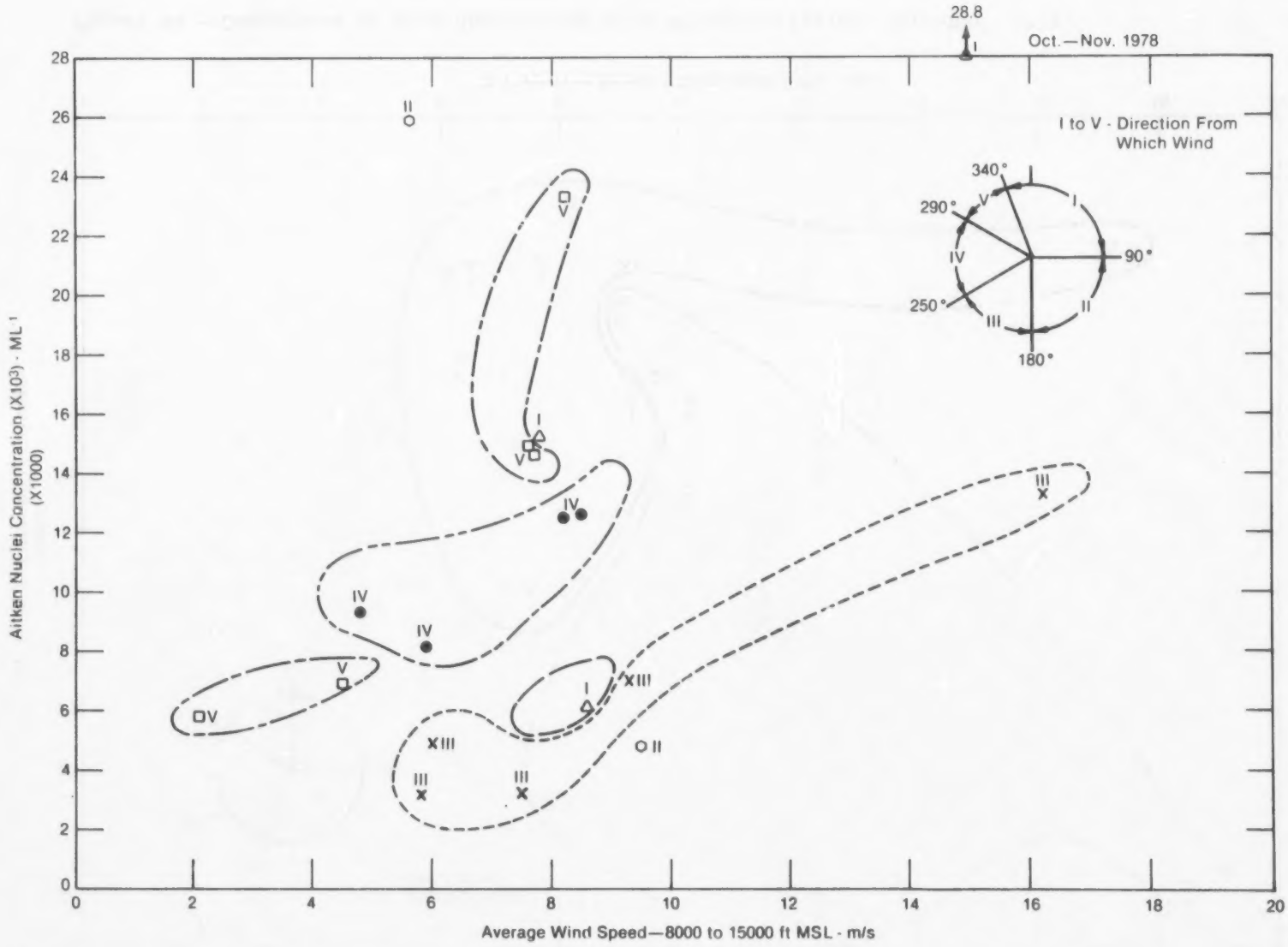

Figure 43.--Comparison of wind observations with AN concentration, Oct.-Nov. 1978.

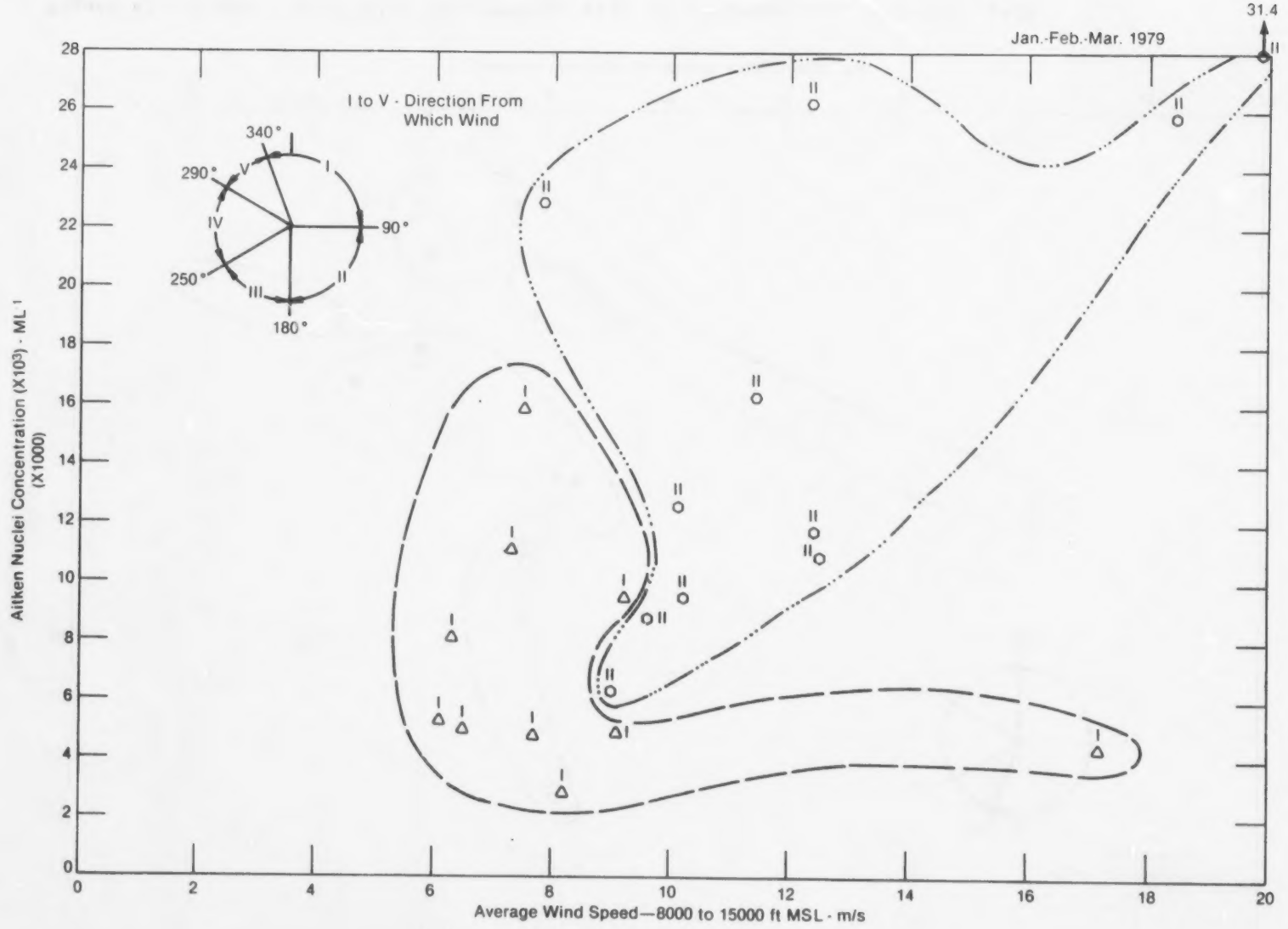

Figure 44.--Comparison of wind observation with AN concentration, Jan.-Mar. 1979.

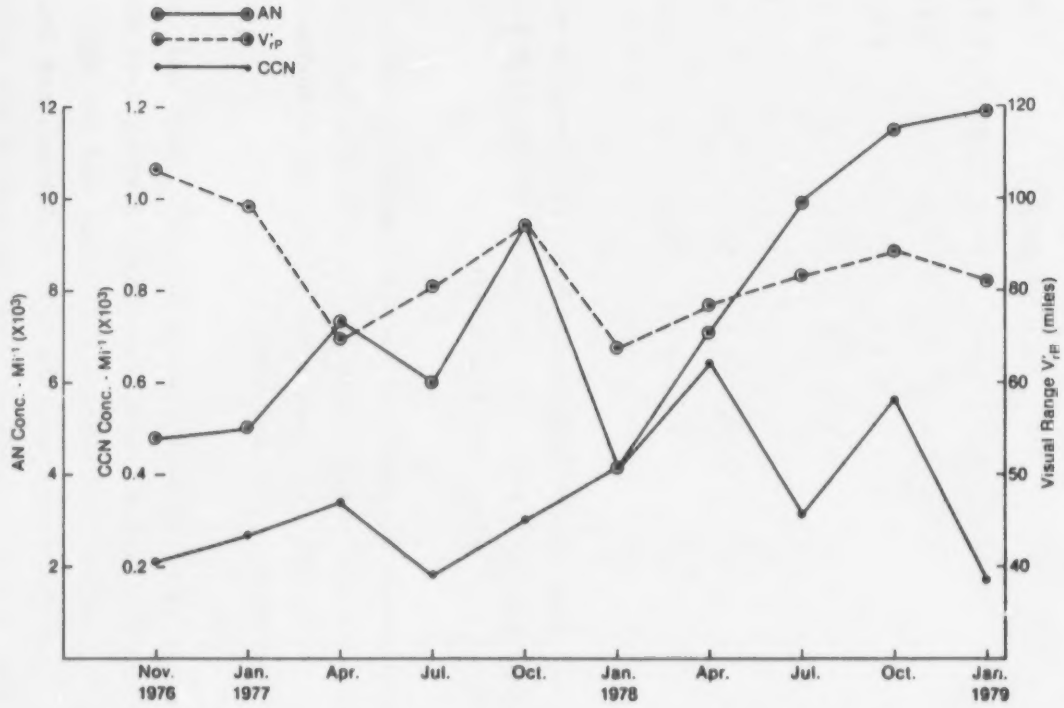

Figure 45.-- Comparison of average monthly concentrations of Aitken nuclei AN and cloud droplet condensation nuclei CCN, with overall photographic monthly average visual range V'_{rP} values for three targets, combining with data for sky behind target and clouds behind target conditions.

Table 18.--AN and CCN concentrations by period

Observation period	AN conc. $m\ell^{-1}$ ($x10^3$)			V'_{rp} (miles)	CCN conc. $m\ell^{-1}$ ($x10^3$)		
	N	AN av.	σ		N	CCN av.	σ
Nov-Dec 1976	31	4.8	2.9	106.5	33	0.72	0.21
Jan 1977	18	5.0	3.5	98.5	15	0.63	0.27
Apr	21	7.3	7.0	69.6	23	0.69	0.34
Jul	27	6.0	4.8	80.8	26	0.82	0.18
Oct	24	9.4	7.1	94.8	26	0.93	0.30
Jan 1978	11	4.2	3.6	67.5	11	0.92	0.41
Apr	21	7.1	6.6	76.5	21	1.11	0.64
Jul	25	9.9	9.3	83.0	23	1.03	0.31
Oct	26	11.5	9.0	88.2	21	1.35	0.56
Jan 1978	26	11.9	8.0	82.0	13	0.30	0.17

When such an air mass is overhead, subsidence still occurs with outflow at the edges of the high-pressure area, and the center of the high pressure is still being ventilated with clean air from aloft.

When the high-pressure air mass has aged and moved on farther south and east of Utah, the stable air traps within its lower layers particulates that originate at the surface. In this case winds aloft have a southerly component associated with lower values of visual range.

From November 20, 1976, through January 30, 1977, Utah and the western portion of the United States had unusual weather. A stationary dynamic ridge at 500 millibars was located off the western U.S. coast and the upper air over Utah was from over the North Pacific Ocean, the Gulf of Alaska, and Canada. The surface was dominated by a high-pressure area centered in the northwest quadrant of the continental United States. The high pressure was replenished by perturbations of air flow that maintained a fresh supply of air to the high-pressure area. Consequently the weather was unseasonably warm, dry, and clear with high values of visual range. For this reason data from these observations periods are best not included in the body of visual range data.

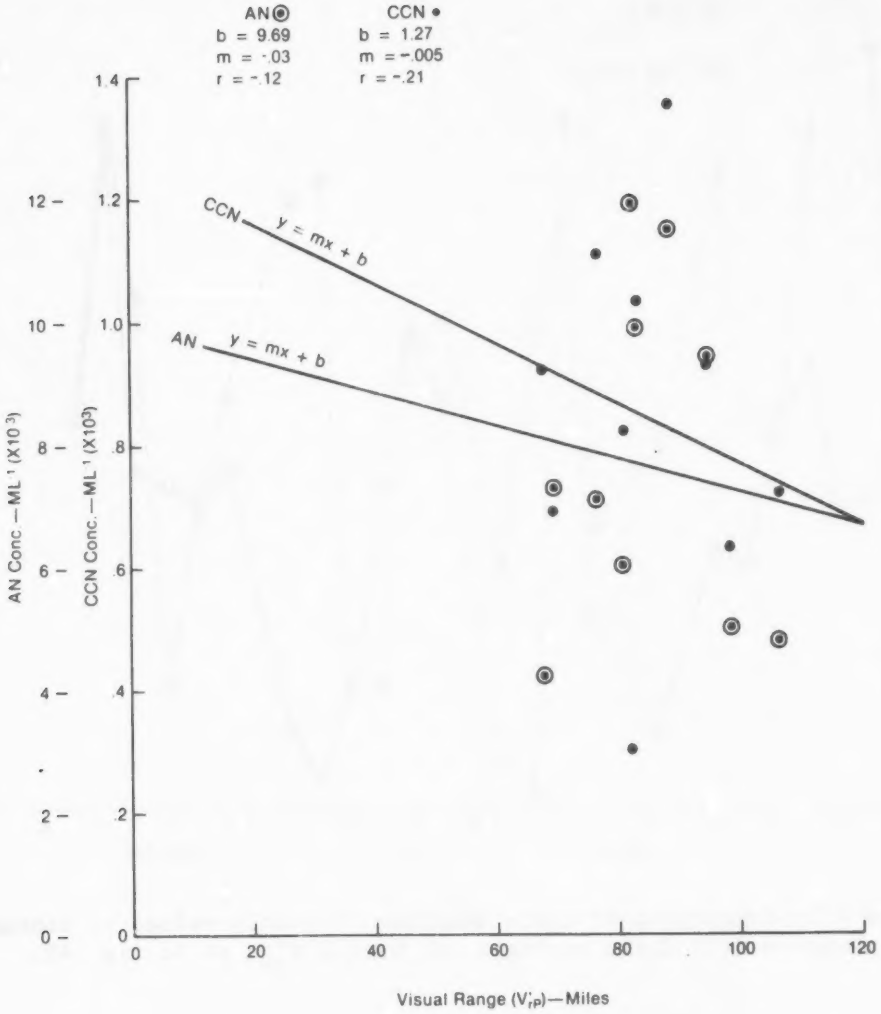

Figure 46.--Comparison of monthly averages of AN and CCN concentrations with overall monthly averages V'_{rP}, as in fig. 45.

Figure 48 is a plot of the average observational period visual range (V'_{rP}) versus the average station pressure during the visibility project. With all data there is a poor correlation coefficient of r = 0.24. With the November-December 1976 and January 1977 data deleted, there is a fair correlation coefficient of r = 0.49. Obviously the pressure is not as good an indicator of the average visual range during an observational period as is the percentage of southerly winds aloft.

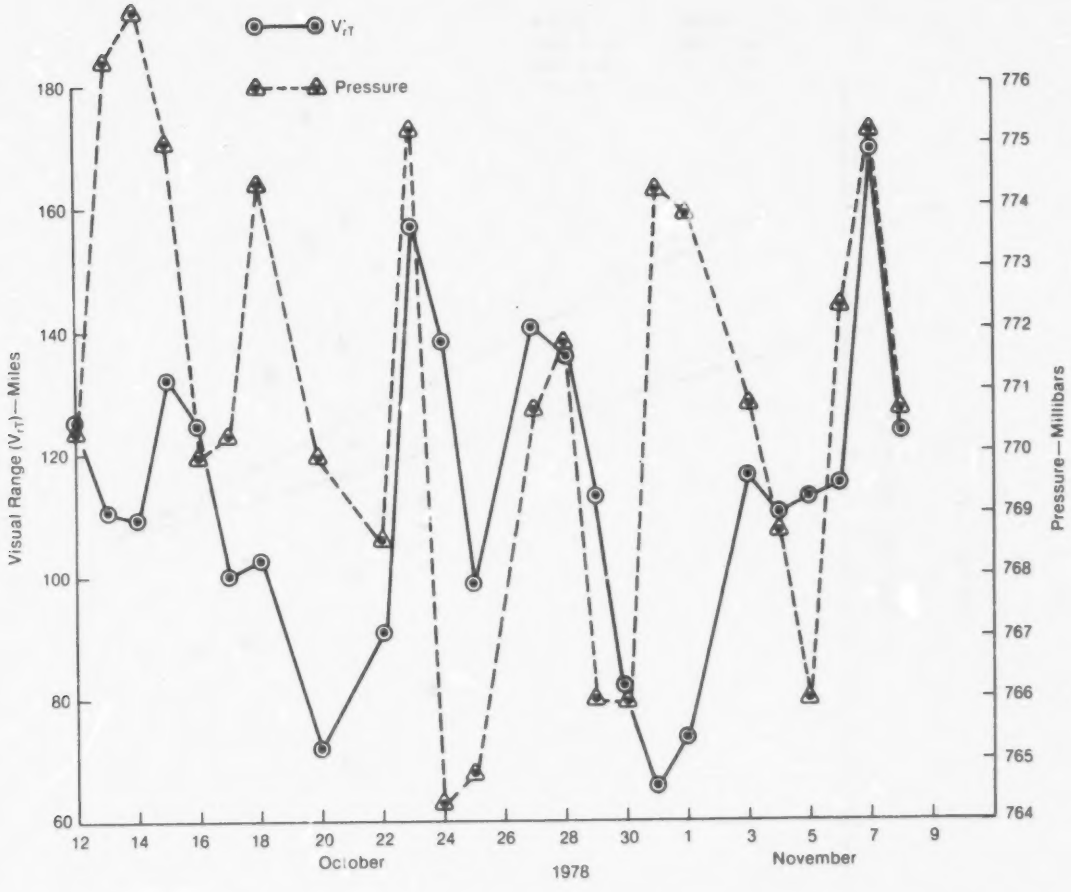

Figure 47.--Comparison of daily averages of hourly values of atmospheric pressure with daily averages of overall V'_{rp}, as in fig. 45.

Table 19 is a listing of the days of October-November 1978 with the associated average visual range and average station pressure. The correlation coefficient between the daily average atmospheric pressure and the daily average visual range is poor at r = 0.15. However, the relationship between visual range and atmospheric pressure patterns is of interest (fig. 47).

The low visibility of October 20 was associated with a closed low at 500 millibars 1,200 miles southwest of Utah, and a falling pressure associated with the system reached a low on October 21.

On October 23 a high value of visual range occurred; a closed low-pressure area at 500 millibars to the southwest was not enough to offset the effect of a

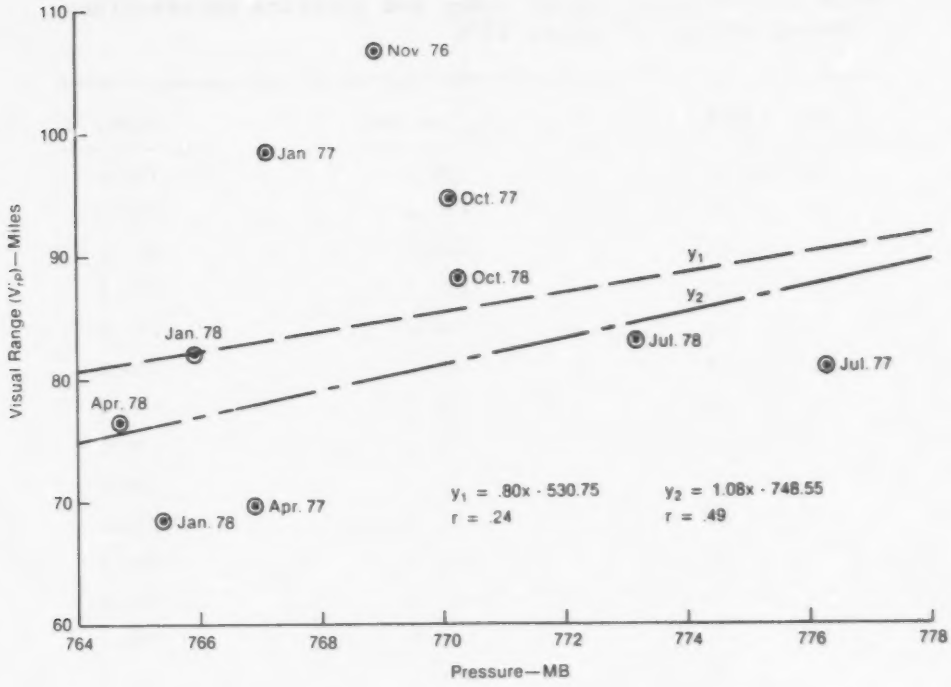

Figure 48.--Comparison of overall average monthly visual range with average monthly station pressure, y_1 (all data) and y_2 (all data except Nov. 1976 and Jan. 1977).

surface high-pressure area 300 miles northwest and the subsequent subsidence of clean air. A high average pressure resulted, the highest noted within a 2-week time period.

On October 31 the lowest visual range of the month occurred. A closed low at 500 millibars was west-southwest of Utah at 700 miles, with no strong high-pressure area at the surface. The lowest pressure in a sequence of about 5 days occurred on the day before the lowest visibility was recorded.

On November 7 a high visual range occurred with a surface high-pressure area centered 600 miles west. There were no noteworthy upper air features at 500 millibars. The atmospheric pressure also reached a concurrent peak on the same day.

A high pressure was noted on October 13 and 14; however, the high-pressure center was northeast of Utah, and air flow to Cedar Mountain would have been

Table 19.--Average visual range and pressure observations during October-November 1978

Date (1978)	V_{rT} (miles)	p(mb)
October 12	125.3	770.4
13	110.6	776.4
14	109.2	777.2
15	132.1	775.1
16	124.6	770.0
17	109.1	770.3
18	142.5	774.4
20	72.1	770.0
22	90.8	768.6
23	157.4	775.3
24	138.3	764.3
25	99.0	764.8
27	140.6	770.7
28	136.1	771.8
29	112.9	766.0
30	81.9	766.0
31	65.9	774.3
November 1	73.7	773.9
3	116.8	770.8
4	110.5	768.8
5	112.9	766.0
6	120.0	772.4
7	169.3	775.2
8	133.3	775.2

from a southerly direction. On October 18, again, the high-pressure center was northeast 1,000 miles, and with a low developing 1,200 miles to the southwest at 500 millibars, the visual range was decreasing. On October 31 the same situation occurred; the surface high pressure center was east-northeast 1,000 miles, with an upper closed low at 500 millibars 700 miles west-southwest, resulting in the lowest visual range observed during this period.

Many intermediate values of visual range occur where surface and upper air features are not pronounced or definitive enough so that we can correlate the

interrelative dependencies. It does appear from the study of the October-November 1978 observation period that some degree of success in forecasting the occurrence of extreme values of the visual range on Cedar Mountain could be made. This would involve forecasting (1) the position of surface low- and high-pressure areas, the position of closed low-pressure systems, troughs, and ridges at the 500-mb pressure level, and assigning priority to the effect of surface high-pressure areas, and (2) the wind direction of low-level winds above the surface, whether (a) southerly wind from an air mass that had been in proximity to the Earth's surface and consequently had accumulated particulates from natural organic and mineral and anthropogenic sources, or (b) northerly wind from an air mass that had its source over or above clean air from polar, maritime, or northern continental locations, or from clean mid-altitude air layers that are undergoing subsidence from a high-pressure area, or (c) indeterminant situations where mid-range values of the visual range are to be expected. The techniques might not be applicable for forecasting visual range values during winter periods in lower valleys of Utah and the West when strong temperature inversions prevent winds aloft from penetrating to the surface within regions that have strong local sources of particulates, such as the Salt Lake City region.

3.1.6 Instability

An analysis of the annual variation of Aitken nucleus concentration in Washington, D.C. (Allee, 1967), showed there was a relationship between a monthly stability index and the average monthly AN concentration of $r = 0.92$ in the morning and $r = 0.87$ in the afternoon. Such an index could be useful to analyze the effect of stable atmosphere on visual range at Cedar Mountain. T_{max} and T_{min} data are available from two Utah locations, Castle Dale and Cedar Mountain. The National Weather Service data archives can be used to determine the 500-mb temperature and derive a suitable stability index for testing this hypothesis.

3.2 Aircraft Measurements

Ground observations were supported by aircraft measurements for two reasons. First, measurements along the path of sight provide information on the homogeneity of the atmosphere. These data help in evaluating the accuracy of visibility observations over long distances. Second, vertical profiles of temperature and

other atmospheric constituents yield information about the depth of the mixing layer and, thereby, about the representativeness of visibility observations conducted at 2,350-m elevation on Cedar Mountain.

The observation platforms were a single-engine Cessna 206 used during 1976 and 1977 and a twin-engine Aero Commander 680E used since 1978. The aircraft were equipped with instruments to measure the parameters listed in table 20.

Aerosol particle and cloud-droplet size spectra are obtained in situ with a forward-scattering aerosol spectrometer (FSSP) and an active-scattering aerosol spectrometer (ASASP-X). Both instruments were manufactured by Particle Measuring Systems, Inc., Boulder, Colorado, as was the data logger, which recorded the aerosol counts and other digital data. The FSSP, mounted outside the aircraft to avoid any loss of particles in ductwork or by alteration of ambient conditions, counts particles with radii between 0.25 and 23.5 micrometers in four partially-overlapping ranges of 15 bins each. The ASASP-X covers the range 0.045 to 1.5 micrometer in the same manner.

An Aitken particle counter records the total particle concentration, and an integrating nephelometer gives the light scattering coefficient, both in a continuous manner.

Aerosol particles are also collected isokinetically on Nuclepore filters (mean pore diameter = 0.1 μm) and on a multistage impactor for post-flight chemical identification of $SO_4^{=}$ and NO_3^{-} by microchemical spot tests and of the elemental composition by X-ray energy dispersion analysis. Trace gases (SO_2, O_3, NO, NO_2) are measured by on-board gas analyzers.

All the data were recorded on magnetic tape in a DAS 64 data acquisition system (fig. 49). Independently, eight analog parameters could be selected for real-time display on an eight-channel strip chart recorder.

Software has been developed to process the data (fig. 50). The time of an event is selected on the basis of the strip chart or log-book records. For these time referrals, the particle counts per unit of time are converted into number, area, and volume size distributions. Light scattering functions are

Table 20.--List of instruments installed in in-situ sensing aircraft

Instrument Manufacturer/Model	Parameter	Method	Typical Operating Range	Minimum Detection Concentration
NOAA	Cloud Condensation Nuclei	Thermal Diffusion Chamber, Photography	20-2000 cm^{-3}	20 cm^{-3}
Environment-One/RICH 100, Gardner/7000 4 G 2	Aitken Nuclei	Expansion chamber	300-10^7 cm^{-3}	1 x 10^2 cm^{-3}
MRI 1550	Light Scattering Coefficient	Integrating nephelometer	0-10 x $10^{-4}m^{-1}$	0.15 x $10^{-4}m^{-1}$
Rosemount 102 AN 1 AF	Temperature	Platinum resistance	-40° to +40°C	
GE 1011	Relative Humidity	Thermoelectric dew point	-75°C to +50°C	
ML 8410	Ozone	Chemiluminescence	0-5 ppm	5.0 ppb
ML 8440	Nitrogen Oxide	Chemiluminescence	0-5 ppm	5.0 ppb
ML 8440	Nitrogen Dioxide	Chemiluminescence	0-5 ppm	5.0 ppb
Teco 43	Sulfur Dioxide	UV Pulsed Fluorescence	0-5 ppm	2.0 ppb
NOAA Sampler, RCA TEM	Aerosol Size	Aerosol Filtration for Electron Microscopy		5.0 cm^{-3}
NOAA Sampler, Coates & Welter SEM, Kevex 5000	Aerosol Composition	Aerosol Filtration for Electron Microscopy X-ray Spectrometry		5.0 cm^{-3}
Thermal Diffusion Chamber, NCAR	Ice Nuclei	Aerosol Filtration		.5 cm^{-3}
Particle Measuring Systems ASASP-X, FSSP	Aerosol Size Distribution	He-Ne laser light Scattering	0.08-50 μm	
NOAA	Potential Gradient	Electric field mill	0-10^6 volts/meter	1 volt/meter
Barnes, PRT-5	Infrared Radiation	Bead Thermistor	-20° to +75°C	
Particle Measuring Systems DAS 64	Data Acquisition	Digital Processing		
Pertec F6x9 formatter, Pertec T7640 transport		Magnetic tape recording		
HP 5055A		Digital printer		
Gulton tmd 840/S-1289		Analog recording		

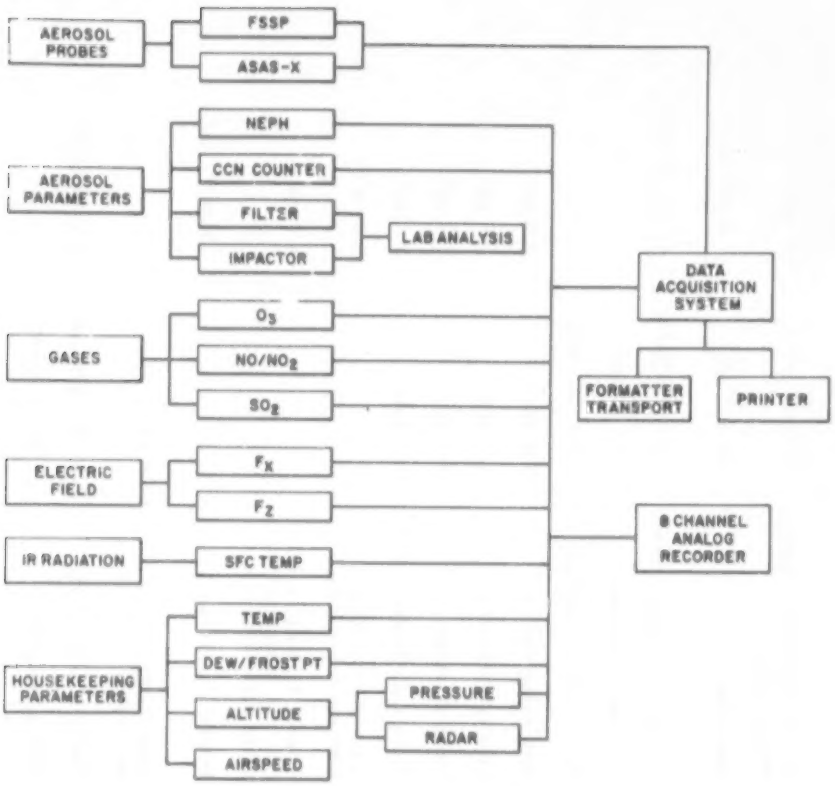

Figure 49.--Instrumentation and data acquisition system of parameters measured by aircraft during the Utah visibility study.

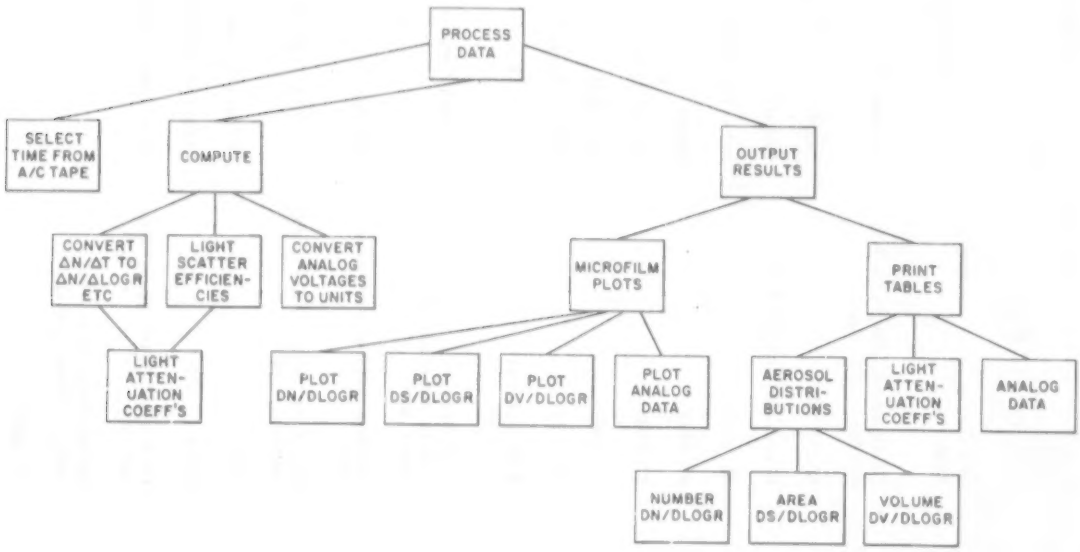

Figure 50.--Data processing flow chart of parameters measured by aircraft during the Utah visibility study.

computed according to Mie theory for the respective particle size distributions, and hard copies of the data are provided in the form of tables and microfilm plots.

3.2.1. Horizontal Atmospheric Homogeneity

In order to show the degree of inhomogeneity that existed in the optical properties of the atmosphere during visibility observations, flights were performed between Cedar Mountain, the ground observer's site, and the west, north and south targets at 200 feet AGL and along the line of sight (see fig. 1). The results are shown in table 21 by the light scatter coefficients from the integrating nephelometer. It follows from table 21 that a relative variability of the optical properties of the atmosphere between 5 and 50 percent can be found, which is independent of season or altitude. Perhaps 5 percent of the measured variability is due to instrument error. This leaves a variability of the atmospheric light scattering coefficient of 0 to 45 percent, which is due to inhomogeneity of aerosol concentration. Such a variability, undoubtedly, affects the accuracy of visibility observations and contributes to the relative accuracy of 10 to 20 percent in the results in tables 3 through 17.

In order to show possible effects of human activities on the optical homogeneity of the atmosphere, flights were also conducted along a valley in which agricultural activities and power plant operation take place (fig. 1, points A and B). The results, shown in table 22, are not much different from those of the surrounding atmosphere.

3.2.2 Vertical Temperature Profiles

The main purpose of this portion of the flight program was to establish the extent of atmospheric stability during some days on which visibility observations were made. Figure 51 shows the results as temperature plots in a skew-T diagram. The elevation of Cedar Mountain (2,350 meters MSL) is indicated on the right side of the diagram.

It follows from fig. 51 that, in general, the atmosphere at Cedar Mountain is neutrally stable. Only in November 1976 and in November 1978 did we observe a

Table 21.--Flight data of light scatter coefficients from integrating nephelometer

Date	Low flight	$\frac{\Delta B}{B}$	High flight	$\frac{\Delta B}{B}$	Low flight	$\frac{\Delta B}{B}$	High flight	$\frac{\Delta B}{B}$	Low flight	$\frac{\Delta B}{B}$	High flight	$\frac{\Delta B}{B}$
11/5/76 PM							0.19±0.09	0.47			0.20±0.09	0.45
11/6/76 AM			0.17±0.11	0.06	0.17±0.09	0.53	.20±0.08	.40	0.16±0.04	0.25		
11/6/76 PM					.18±0.08	.44					.21±0.08	.38
12/13/76 AM			.20±0.01	.05							.18±0.02	.11
1/27/77 AM	0.50±0.18	0.36	.25±0.05	.20	.36±0.13	.36	.23±0.05	.22	.38±0.12	.32	.36±0.05	.14
1/27/77 PM	.29±0.10	.35			.25±0.07	.28	.21±0.03	.14				
1/28/77 PM	.60±0.08	.13			.35±0.09	.26			.35±0.10	.29	.28±0.06	.21
4/19/77 AM	.42±0.06	.14			.28±0.06	.21			.34±0.06	.18	.34±0.08	.24
4/20/77 AM	.27±0.09	.33	.19±0.06	.32	.20±0.05	.25	.18±0.05	.28	.24±0.05	.21	.19±0.04	.21
7/9/77 AM	.27±0.05	.19			.19±0.02	.11	.20±0.02	.10	.19±0.01	.05	.19±0.01	.05
8/3/77 AM	.44±0.05	.11	.40±0.05	.13	.36±0.04	.11	.33±0.03	.09	.38±0.03	.08	.36±0.05	.14
8/4/77 AM	.49±0.08	.16	.50±0.04	.10	.48±0.10	.21	.47±0.04	.09	.43±0.14	.33	.47±0.04	.09
8/5/77 AM	.55±0.03	.05	.55±0.05	.09	.54±0.04	.07	.47±0.04	.09	.56±0.02	.04	.47±0.04	.09
10/19/77	.21±0.01	.05	.20±0.02	.10								
10/20/77	.20±0.01	.05	.21±0.01	.05								
10/21/77	.20±0.02	.10	.25±0.02	.08	.21±0.01	.05	.19±0.01	.05	.23±0.01	.04		
10/13/78			.18±0.02	.11							.19±0.05	.26
10/18/78											.19±0.05	.26
11/6/78			.18±0.03	.17							.19±0.02	.11
11/8/78			.18±0.02	.11							.20±0.01	.05

Table 22.--Temporal and spatial variations of light scattering coefficients, $B(10^{-4}m^{-1})$, around Cedar Mountain, Utah

Date	Low flight	$\frac{\Delta B}{B}$	High flight	$\frac{\Delta B}{B}$
1/27/77 AM	0.55±0.19	0.35	0.24±0.07	0.29
1/27/77 PM	0.35±0.12	0.34		
1/28/77 PM	0.71±0.17	0.24		
4/19/77 AM	0.41±0.06	0.32	0.35±0.07	0.20
4/20/77 AM	0.28±0.09	0.24	0.22±0.05	0.14
7/9/77 AM	0.38±0.09	0.11	0.28±0.04	0.07
8/3/77 AM	0.45±0.05	0.15	0.41±0.03	0.08
8/4/77 AM	0.53±0.08	0.14	0.48±0.04	0.06
8/5/77 AM	0.49±0.07	0.14	0.49±0.03	0.06

distinct temperature inversion at 2,900 meters MSL. Interestingly, the time-averaged visibility data of fig. 21 show relatively high values during these periods. This is contrary to what one would expect if temperature inversions were to increase the aerosol load by limiting the volume into which particles of local origin can be dispersed. The important conclusion from this finding is that advected, rather than locally emitted, aerosol strongly affects the visibility in east-central Utah. (See Section 3.2.3.)

3.2.3 Aerosol Dynamics

The aerosol dynamics, discussed in terms of the lumped-mode heterodisperse-coagulation model (Whitby et al., 1978), show that there is an appreciable rate of formation of particles of nucleus-mode size in east-central Utah. These particles, initially too small to be optically active, interact rapidly with the accumulation-mode aerosol. The resulting aerosol is most persistent and important for environmental effects, including visibility.

Figure 52 shows a typical aerosol size distribution for east-central Utah. For radii between 0.05 and 23.5 micrometers, the size distributions are derived from the records of the FSSP and ASASP-X aerosol probes. Within this size range, two modes, one at around 0.1-μm radius, henceforth referred to as the accumulation mode, and one at radii larger than 1 micrometer, from now on called the coarse-

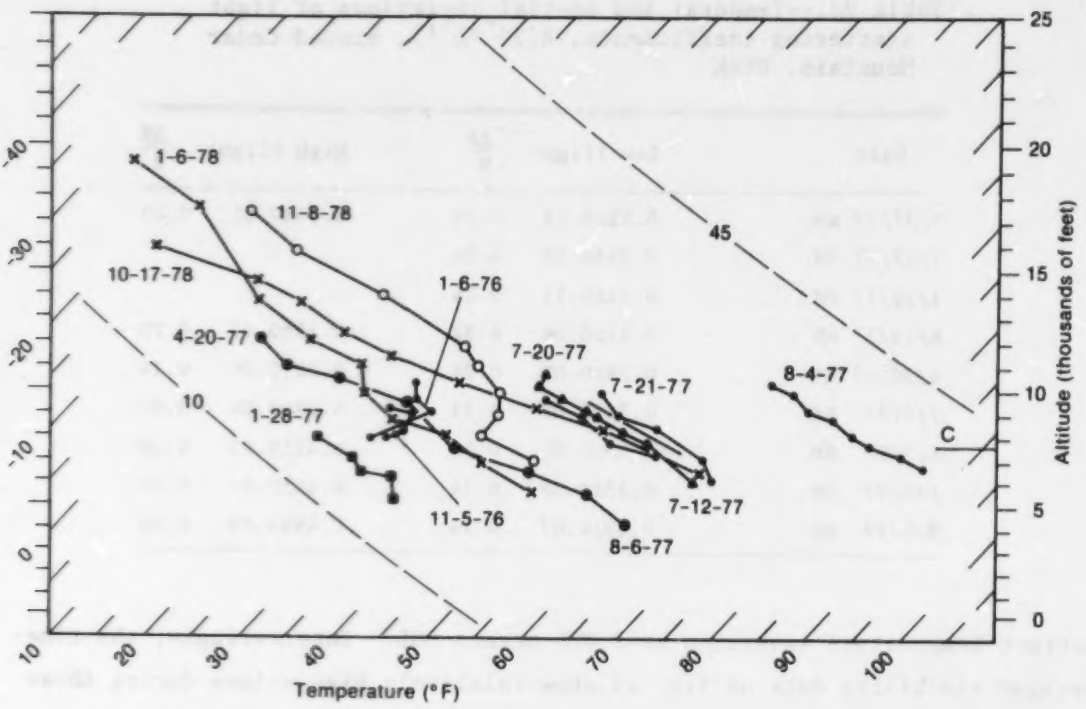

Figure 51.--Temperature profiles measured by aircraft on selected days during the Utah visibility study.

particle mode, are clearly distinguishable. The bar at radii 0.01 μm < R < 0.05 μm represents the total Aitken particle concentration measured with the Environment-One condensation nucleus counter, which, like any other counter operated at around 300 percent supersaturation, detects particles as small as 0.01-μm radius. The Aitken particle concentration, therefore, is characteristic of the very fine particles that determine the condensation nucleus mode at or above 0.01-μm radius.*

By far the largest (about two orders of magnitude) increase of concentration is found in the condensation nucleus mode. The measured concentration $N_N = 3 \times 10^4$ cm^{-3} in rural Utah is surprisingly high for a region that is several hundred kilometers away from any industrial activity. Because of this, and because of

*We adopted Whitby's (1978) terminology in calling very fine particles condensation nuclei, although condensation nuclei in cloud physics usually mean larger particles.

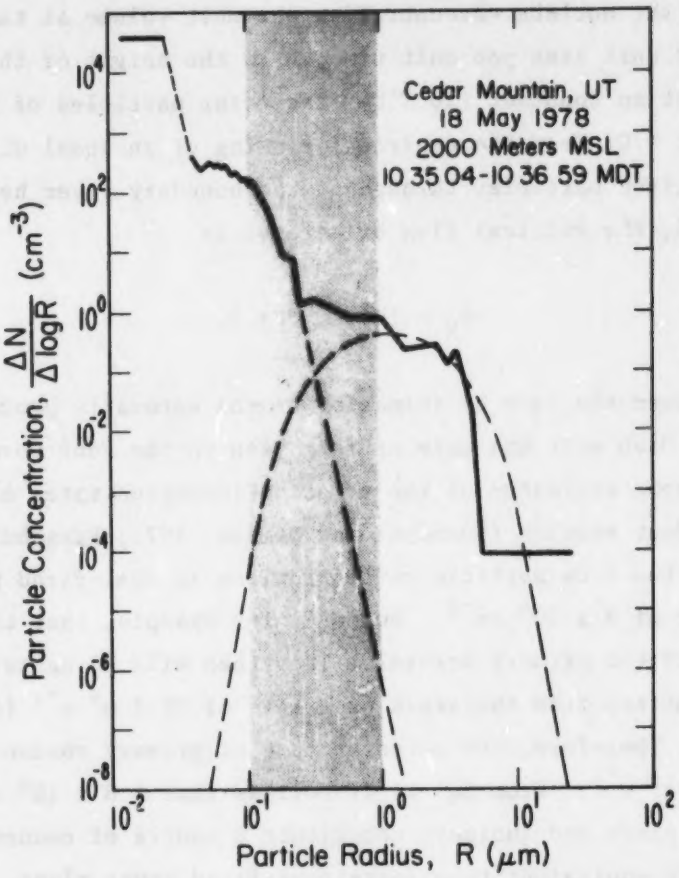

Figure 52.--Typical aerosol size spectrum measured near Cedar Mountain during the Utah visibility study.

the low concentrations of SO_2 and NO_x that we measured in this region, we postulate that the condensation nuclei in rural Utah originate from polymerization of terpenes (Went, 1965) emitted by juniper and piñon trees that make up a thin forest in this area, rather than from the photo-oxidation of either SO_2 or NO_2.

The evolution of condensation nuclei as a function of time from a forest canopy can be expressed (Lopez et al., 1974) as

$$\frac{dN}{dt} = \frac{\Phi_N}{h} - K N_N^2 (t), \qquad (20)$$

where N_N (t) is the nucleus concentration per unit volume at time t, ϕ_N is the nucleus flux per unit area per unit time, h is the height of the mixing layer, and K is the coagulation constant (10^{-9} cm^3 sec^{-1} for particles of radius R = 3 x 10^{-2} μm). With dN/dt = 0, from the empirical finding of an equal distribution of condensation nucleus particles throughout the boundary layer between 2,000 and 3,000 meters MSL, the vertical flux of aerosol is

$$\phi_N = 10^3 \text{ cm}^{-2} \text{ s}^{-1}. \quad (21)$$

In order to compare the rate of formation of the naturally produced condensation nuclei in rural Utah with the rate of formation in the Four Corners power plant plume, we need some estimates of the emission/formation rates of the power plant plume. Independent studies (Pueschel and Mamane, 1979; Pueschel et al., 1979) have shown that the fine particle concentrations in coal-fired power plant plumes are of the order of 8 x 10^4 cm^{-3}. Suppose, for example, that the nuclei in the plume are part of the primary aerosol. They then will be contained in the effluents that are emitted from the stack at a rate of 59.7 m^3 s^{-1} (Arizona Public Service, 1975). Therefore, the emission rate of primary condensation nuclei will be 4.8 x 10^{12} s^{-1}. From Eq. 21 it follows that 4.8 x 10^5 m^2 of sparse forest of piñon pines and junipers constitute a source of condensation nucleus particles that is equivalent to a large coal-fired power plant.

A separate study (Pueschel and Van Valin, 1978) has shown that the Four Corners power plant produces secondary aerosols at a rate of 10^{15} to 10^{16} per second. From Eq. 21 it follows that 100 km^2 of forest would produce that amount of Aitken particles per unit time.

The information in fig. 52 adds weight to the evidence that aerosol size distributions are typically trimodal (Whitby, 1978). All three modes are clearly evident in all of the distribution weightings utilizing the Knollenberg probes in conjunction with the Environment-One Aitken nucleus counter.

According to Whitby, in a typical trimodal size distribution when all particles are considered to be lumped at one mean size for each mode, the rate of change of the number concentration in the three modes can be described by the following equations.

Table 23.--Experimentally-determined modal radii and calculated transfer rates and residence times of the atmospheric background aerosol in Utah

Modal radii (μm)			Particle concentrations (cm^{-3})		
R_N	R_A	R_C	N_N	N_A	N_C
0.01	0.08	2.0	3×10^4	5×10^2	0.5

Particle Transfer Rates (cm^{-3} sec^{-1})			Residence times (days)	
QN_N	QN_A	QN_C	τ_N	τ_A
1.17	1.5×10^{-4}	7.5×10^{-11}	0.3	39

Nucleus mode:

$$\frac{dN_N}{dt} = Q\bar{N}_N - K_{NN}\bar{N}_N^2 - K_{NA}\bar{N}_N\bar{N}_A - K_{NC}N_NN_C - (N_{NP} - N_{NB})\frac{dV_p}{V_p dt} \quad (22)$$

Accumulation mode:

$$\frac{dN_A}{dT} = Q\bar{N}_A - K_{AA}\bar{N}_A^2 - K_{AC}\bar{N}_A\bar{N}_C - (\bar{N}_{AP} - \bar{N}_{AB})\frac{dV_p}{V_p dt} \quad (23)$$

Coarse particle mode:

$$\frac{d\bar{N}_C}{dt} = Q\bar{N}_C - K_{CC}\bar{N}_C^2 - S(t) - (\bar{N}_{CP} - \bar{N}_{CB}) \times \frac{dV_p}{V_p dt} \quad (24)$$

where N (cm^{-3}) = the average number concentration, QN = the average rate insertion of new particles (cm^{-3} s^{-1}), S(t) = a settling function for the coarse particles, K = the coagulation constant (cm^3 s^{-1}), and V_p = the volume of the plume in which the particles are being dispersed. The subscripts P and B denote plume and background situations, respectively.

For the Utah background aerosol, at any given time, dN/dt = 0 and dV/dt = 0, and the particle transfer rates can be calculated directly from the data in fig. 52 and coagulation constants from Fuchs (1964). Table 23 shows the parameters used for the results of the calculations.

The atmospheric residence time of the nuclei is determined by the turnover times of both the nucleus mode and the accumulation mode. The atmospheric residence time is obtained by dividing the total number in a reservoir (plume, boundary layer) by the emission or removal rate.

The values in table 23 indicate that the interaction between the nucleus mode and the coarse particle mode is negligible. It is the accumulation mode that will absorb most or all of the condensation nuclei as time progresses. The nucleus-mode particles are transferred into the accumulation mode within hours to days. The residence time of the accumulation-mode particles, on the other hand, is between weeks and months in the absence of efficient removal processes, e.g., rain and snow. We conclude that the turnover times of the more persistent accumulation mode determine the atmospheric residence times and, therefore, the effects on visibility of nucleation/condensation-produced aerosols. Consequences of the interaction between condensation and accumulation modes are possible changes in chemical composition, size, and concentration of the accumulation mode aerosols.

3.3.4 Aerosol Chemistry

Qualitatively, it has been known for a long time that Aitken nucleus counts are higher in the daytime than at night (Junge, 1953). Bricard (1974) and Hogan (1976) suggest that the generally observed 50 percent increase in Aitken nuclei is caused by SO_2-to-aerosol conversion. We cannot accept this hypothesis as an explanation for the Aitken nucleus formation rate that we measured in rural Utah. We measured SO_2 concentrations of less than 13 $\mu g\ m^{-3}$ for Utah, as opposed to up to $4 \times 10^3\ \mu g\ m^{-3}$ close in and $1 \times 10^2\ \mu g\ m^{-3}$ 80 kilometers downwind from the stacks in the Four Corners power plant plume (Pueschel and Van Valin, 1978). However, the nucleus formation rate at 80 kilometers in the plume is only a few percent of what it is in rural Utah.

Information on the physical and chemical properties of the Utah background aerosol shows conclusively that the accumulation mode is not dominated by sulfur-containing aerosol. The data are the results of an application of the combined techniques of scanning electron microscopy and X-ray energy dispersive analysis to individual particles of samples on Nuclepore filters that were collected during 1976-1978 on Cedar Mountain, Utah.

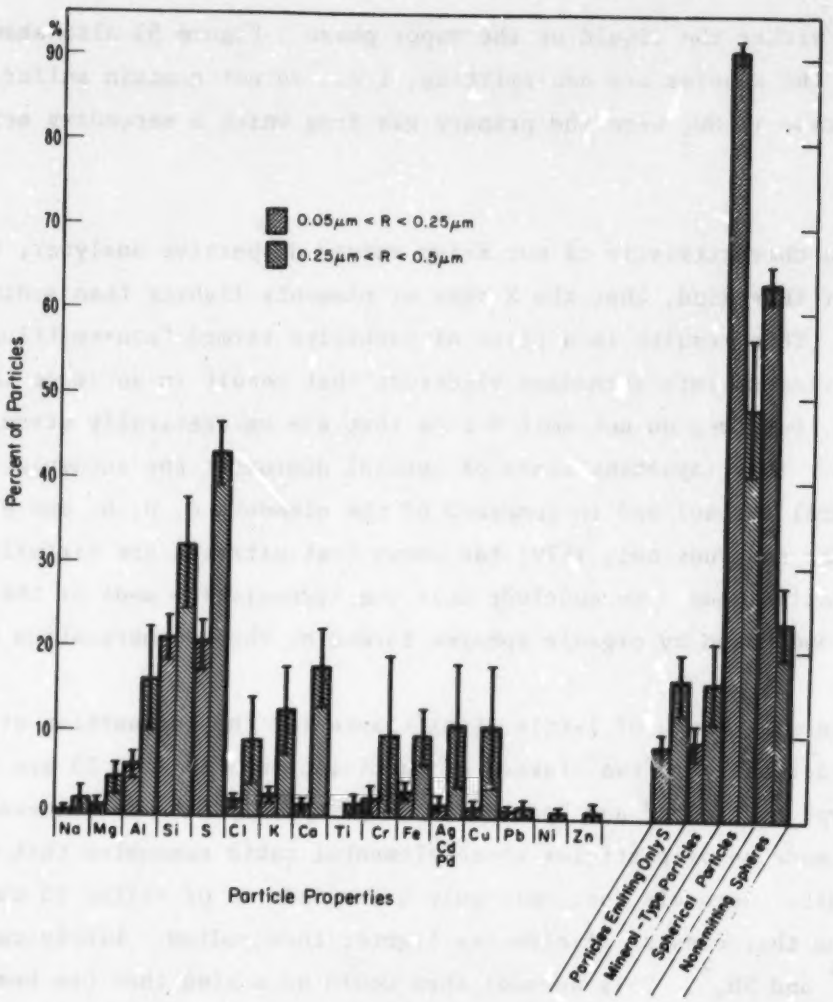

Figure 53.--Percent (by number) of the particles collected at Cedar Mountain that contain elements and show the properties listed on the abscissa.

The results are shown in fig. 53. The ordinate represents the mean and standard deviation of fractions (in percent) of the total number concentration. The abscissa lists the properties (elemental composition, shape) of the aerosol. The data were derived from particles of radii from 0.05 to 0.5 micrometers, the size range in which the accumulation mode is typically found.

The values in fig. 53 indicate that the accumulation mode is dominated by spherical particles formed by a mechanism that involves a phase transition to

solids from either the liquid or the vapor phase. Figure 53 also shows that the majority of the spheres are non-emitting, i.e., do not contain sulfur. This would not be the case if SO_2 were the primary gas from which a secondary aerosol had formed.

It is a characteristic of our X-ray energy dispersive analyzer, as with most analyzers of this kind, that the X rays of elements lighter than sodium are not detectable. This results in a class of particles termed "non-emitting spheres." These particles do emit secondary electrons that result in an image that identifies their shape, but they do not emit X rays that are energetically strong enough to be detected. This important class of aerosol dominates the accumulation mode in the Utah rural aerosol and is composed of the elements C, O, H, and N. A separate study (Mamane and Pueschel, 1979) has shown that nitrates are virtually absent in the accumulation mode. We conclude that the accumulation mode of the Utah rural aerosol is dominated by organic spheres formed by the polymerization of terpenes.

Of interest though of little significance for the composition of the Utah background aerosol, are two classes of particles that in fig. 53 are termed "mineral-type particles" and "particles emitting only S." The mineral-type aerosol is made up of particles whose elemental ratio resembles that of the Earth's crust. Aerosols that emit only S are made up of sulfur in combination with cations that consist of elements lighter than sodium. Likely candidates are the ions H^+ and NH_4^+. This aerosol then would be a kind that has been found to predominate in several midwestern and southern sites (Weiss et al., 1977).

The data in fig. 53 are derived from the energy-dispersive analysis X rays generated when 15-KeV electrons impinge upon the particles in a scanning-electron microscope. To validate these results and to extend the analysis to heavier elements such as lead, samples were analyzed per separate contract by the Air Quality Group, Crocker Nuclear Laboratory, University of California at Davis, utilizing X rays that were generated when 15-MEV α-particles impinge upon aerosols deposited on Nuclepore filters.

The sampler consisted of a filter stack (Cahill et al., 1979) of a 5-μm pore size filter followed by a 0.1-μm pore size filter in order to separate the coarse particle fraction from the fine particle load. The cutoff size, defined as the

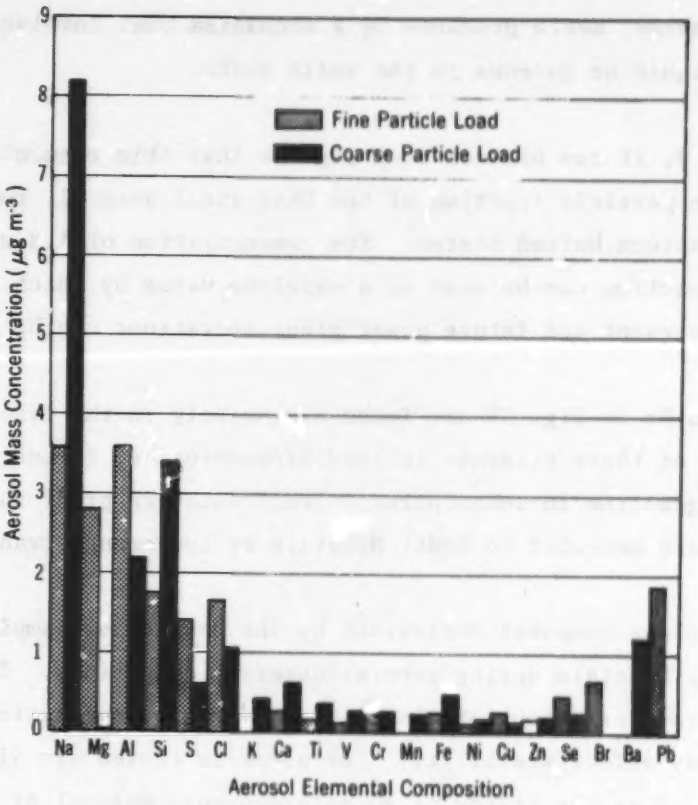

Figure 54.--Concentration of elements in the atmospheric aerosol at Cedar Mountain.

particle size for which the 5-μm pore size filter is 50 percent efficient (Spurny and Lodge, 1972), was 1-μm particle radius.

Figure 54 shows the data, resulting from the averages of 33 samples that were collected between April and November 1978. With the exception of the data for Na which, due to the relatively soft X rays emitted by Na could be erroneous, it follows from fig. 54 that the Si dominates the coarse particle mode with a concentration of about 3.3 μg m^{-3}. The fraction of 1.7 μg m^{-3} of Si in the fine particle load is surprisingly high, however, as is the relatively large amount (3.6 μg m^{-3}) of Al. This finding of a relatively high concentration of aluminum silicates of submicron size leads to the speculation that combustion-produced fly ash from smelter or power plant operations is a significant fraction of the Utah background aerosol. This notion is supported by the findings of the scanning electron microscope single particle analysis, described previously, which identifies those

particles as spheres, hence produced by a mechanism that involves a phase transition from the liquid or gaseous to the solid state.

Turning to S, it can be seen from fig. 54 that this element does not predominate in the fine particle fraction of the Utah rural aerosol, contrary to what is known for the Eastern United States. The concentration of 1.3 $\mu g\ m^{-3}$ of S in the fine particle fraction can be used as a baseline value by which the effects on the environment of present and future power plant operations can be judged.

Both Pb and Br in fig. 54 are found exclusively in the fine particle fraction. A likely source of these elements is lead-bromochloride, formed during the combustion of leaded gasoline in automobiles. These data are proof that anthropogenic urban aerosols are advected to Cedar Mountain by long-range transport.

Figure 55 shows temporal variations by the results of samples collected over 4 hours on Cedar Mountain during several observation periods. The data are presented as temporal variations of visibility and the concentration of various elements that may affect visibility. The elements chosen are Si as an example of mineral aerosol, S as the tracer of an anthropogenic aerosol of coal combustion, and Pb as an anthropogenic aerosol generated by combustion of leaded gasoline.

It follows from fig. 55 that no correlation of any statistical significance can be found between the prevailing visibility and the presence of a specific element. It further follows from fig. 55 that Si is as abundant as S in the elemental composition of the Utah rural aerosol, and that Pb occasionally dominates the aerosol elemental composition. This is entirely contrary to what is known of the atmospheric aerosol along the eastern seaboard where S usually dominates the elemental composition of the aerosol. Hence, an air quality picture for Utah is evolving which, if typical for the Western United States, could be used as a criterion for the impact on the local/regional environment of power plant operations.

Of importance for evaluating the potential impact on visibility of local power plant operations are the effects on visibility of aerosols that are advected from remote areas. An example of the dominating effect on visibility of air masses that have undergone long-range transport is contained in fig. 56 of the

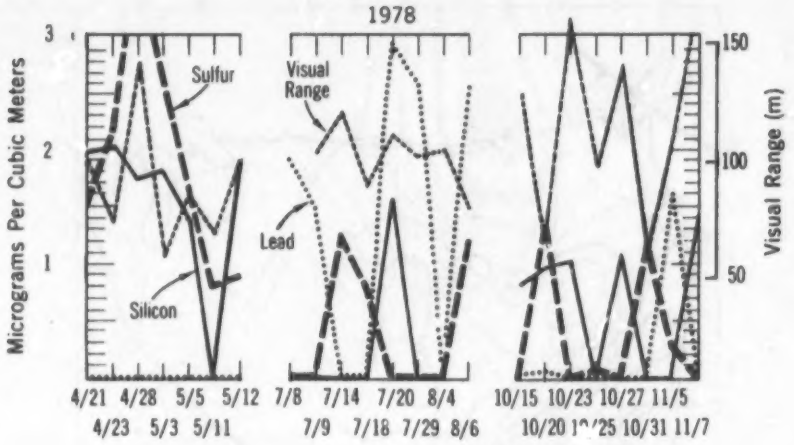

Figure 55.--Temporal variation of the atmospheric concentration of selected elements in aerosols at Cedar Mountain, Apr.-Nov. 1977.

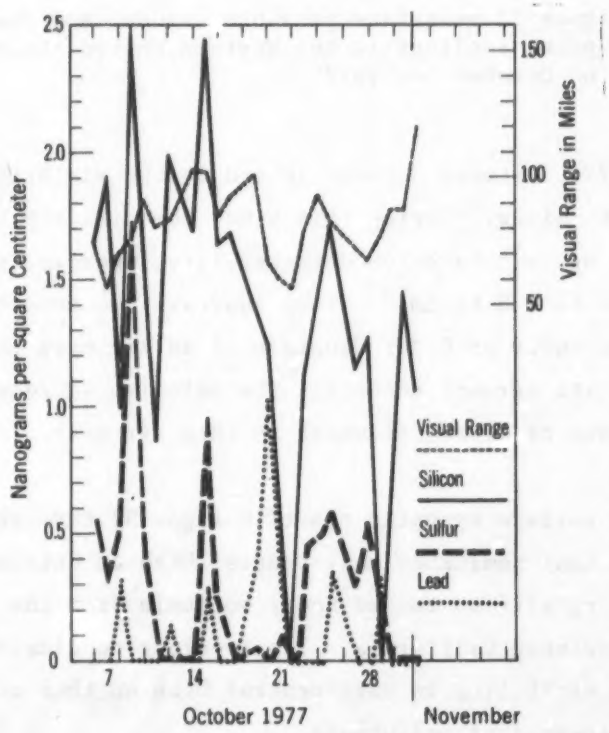

Figure 56.--Temporal variation in the concentration of selected elements in aerosol collected at Cedar Mountain, Oct. 1977.

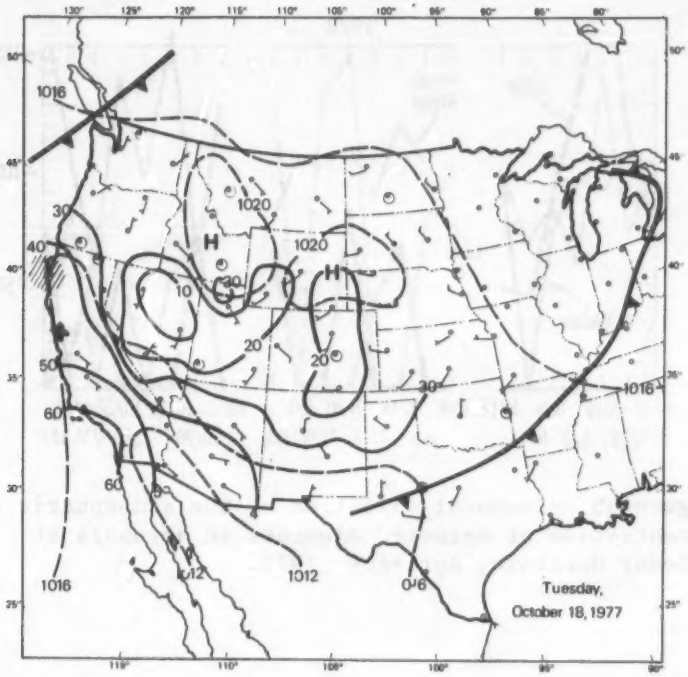

Figure 57.--Surface pressure, winds, and dew-point isolines in the Western United States on October 18, 1977.

data of October 1977. Between October 18 and 19 the visibility decreased rapidly from 100 miles to 65 miles. During this time, the silicate content of the aerosol decreased from 1.4 ng cm^{-2} to below detectability, whereas lead increased from below detectability to 1.0 ng cm^{-3}. This suggests the advection, within less than 24 hours, to the vicinity of Cedar Mountain of an air mass that is characteristically different in its aerosol content. The relative increase in lead strongly suggests the presence of urban effluents in this air mass.

A look at the surface synoptic chart in figs. 57 through 59 shows that the high-pressure area that dominated east-central Utah on October 18 had moved to the southeast, permitting airflow toward Cedar Mountain from the southwest, i.e., from the direction of southern California. The apparent conclusion from this result is that deteriorating visibility in east-central Utah on this occasion was associated with long-range transport of pollutants.

Regarding the cause-effect relationship of the visiblity change on October 18-19, 1977, the high lead content of the advected air mass seems to implicate

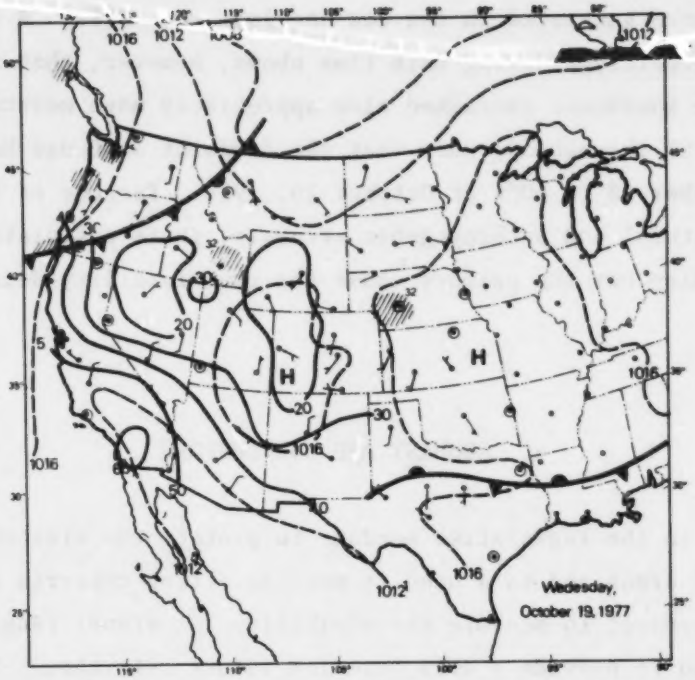

Figure 58.--Surface pressure, winds, and dew-point isolines in the Western United States on October 19, 1977.

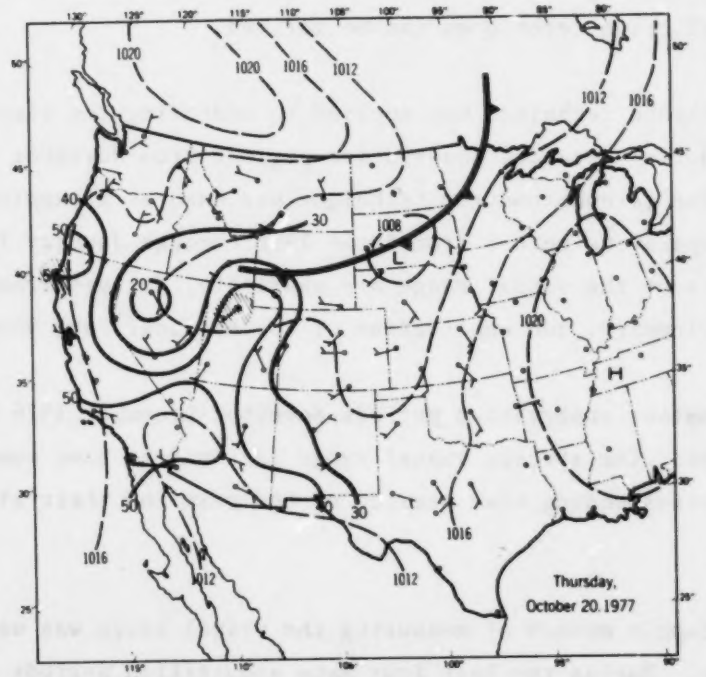

Figure 59.--Surface pressure, winds, and dew-point isolines in the Western United States on October 20, 1977.

pollutants that were generated in the Los Angeles [illegible] area. A closer look at the prevailing meteorology during this time shows, however, that the air mass that originated to the southwest contained also appreciably more moisture. The dewpoint isotherms (figs. 57 through 59) show that the dewpoint at Cedar Mountain increased from 20°F on October 18 to 40°F on October 20, 1978. Because of the hygroscopic nature of many natural and anthropogenic aerosols, it is postulated that the increase in humidity was the primary cause for the visibility decrease during this time.

4. SUMMARY AND CONCLUSIONS

In response to the legislative mandate to protect the visibility in and near mandatory Class I areas and to a need to provide siting criteria for coal-fired power plants, a project to measure the visibility (or visual range) in east central Utah was initiated to provide a data base for future reference. Meteorological parameters and aerosol characteristics were measured concurrently to furnish data for the correlation of visual range to these data. With these visual range data, decisions can be made on monitoring methodology and cause/effect relationship studies, and predictive techniques can be derived.

The photographic technique was applied to measuring the visual range within the atmosphere during selected observation periods from November 1976 through January 1979. The telephotometric technique was used as a supplementary and transitional comparative method from April 1978 through January 1979. Supplementary measurements of the visual range are available, derived from turbidity, solar radiation, nephelometry, and application of the National Park Service Program.

If the anomalous observation periods November-December 1976 and January 1977 are not considered, the average visual range is found to have remained essentially constant when corresponding time periods of the year and their standard deviation are compared.

The photographic method of measuring the visual range was used to establish a 2-yr data base. During the last four data acquisition periods the telephotometric method was also used to derive the visual range. This gives a transitional

time period for comparison between the photographic and telephotometric methods so there will be a calibration between the two methods when telephotometric equipment is permanently installed on Cedar Mountain.

Turbidity measurements can be converted to values of visual range--however, such measurements must be made when there are no clouds obscuring the direct sunlight. Turbidity measurements indicate that over the project time period the amount of particulate material in the atmosphere above Cedar Mountain has increased even though the visual range has not been impaired.

As in most localities there is an inverse relationship between the relative humidity and the visual range, with a correlation coefficient of r = -0.37 (fig. 30).

However, the strongest correlation is found between the southern component of the upper air flow and the visual range, with r = -0.93 (fig. 34). Since the direction of the upper air flow can be interpreted from the location of low- and high-pressure areas, it appears feasible to forecast periods of extreme visual range. Whether daily values of instability are useful in determining the daily variation of visual range has yet to be investigated.

The visual range in Utah is determined by regional air masses and the history of those air masses. Specific incidents of low and high visual range have been correlated to the location of low-pressure areas, the advection of surface air containing anthropogenic and organic particulates of the southern regions, or from source regions of clean air that subsides over the Utah region from areas of high pressure.

At the present time the average annual photographic visual range (V'_{rP}) is about 80 miles, a telephotometric value determined with a photopic filter (V_{rT}) is about 100 miles. During a given observation period the average daily visual range (V_{rT}) varies by a factor of about 2.5 in response to changes of mesoscale meteorology. The average visual range (V_{rT}) varied by a factor of 3.2 over a period of 1 year. In contrast, local and nearby regional industrial activities could not be identified as sources for short- or long-term changes of visual range during the period of operation of the visibility project in east central Utah.

5. ACKNOWLEDGMENTS

We wish to acknowledge the dedication of the co-op university and college students who were observers at the Cedar Mountain, Utah, field observation site and their participation in reduction and analysis of the data; they are Richard Ochoa, Michael A. Dias, William F. Roberts, Gary M. Williams, L. Gwen Lowery, and Mark B. Cozad. We also wish to thank Dennis L. Wellman and Billy R. Caldwell for development and maintenance of the equipment in the mobile field unit. The project was supported by the Environmental Protection Agency through Interagency Agreement IAG-EPA-78-D-F0305 and the Bureau of Land Management through Interagency Agreement YA-515-IA6-26.

6. REFERENCES

Allee, P. A., 1967: Annual variation of Aitken nuclei concentration at Washington, D.C. Mon. Wea. Rev. 95:925-928.

Allee, P. A., and M. B. Cozad, 1979: Telephotometric study of baseline visual range at Cedar Mountain, Utah--October 12 to November 10, 1978. NOAA Data Report ERL APCL-5, U.S. Dept. Comm., Boulder, Colo.

Allee, P. A., and L. G. Lowery, 1979: Telephotometric study of baseline visual range at Cedar Mountain, Utah--July 7 to August 6, 1978. NOAA Data Report ERL APCL-3, U.S. Dept. Comm., Boulder, Colo.

Allee, P. A., W. F. Roberts, L. G. Lowery, and G. M. Williams, 1979: Telephotometric study of baseline visual range at Cedar Mountain, Utah--April 21 to May 16, 1978. NOAA Data Report ERL APCL-4, U.S. Dept. Comm., Boulder, Colo.

Arizona Public Service, 1975: Four Corners power generating plant and Navajo coal mine. Environmental report prepared by Westinghouse Environmental Systems Department, Arizona Public Service Co., Phoenix, Ariz.

Bricard, J., 1974: Aerosol production in the atmosphere. Proc. Annual Meeting: Aerosols in nature, medicine and technology, German Aerosol Foundation, Vorderhinderlang, Germany.

Cahill, T. A., R. A. Eldred, J. Barone, and L. Ashbaugh, 1979: Ambient aerosol sampling with stacked filter units. Report No. FHWA-RD-78-178, Federal Highway Administration, Washington, D.C.

Daily Weather Maps, Weekly Series, 1976-79: U.S. Dept. Comm., EDIS, Washington, D.C.

Elterman, L., 1968: UV, visible and IR attenuation for altitudes to 50 km., 1968. Environmental Research Papers, No. 285, AFCRL-68-0153, Air Force Cambridge Research Laboratories, L. G. Hanscom Field, Bedford, Mass., 57 pp.

Flowers, E. C., R. A. McCormick, and K. R. Kurfis, 1969: Atmospheric turbidity over the United States, 1961-1966. J. Appl. Meteor. 5:955-962.

Flowers, E. C., R. A. McCormick, K. R. Kurfis, and T. H. Bilton, 1974: Atmospheric measurements with the dual-wavelength sunphotometer. Proc. WMO/WHO Technical Conference on Observation and Measurement of Atmospheric Pollution, Helsinki, Finland, July 30 to August 4, 1973.

Fuchs, N. A., 1964: The Mechanics of Aerosols. Macmillan, New York, 408 pp.

Glossary of Meteorology, 1959: R. E. Huschke (ed.), American Meteorology Society, Boston, Mass.

Harrison, G. B., 1945: The scattering of light in the atmosphere. Photogr. J., Sect. B, 85:57-62.

Hogan, A. W., 1976: Physical properties of the atmospheric aerosol. State University of New York, Atmospheric Sciences Research Center, Publ. No. 408, Albany, N. Y., 167 pp.

Junge, C. F., 1953: Die Rolle der Aerosole und der gasförmigen Beimengungen der Luft in Spurenstoffhaushalt der Troposphäre. Tellus 5:1-26.

Kasten, F., 1964: A new table and approximation formula for the relative optical air mass. U.S. Army Materiel Command, Cold Regions Research and Engineering Laboratory, Hanover, N. H., 11 pp.

Lopez, A., J. Fontan, and J. Servant, 1974: Mesoscale determination of Aitken nuclei flux near the ground, in atmosphere-surface exchange of particulates and gaseous pollutants. U.S. Energy Research and Development Administration, 171-191.

Mamane, Y., and R. F. Pueschel, 1980: A method for the detection of individual nitrate particles in the atmosphere. Atm. Environ. (accepted for publication).

Martin Marietta Corporation, 1976-1979: A study of baseline visibility at Cedar Mountain, Utah (9 Vols.). Work performed under NOAA contract No. 03-7-022-35107, Martin Marietta Corp., Denver Division, Denver, Colo.

Middleton, W. E. K., 1952: Vision Through the Atmosphere. University of Toronto, Canada, 230 pp.

Nautical Almanac, 1976-79: United States Naval Observatory, Washington, D.C.

Pueschel, R. F., and Y. Mamane, 1979: Mechanisms and rates of formation of sulfur aerosols in power plant plumes. Proc. WMO Conference on Long-Range Transport, Sofia, Bulgaria, 1-5 Oct. 1979.

Pueschel, R. F., R. C. Schnell, H. K. Weickmann, and D. L. Wellman, 1979: Aerosol and ice nuclei measurements in the plume of the Homer, PA, power plant. Geophys. Res. Lett. 6:371-374.

Pueschel, R. F., and C. C. Van Valin, 1978: Cloud nucleus formation in a power plant plume. Atmos. Env. 12:307-312.

Spurny, K. R., and J. P. Lodge, Jr., 1972: Collection efficiency tables for membrane filters used in the sampling and analysis of aerosols and hydrosols. Rept. No. NCAR-TN/STR-77 (3 Vols.), National Center for Atmsopheric Research, Boulder, Colo.

Walther, E. G., and W. C. Malm, 1979: The excellent but deteriorating air quality in the Lake Powell region. J. Air Pollut. Control Assoc. 29:378-80.

Weiss, R. E., A. P. Waggoner, R. J. Charlson, and N. C. Ahlquist, 1977: Sulfate aerosol: its geographical extent in the midwestern and southern United States. Science 195:979-981.

Went, F. W., 1965: The nature of Aitken condensation nuclei in the atmosphere. Proc. Nat. Acad. Sci. 51:1259-1267.

Whitby, K. T., 1978: The physical characteristics of sulfur aerosols. Atmos. Environ. 12:135-159.

Whitby, K. T., B. K. Cantrell, and D. B. Kittelson, 1978: Nuclei formation rates in a coal-fired power plant plume. Atmos. Environ. 12:313-321.

Williams, G. M., and P. A. Allee, 1979: Telephotometric study of baseline visual range at Cedar Mountain, Utah--January 19 to March 6, 1979. NOAA Data Report ERL APCL-6, U.S. Dept. Comm., Boulder, Colo.